



University Library

Author/Filing Title YANG

Class Mark T

Please note that fines are charged on ALL
overdue items.

--	--	--

0402940962



Data Extraction in Holographic Particle Image Velocimetry

By Hui Yang

Doctoral Thesis

Submitted in partial fulfilment of the requirement for the award
of Doctor of Philosophy at Loughborough University

October 2004

© by H. Yang 2004.

 Loughborough University	
Date	SEP'05
Class	T
Acc No	40294096

Table of Contents

Table of Contents	1
Nomenclature	3
Abstract	5
Acknowledgements	6
List of Figures	7
List of Tables	9

Chapter 1 Introduction

1.1 Overview of optical methods for fluid metrology	1-1
1.2 Research objectives	1-3
1.3 Outline of the thesis.....	1-5
1.4 References	1-6

Chapter 2 Literature Review of HPIV

2.1 Introduction	2-1
2.2 Review of HPIV	2-1
2.3 Particle tracking.....	2-3
2.4 Intensity correlation analysis	2-6
2.5 Optical complex amplitude correlation	2-12
2.6 Digital HPIV.....	2-18
2.7 Summary	2-21
2.8 References	2-21

Chapter 3 Theoretical Background of Complex Amplitude Correlation

3.1 Introduction	3-1
3.2 3D complex amplitude correlation	3-1
3.3 Digital 3D complex amplitude correlation	3-7
3.4 Summary	3-9
3.5 References	3-10

Chapter 4 Digital Shearing Method

4.1 Introduction	4-1
4.2 Theory of digital shearing method.....	4-1
4.3 Simulated experiment.....	4-8

4.4	Comparison between digital shearing and CAC method.....	4-17
4.4.1	Computational performance	4-17
4.4.2	Accuracy.....	4-18
4.5	Experimental results	4-23
4.6	Summary	4-29
4.7	References.....	4-30

Chapter 5 Micro Holographic Particle Image Velocimetry

5.1	Introduction	5-1
5.2	Review of μ PIV	5-2
5.3	Digital μ HPIV	5-5
5.3.1	Digital recording.....	5-6
5.3.2	Numerical reconstruction	5-11
5.3.3	Data extraction.....	5-12
5.4	3C-3D measurement of the micro-scale jet flow.....	5-14
5.4.1	Experimental layout.....	5-14
5.4.2	Experimental results	5-18
5.4.3	Vector cluster analysis.....	5-23
5.5	Summary	5-27
5.6	References	5-28

Chapter 6 Conclusions and Further Work

6.1	Conclusions and main contributions.....	6-1
6.2	Suggestions for further work	6-4

Nomenclature

3C	Three-component
3D	Three-dimensional
CAC	Complex Amplitude Correlation
f	Focal length
f_x	Spatial frequency of carrier fringes
FFT	Fast Fourier Transformation
HPIV	Holographic Particle Image Velocimetry
$h(x_i, y_i)$	The impulse response
$I(x_i, y_i)$	Intensity distribution
$\mathbf{k}=(k_x, k_y, k_z)$	Wave vector
K_x, K_y	Wave vector components with a change of co-ordinate
lp/mm	Line pair per millimetre
M	Magnification of the optical system
N	Pixel number
NA	Numerical Aperture
$P(\mathbf{k})$	Power spectral density
PIV	Particle Image Velocimetry
$P(k_x, k_y)$	The x - y projection of the power spectral density
$\mathbf{r}=(r_x, r_y, r_z)$	Position vector
$R(\mathbf{r})$	Correlation of the optical field
$\mathbf{s}=(s_x, s_y, s_z)$	Particle image displacement
$S(\mathbf{k})$	Spectrum of complex amplitude
$U(\mathbf{r})$	Complex amplitude

$W(k_x, k_y)$	Isolated power spectral density
α	Angle between the reference beam and the object beam
δ	Delta function
λ	Wavelength
μHPIV	Micro Holographic Particle Image Velocimetry
μPIV	Micro Particle Image Velocimetry
*	Complex conjugate
\otimes	Convolution

Abstract

Holographic Particle Image Velocimetry (HPIV) is potentially the best technique to obtain instantaneous, three-dimensional, flow field information. Several researchers have presented their experimental results to demonstrate the power of HPIV technique. However, the challenge to find an economical and automatic means to extract and process the immense amount of data from the holograms still remains. This thesis reports on the development of complex amplitude correlation as a means of data extraction. At the same time, three-dimensional quantitative measurements for a micro scale flow is of increasing importance in the design of microfluidic devices. This thesis also reports the investigation of HPIV in micro-scale fluid flow.

The author has re-examined complex amplitude correlation using a formulation of scalar diffraction in three-dimensional vector space. Three-dimensional complex amplitude correlation has been implemented digitally to replace optical methods. However, the computation of three-dimensional complex amplitude correlation is intensive. A digital shearing method has been proposed and implemented for data extraction. It has been shown that all three components of particle image displacement can be retrieved using two-dimensional fast Fourier transform operations and appropriate co-ordinate transformations. Simulated and experimental results show that the digital shearing method has comparable accuracy to three-dimensional correlation but is significantly faster.

The potential of the digital μ HPIV has also been investigated in this thesis. A forward-scattering microscopic holographic system was used to record three-dimensional images of interest. The whole optical field complex amplitude was then reconstructed by fast Fourier transformation based on a convolution approach. Vector cluster analysis method was used to assign the measured displacement to a velocity at a particular point in the flow. These techniques were demonstrated using a free jet flow in a microchannel.

Acknowledgements

I would like to thank my supervisors, Dr. Jeremy Coupland and Prof. Neil Halliwell, for their help and encouragement during the course of my studies. I am very grateful for the study opportunity they offered me, which opened my eyes well beyond the PhD research. The fact that I am able to complete the PhD research and present this thesis mainly contributes to Dr. Jeremy Coupland. Without his support and push, this thesis would not be possible.

I would also like to thank Dr. Graham Hargrave for his advice and support as my Director of research and Rob Alcock for his technical support with digital μ HPIV experiments.

My gratitude is also extended to all of my friends and colleagues at Loughborough who helped, supported or entertained me during the course of this work. Special thanks are due to the families of Mr. Francis Maccabee and Dr. Feng Gao for the happy times together.

I wish to thank my parents, my brother and my two sisters for their importance in my life. I also wish to acknowledge my parents-in-law, all of my brothers-in-law and my sisters-in-law for their help and financial support.

Finally, I would like to thank my wife, Fangmin Shi, and our daughter, Chuyi Yang for their patience and encouragement.

List of Figures

Figure 2-1 Double exposure input interrogation area and the corresponding output auto-correlation plane	2-7
Figure 2-2 Two single exposure input interrogation areas and the corresponding output cross-correlation plane	2-7
Figure 2-3 (a) Recording of hologram (b) Object-conjugate reconstruction of hologram	2-15
Figure 2-4 Reconstruction geometry with fibre optic illumination probe	2-16
Figure 3-1 The wave vector \mathbf{k}	3-3
Figure 3-2 Ewald Sphere.....	3-4
Figure 3-3 3D complex amplitude auto-correlation output.....	3-6
Figure 3-4 k-space mapping	3-8
Figure 3-5 Flow chart of digital 3D-CAC.....	3-9
Figure 4-1 Wave-vector geometry	4-4
Figure 4-2 Flow chart of digital shearing method	4-7
Figure 4-3 Geometry of fringe pattern generation	4-7
Figure 4-4 The far field fringe pattern	4-9
Figure 4-5 The far-field fringe pattern as a function of wave vector components.....	4-9
Figure 4-6 Phase-only map of the curved wavefront (modulo 2π).....	4-10
Figure 4-7 Sheared phase distribution (modulo 2π)	4-11
Figure 4-8 Sheared phase distribution with a variable change.....	4-11
Figure 4-9 Squared modulus of FFT of complex exponential of the phase shown in Figure 4-8	4-12
Figure 4-10 Original phase-only map (Figure 4-5) with curvature (due to sz displacement) subtracted	4-13
Figure 4-11 Squared modulus of FFT of complex exponential of the phase shown in Figure 4-10	4-13
Figure 4-12 A comparison between the computed and pre-assigned displacement in z direction (pre-assigned displacements in x and y directions are $10\mu\text{m}$, respectively)	4-15
Figure 4-13 A displacement comparison in x -direction.....	4-15
Figure 4-14 A displacement comparison in y -direction.....	4-16
Figure 4-15 Variation of RMS error for digital shearing and 3D correlation methods.....	4-20
Figure 4-16 Variation of mean bias error for digital shearing and 3D correlation methods	4-22
Figure 4-17 Recording geometry	4-23

Figure 4-18 First and second exposure hologram	4-25
Figure 4-19 Reconstructed particle images from Figure 4-18 a) and b)	4-26
Figure 4-20 Phase map of cross-spectrum	4-26
Figure 4-21 Co-ordinate transformed sheared cross-spectrum	4-27
Figure 4-22 Squared modulus of FFT of complex exponential of the phase illustrated in Figure 4-21 (after zero padding)	4-28
Figure 4-23 Original phase map of cross-spectrum (Figure 4-19) with curvature subtracted	4-28
Figure 4-24 Squared modulus of FFT of complex exponential of the phase illustrated in Figure 4-23 (after zero padding).	4-29
Figure 5-1 Schematic of a μ PIV system (after Meinhart et al).....	5-3
Figure 5-2 Digital μ HPIV	5-7
Figure 5-3 Phase curvature match.....	5-9
Figure 5-4 A holographic recording of the optical field in the object plane of the objective.....	5-9
Figure 5-5 Flow chart of μ HPIV	5-13
Figure 5-6 Off-axis forward scattering μ HPIV imaging system.....	5-15
Figure 5-7 Micro channel.....	5-16
Figure 5-8 (a) First and (b) second exposure hologram.....	5-17
Figure 5-9 Reconstructed particle image from Figure 5-8.....	5-19
Figure 5-10 Reconstructed particle image at $z=-0.12mm$	5-20
Figure 5-11 Reconstructed particle image at $z=-0.21mm$	5-21
Figure 5-12 3D cross-correlation intensity of marked sub-pictures in the (a) Figure 5-9, (b) Figure 5-10 and (c) Figure 5-11 (the centre pixel is a zero velocity reference)	5-22
Figure 5-13 The correlation peaks of marked sub-pictures throughout the z-direction....	5-24
Figure 5-14 The calculated three-component displacement vectors from the correlation peaks position throughout the depth-direction of the flow volume.....	5-24
Figure 5-15 In-plane two components velocity map in the image plane (a) before and (b) after the measurement data is identified	5-26
Figure 5-16 Three-dimensional velocity map of free jet fluid flow (137 vectors in the size of $0.5 \times 0.6 \times 0.6mm^3$ volume).....	5-26

List of Tables

Table 1-1 Techniques for optical flow velocimetry	1-3
Table 4-1 Independence of x , y and z displacement measurements	4-15
Table 4-2 Computational performance of digital shearing and 3D correlation methods .	4-17
Table 4-3 Mean errors magnitude over the complete 11-20 μm range	4-21

Chapter 1: Introduction

1.1 Overview of Optical Methods in Fluid Metrology

Since the advent of the laser, optical metrology has played a major role in the understanding of fluid flow phenomena and the subsequent development of complex computational models. Laser Doppler Anemometry (LDA) quickly showed the power of optical metrology, allowing three-component (3C), time-resolved velocity measurements to be made at a single point in the fluid flow field (Yeh *et al.* 1964). This method relies on a direct measurement of the frequency shift that occurs when light is scattered from moving particles suspended in the flow. Recently, Doppler techniques have been used for whole field measurements. Doppler Global Velocimetry (DGV), also known as Planar Doppler Velocimetry (PDV), is another 3C velocimetry measurements technique which is capable of providing planar velocimetry measurements (Meyers 1995). This method usually uses an absorption edge of an iodine filter to demodulate Doppler scattered light. Finally, Combined LDA and Optical Coherence Tomography (OCT), Doppler OCT has been demonstrated as a means to measure velocity in different planes through a volume of fluid (Chen *et al.* 1997).

Although whole Laser Doppler techniques have much potential, Particle Image Velocimetry (PIV) is the preferred technique for simultaneous two-dimensional (2D) measurement of fluid velocity (Adrian 1991). In essence PIV employs laser light sheet imaging (using photographic films or digital cameras) to measure the two in-plane components (2C) of fluid velocity from a single plane in a flow. The component of out-of-plane velocity cannot be measured directly, but can be derived from the planar

measurements in a stereoscopic set-up (Prasad *et al.* 1993). The development of PIV clearly marks a significant advancement in experimental fluid mechanics from single-point to multi-point velocity measurement (Adrian 1997). This progress, however, is only half-way towards the full-field three-component measurement of turbulent flows. Attempts have been made to generalise planar PIV techniques into volumetric field measurement through scanning (Bruecker 1995), however there are severe limitations in spatial and temporal resolution. Hence, planar PIV techniques are unable to provide detailed space-resolved experimental data in highly transient and three-dimensional (3D) turbulent flows.

Holographic Particle Image Velocimetry (HPIV) is an emerging technology that provides instantaneous three-dimensional flow field information (Hinsch 2002). HPIV works on holographic rather than photographic principles to record a 3D image. Holography is a method for recording and reconstructing the amplitude and the phase of a wavefield (Gabor 1948). A hologram is a recorded interference pattern between a wavefield scattered from the object and a coherent background, called reference wave. The processed interference pattern is used to reconstruct the original wavefield by illuminating it with a replica of the reference wave. HPIV records the 3D information of particles in a fluid volume instantaneously on a double-exposure hologram (or two single-exposure holograms) separated by a short time lapse and generally reconstructs the particle images in a 3D space. From the reconstructed image field, the 3D velocities of these particles in the volume can be obtained. Based on the 3D nature of the holographic image as well as advanced image processing technology, HPIV is the most promising candidate for the next generation full-field velocimetry that can measure high spatial resolution of instantaneous 3D velocity fields. Table 1.1 shows a comparison of various techniques for optical flow velocimetry and their attainable dimensions of data space (Hinsch 1995).

Table 1-1 Techniques for optical flow velocimetry

Measurement techniques	Velocity components	Spatial dimensions
LDA	1	0
3D LDA	3	0
PIV	2	2
Stereoscopic PIV	3	2
HPIV	3	3

1.2 Research objectives

The research of this thesis was motivated by the desire to develop an automatic, three-component velocity measurement system for the efficient and accurate study of three-dimensional fluid flow. A number of research groups (Hinsch *et al.* 1990; Coupland *et al.* 1992; Meng *et al.* 1993; Barnhart *et al.* 1994) have investigated HPIV as a means to make three-component velocity measurement from a three-dimensional volume of interest. Over the past decade, several groups (Herrmann *et al.* 2000; Pu *et al.* 2000; Barnhart 2001; Sheng *et al.* 2001) have successfully produced instantaneous, high-spatial resolution, volumetric field measurement of turbulent flow. It is clear that the enormous potential of HPIV has been demonstrated, however, the challenge of how to find an economical and automatic means to extract and process the immense amount of data from the holograms still remains to be overcome before the method reaches the level of maturity of LDA or PIV.

The main aim of this thesis is to examine a high speed digital analysis approach to extracting 3C-3D data from holograms. The method proposed in this thesis is called the digital shearing method, which is based on complex amplitude correlation (CAC) theory (Coupland *et al.* 1992).

The formidable cost and the technical complexity of film-based HPIV systems have also hampered the wide application of HPIV in practice. For this reason many researchers have replaced holographic films with a digital camera (Hinsch 2002; Meng *et al.* 2004). Digital HPIV directly records a time series of holograms onto a CCD sensor and reconstructs the 3D flow field numerically. It benefits from the simplicity of hardware and the ease of operation with which digital images can be transferred to a computer for further analysis. For the most part in digital HPIV, a small numerical aperture (NA) recording has been used to record the large flow. This means recordings are generally low resolution and measurements are possible on a sparse grid. It is possible, however, to make high numerical aperture recordings provided that the field is limited in spatial extent. With present recording capability this means a flow field of the order of $0.5 \times 0.5 \times 0.5 \text{ mm}^3$ can be recorded. Interestingly, flow fields of this scale have recently become of major interest with the development of so-called lab on a chip technologies and microfluidics. The other aim of this thesis therefore is to investigate digital HPIV for the measurement of micro-scale flow structures. This is called digital Micro Holographic Particle Image Velocimetry (μ HPIV). The techniques of digital μ HPIV and CAC are then demonstrated by measuring the free jet flow in a micro-channel.

The specific objectives of this thesis are summarized as follows:

- (1) Examination of the basic principles of CAC mathematically using a formulation of scalar diffraction in 3D vector space and implementation of 3D-CAC digitally;

- (2) Development, formulation and implementation of a new method, named the *digital shearing method*, to extract 3C-3D data from the holograms efficiently and accurately;
- (3) Evaluation of the performance of the digital shearing and 3D-CAC methods in terms of their computational efficiency and measurement accuracy;
- (4) Exploration of digital μ HPIV for the 3C-3D measurement of flow structures within micro-fluidic devices;
- (5) Application of digital μ HPIV and CAC to measure the free jet flow in a micro-channel.

1.3 Outline of the thesis

There are six chapters in this thesis. Each chapter starts with an introductory section and is concluded with a summary of the chapter and references. Generally each chapter follows a structure of review, related theory, development and implementation, results and discussion.

Chapter 2 reviews various HPIV measurement techniques as they have been developed for the study of fluid mechanics. In particular, quantitative analysis of particle holograms is examined including particle tracking, particle intensity correlation and optical complex amplitude correlation.

Chapter 3 presents the theoretical background of CAC for 3C-3D displacement measurement using a formulation of scalar diffraction in 3D vector space and implementation of 3D-CAC digitally.

These are followed by the main investigation in Chapters 4 and 5. Chapter 4 introduces and defines a new measurement method based on CAC analysis, which is called the digital shearing method. It begins with the formulation and its fast implementation. Then the performance of the digital shearing and 3D-CAC methods, in terms of their computational efficiency and measurement accuracy, is evaluated.

Chapter 5 explores digital μ HPIV as a means to make 3C-3D measurements in micro-fluidics. The principle and practical issues of digital μ HPIV are analysed. A micro-scale free jet fluid flow is measured and the experimental result is discussed.

Finally, Chapter 6 presents a summary of the work covered by the thesis, lists and describes the contributions of the thesis and makes some suggestions for future work.

1.4. References

- Adrian, R. J., 1991, "Particle-imaging technique for experiment fluid dynamics", *Ann. Rev. Fluid. Mech.*, vol.23, p261-304.
- Adrian, R. J., 1997, "Dynamic ranges of velocity and spatial resolution of particle image velocimetry", *Measurement Science and Technology*, vol.8, p1393-1398.
- Barnhart, D. H., 2001, Whole-field holographic measurements of three-dimensional displacement in solid and fluid mechanics, PhD thesis, Loughborough University, UK.
- Barnhart, D. H., Adrian, R. J. and Papen, G. C., 1994, "Phase-conjugate holographic system for high-resolution particle-image velocimetry", *Applied Optics*, vol.133(30), p7159-7170.
- Bruecker, C., 1995, "3-D PIV using a scanning light-sheet and stereoscopy: study of flow development around a spherical cap", *ASME*, vol.229, p497-503.
- Chen, Z. and Milner, T. R., 1997, "Doppler OCT", *Optical Letter*, vol.22(64).

Coupland, J. M. and Halliwell, N. A., 1992, "Particle image velocimetry: three-dimensional fluid velocity measurements using holographic recording and optical correlation", *Applied Optics*, vol.131(8), p1005-1007.

Gabor, D., 1948, "A new microscopic principle", *Nature*, vol.1161, p777-778.

Herrmann, S. F., Geiger, M., Hinsch, K. D. and Peinke, J., 2000, "Light-in-flight holography with switched reference beams for cross-correlation in deep volume PIV", 10th International Symposium on Applications of Laser Techniques to Fluid Mechanics, Lisbon.

Hinsch, K. D., 1995, "Three-dimensional particle velocimetry", *Measurement Science and Technology*, vol.6, p742-753.

Hinsch, K. D., 2002, "Holographic Particle Image Velocimetry", *Measurement Science and Technology*, vol.13, pR61-R72.

Hinsch, K. D., Hinrichs, H., Kuhfahl, G. and P. Meinlschmidt, 1990, "Holographic recording of 3-D flow configurations for Particle Image Velocimetry (PIV)", *ICALEO*, vol.12, p121-130.

Meng, H., Anderson, W. L., Hussain, F. and Liu, D. D., 1993, "Intrinsic speckle noise in in-line particle holography", *Journal of the Optical Society of America A (Optics and Image Science)*, vol.10(9), p2046-2058.

Meng, H., Pan, G., Pu, Y. and Woodward, S. H., 2004, "Holographic particle image velocimetry: from film to digital recording", *Measurement Science and Technology*, vol.15, p673-685.

Meyers, J. F., 1995, "Development of Doppler Global Velocimetry (DGV) as a flow diagnostics tool", *Measurement Science and Technology*, vol.6(5), p769-783.

Prasad, A. K. and Adrian, R. J., 1993, "Stereoscopic particle image velocimetry applied to liquid flows", *Experiments in Fluids*, vol.15, p49.

Pu, Y. and Meng, H., 2000, "An advanced off-axis holographic particle image velocimetry (HPIV) system", *Experiments in Fluids*, vol.29, p184-197.

Sheng, J., Malkiel, E. and Katz, J., 2001, "One beam two view holographic particle image velocimetry system (CD-Rom)", *Proceedings of 4th International Symposium on Particle Image Velocimetry*, Gottingen, p1022.

Yeh, Y. and Cummins, H., 1964, "Localised fluid measurements with a HeNe laser spectrometer", *Applied Physics Letters*, vol.4, p176-178.

Chapter 2 : Literature Review of HPIV

2.1. Introduction

The purpose of this literature review is to provide a detailed account of the various HPIV measurement techniques as they have been developed for the study of fluid mechanics. Firstly, the historical foundations of HPIV in flow measurement are provided by section 2.2. Then, research efforts undertaken to utilize the general methods of particle tracking and image intensity correlation for quantitative analysis of particle holograms are examined in sections 2.3 and 2.4, respectively. Section 2.5 reviews far-field interferometry and initial work on complex amplitude correlation (CAC) using optical methods, which is the basis of the theory proposed in this thesis. Finally, digital HPIV is examined in section 2.6, and leads to a discussion of the digital μ HPIV system.

2.2. Review of HPIV

There are two basic HPIV configurations classified by the nature of the holographic scheme: in-line and off-axis holography. An in-line holographic system employs only one beam to produce both the object wave and reference wave, but off-axis holography introduces separate object beam and reference beam(s). In-line holography has the advantages of simplicity of optical geometry and low requirements for laser coherence and energy, but has severe drawbacks (Meng *et al.* 1993). Due to the superposition of the real image, virtual image and reference waves, together with recordings of light scattered from all the components along the optical path, excessive speckle noise is produced and interferes with the recognition of particle images. To improve the practicality of in-line

HPIV while maintaining its merits, efforts have been made to suppress the speckle noise and improve the signal-to-noise ratio (SNR) of the reconstructed particle images, e.g. the in-line recording and off-axis viewing technique (Meng *et al.* 1995). However, at a seeding density of no more than a few particles per mm^3 , the unscattered waves that form the reference beam can be severely perturbed and the achievable spatial resolution of in-line HPIV is still far from resolving turbulent flows to the request level.

Compared with in-line techniques, off-axis holography has several significant advantages. Firstly, off-axis holography tolerates higher seeding densities, which yields higher spatial resolution. Then, with proper design it resolves the overlapping real and virtual image problem and hence reduces the speckle noise substantially. This offers a much better image signal-to-noise ratio (SNR). Also the directional ambiguity problem inherent in double-exposure in-line HPIV can be solved by employing dual reference waves at different angles (Barnhart *et al.* 1993). These make off-axis HPIV a preferable configuration, which is employed in the work described in this thesis.

Various more sophisticated off-axis methods have been proposed and implemented since the early years of HPIV development, that successfully tackle practical problems such as low scattering efficiency, inferior depth resolution or aberration in the reconstruction (Barnhart *et al.* 1994; Hinrichs *et al.* 1997; Zhang *et al.* 1997; Pu *et al.* 2000). Barnhart *et al.* developed a phase-conjugated, off-axis HPIV system, where two separate channels of near-forward scattering are used to achieve an effective large numerical aperture (NA) recording of particle images (Barnhart *et al.* 1994). Zhang *et al.* constructed a hybrid HPIV system, where two orthogonal views with forward scattering are implemented to overcome the large depth of focus. An optical high-pass spatial filter is utilised to remove the directly transmitting wave (dc term) in the object beam (Zhang *et al.* 1997). Hinrichs *et al.* developed light-in-flight HPIV system with a backscattering geometry to efficiently suppress speckle noise (Hinrichs *et al.* 1997). Pu *et al.* reported the Gemini off-axis HPIV

system to use a double-referenced, off-axis holographic recording with 90° side-scattered particle illumination to obtain a large angular aperture and *in situ* reconstruction to minimize the aberration (Pu *et al.* 2000). The details of these methods will be introduced in the following sections.

Once particle images have been reconstructed, the real challenge is to extract the particle displacement required to compute a velocity map. Most HPIV data extraction methods can be categorised into three types: particle tracking, particle image intensity correlation and complex amplitude correlation (CAC). Particle tracking and particle image intensity correlation are applied in a way similar to those in PIV. The choice of a processing technique primarily depends on the density of seeding particles. CAC is a unique method used in HPIV, which utilises both the amplitude and phase information to calculate the particle displacement. In the next three sections a comprehensive survey of published research in these fields, as they relate to the present thesis objectives, is presented.

2.3. Particle tracking

Particle tracking (Trolinger *et al.* 1969) is the most basic technique to extract the displacement vectors from particle images. It depends on the idea of following the movement of individual particles in consecutive image frames separated by a small time interval. In the particle tracking process, the positions of individual particles within a recorded image are first identified and then cross-matched with a particle record taken from a different instant of time. By locating the matched particle pair positions, the displacement between the matched particle pair positions can be obtained. The particle velocity is finally determined by dividing the displacement by the time interval between the two recordings.

The computationally intensive processing operations required to track many particles in a 3D volume restricted the development of particle tracking for practical holographic velocimetry. Relatively, few papers were published concerning holographically recorded flows with automatic particle tracking procedures after the initial developments of holographic particle measurement were made in the sixties. By the early 1990s, computer and image processing techniques had advanced sufficiently to perform most of the requirements of holographic particle studies, which led to renewed efforts by researchers to develop holographic velocimetry further. Bernel *et al.* achieved one of the first truly successful three-component, volumetric measurements with holographic particle tracking (Bernel *et al.* 1993). In their experiment two orthogonal in-line holographic recordings were used. Glass micro-balloons with a size of 15-20 micron were seeded in air and illuminated with a copper vapour laser. By using two orthogonal views, they could obtain all three displacement components with high measurement resolution. Quantitative volumetric plots of three-component velocity were displayed in their published results, which contain many hundreds of individual vectors in each plot. However, these measurements still relied on a human operator to identify the particle positions within the holographic images. Their semi-automated methods could process roughly 200 vectors per hour. Obviously, further research efforts were required to increase the processing speed and efficiency of particle tracking.

Trolinger *et al.* reported their research results taking place aboard the space shuttle in a micro-gravity environment (Trolinger *et al.* 1997). Trolinger's team used multiple holographic frames to track the volumetric time sequence of particle events. They developed an automatic procedure to locate, size, and track the particles between the sequences of holographic frames. Although the velocity measurements were somewhat sparse in number, they had successfully demonstrated an important practical 3D application of quantitative holographic particle tracking for their unique research objectives.

Holographic particle tracking methods had also been applied to the measurement of pipe flow (Chan *et al.* 1998) and 3D sprays (Feldmann *et al.* 1998).

Sheng and Meng presented a Genetic Algorithm Particle Pairing (GAPP) method for automatic particle pairing in holographic images (Sheng *et al.* 1998). They used the principles of fluid dynamics as its filtering criteria to pair a group of particles instead of statistical averaging. It was a suitable method for large velocity gradients and low particle density regions in a 3D volume. Their simulated experimental results demonstrated that GAPP had sufficient processing speed to measure 10^5 vectors per hour and was a promising practical alternative to correlation techniques for HPIV data processing.

In some instances, particle tracking has been used after correlation processing to provide “super resolution” particle velocity maps. More recently, particle tracking in PIV has been named particle tracking velocimetry (PTV) (Stitou *et al.* 2001). PTV researchers have developed some new innovative particle tracking techniques, e.g. using fuzzy logic and neural networks (<http://www.grc.nasa.gov/www/optinstr/piv/fuzzyptv.htm>). Fuzzy logic techniques utilize a rule base (flow continuity) for allowed particle displacements. Particle pairs close together must move in similar directions and must have similar displacements. Neural network techniques for data extraction rely on training the nets to identify patterns. The nets must be trained on flows similar to those that they will be used to process. These methods can also be applied for extracting the individual particle displacements in HPIV.

2.4. Intensity correlation analysis

Intensity correlation techniques in HPIV are based on the well-established correlation principles found in speckle photography and PIV. Speckle photography was originally developed to measure the surface displacement in solid mechanics (Burch *et al.* 1968). Later, the technique had been successfully applied to the measurement of fluid velocity fields and been renamed as speckle velocimetry (Dudderar *et al.* 1982; Halliwell 1982). As particles in fluid flows were illuminated by a light sheet it was noted that the image plane would contain images of individual particles. Once again the technique was re-named Particle Image Velocimetry (PIV) (Adrian 1984; Pickering *et al.* 1984) to distinguish it from speckle velocimetry.

Intensity correlation techniques produce spatially averaged velocity estimates. Each image frame reconstructed from a hologram is divided into a grid of small sections known as interrogation areas, each containing particle images. By processing the image over a regular grid of small interrogation areas, a velocity vector map is generated. There are two correlation techniques that are used to process particle images: auto-correlation and cross-correlation. In auto-correlation technique a single hologram is double-exposed. The displacements are determined by computing the auto-correlation of the interrogation areas. Figure 2-1 shows a sample input double exposure interrogation area and the resulting auto-correlation plane output. In cross-correlation, two single exposure holograms revealing the positions of tracer particles within a fluid must be recorded a short time, Δt , apart. The corresponding interrogation areas within each of the two reconstructed images are then cross-correlated. The correlation produces a signal peak, identifying the common particle displacement. Figure 2-2 shows a pair of input single exposure interrogation areas and the resulting cross-correlation output plane. By scaling this displacement by the magnification of the camera lens and dividing by Δt , an average velocity for the fluid within the interrogation area can be obtained. This process is

repeated at each grid point within the image, resulting in a map of velocity vectors to describe the flow.

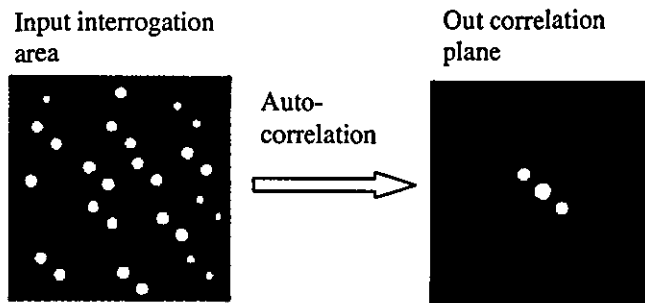


Figure 2-1 Double exposure input interrogation area and the corresponding output auto-correlation plane

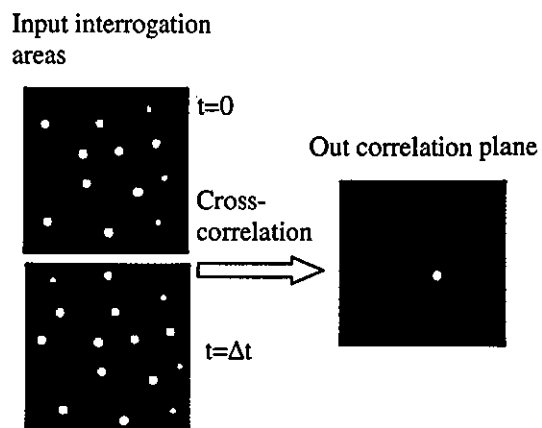


Figure 2-2 Two single exposure input interrogation areas and the corresponding output cross-correlation plane

The concept of particle image intensity correlation was extended to holographic particle measurements at the start of the nineties (Hinsch *et al.* 1990). Initially, the technique retained its 2D nature, but was extended to a light-sheet recording with off-axis holography. However, the holographic recording of light sheets had some added advantages. As a laser source with limited coherence was used, several image planes were simultaneously recorded by an off-axis hologram without adding additional image noise from the superimposed images. In doing this, Hinsch had partially extended the principles of PIV into three dimensions, but only measured two components of displacement. More importantly, the application of particle image intensity correlation techniques to holographic velocimetry made it possible, for the first time, to produce fully automatic velocity vector analysis of particle holograms (Barnhart 2001). Other researchers soon reported their initial works on intensity correlation based HPIV techniques to measure three components of displacement in 3D space. Many of the studies were based on some form of stereoscopic viewing of the particle images (Barnhart *et al.* 1993; Hinsch *et al.* 1993; Hussian *et al.* 1993; Katz *et al.* 1993), while some also considered the use of two orthogonal-view holograms (Hussian *et al.* 1993; Katz *et al.* 1993).

In 1994, Barnhart *et al.* reported a fully automatic volumetric holographic system that was capable of measuring almost a million 3C velocity vectors from a single hologram (Barnhart *et al.* 1994). The system employed a double reference beam resulting in cross-correlation image analysis. An important aspect of the system was its use of stereo-projected image-plane holographic recording combined with phase-conjugate reconstruction through the recording camera optics to cancel the optical aberrations. This requires placing everything, including the original flow medium and its window, which appeared between the particles and the hologram during the recording, back into the reconstruction system. The system employed a parallel computer that could perform the complete automatic hologram analysis within a single day (0.5 million vectors in 10 hours).

In 1995, Meng *et al.* reported a special holographic velocimetry system (Meng *et al.* 1995). The method used the in-line single-beam holographic recording with off-axis stereo viewing. Image intensity correlation was used in the hologram analysis for regions of the hologram with a sufficiently high SNR. Manual assistance particle tracking was used for regions with a low SNR, so Meng's method was not entirely automated. However, it demonstrated for the first time the in-line production of high-quality 3D velocity measurements based on image intensity correlation. The work has been further developed recently and will be discussed in detail at the end of this section.

Two years later, Zhang *et al.* reported a hybrid correlation-based HPIV system (Zhang *et al.* 1997). The holographic arrangement used two orthogonal off-axis views with forward scattering. An optical high-pass filter was introduced to remove a large portion of the background light before it reached the holographic plate. The two orthogonal-crossed holographic arrangements maximised the displacement measurement resolution. One of the special features of this technique was its method of data extraction. The holographic image volume was sampled with a series of planar slices. Each planar slice was composed of 270 image frames taken by a CCD camera. Unusually, each of the 270 image frames digitized from a slice were then patched together to form a single image. The auto-correlation method was then performed with windowed sections of the compressed image to produce the two-dimensional vector data. 800,000 final velocity vectors each for both viewing directions were obtained, which took more than 200 hours. Although this technique may have offered greater flexibility during the correlation analysis procedures, it came at the expense of a large image data storage requirement. A recent development was to modify the setup for a simpler layout (Sheng *et al.* 2001).

Meanwhile, Hinsch and Hinrichs's research group demonstrated the ability of light-in-flight HPIV technique (Hinrichs *et al.* 1997). The most important advantage of light-in-flight holography was its tolerance to image noise and its ability to isolate particle

information at different depths. This was a natural consequence of the limited coherence light source coupled with a carefully arranged recording geometry. Herrmann *et al.* reported the use of traditional 2D cross-correlation analysis in order to extract two components of velocity field data at different 3D surfaces in space (Herrmann *et al.* 2000). In later work, a 3D grey-value cross-correlation was performed on each 128x128x128 pixels-sub-volume to extract 3C-3D velocity field (Herrmann *et al.* 2002). More than 13GB of image data were scanned and 16,640 vectors were finally obtained. Due to the need to move the circular aperture over the hologram, reconstruction was a time-consuming operation, taking over 35 hours.

Lozano *et al.* reported another related HPIV effort in 1999 (Lozano *et al.* 1999). In their work, the flow illumination was directed parallel with the holographic plate and particle side-scatter was recorded by the hologram. The virtual particle image was then reconstructed by placing the recorded hologram back into the original recording system. Later on, the reconstructed virtual image was used for correlation analysis. As the double-exposed hologram was recorded with different reference wave directions, the images could be separated for cross-correlation analysis. They presented the results of 2C measurements at simultaneous, multiple planes in space. However, they did not attempt to obtain all three components of the displacement.

Recently, a Gemini off-axis HPIV system has been developed by Pu *et al.* (Pu *et al.* 2000). Their technique used two reference beams with 90° scattering particle illuminations to record the hologram, which was the same setup as Lozano's. However, reconstruction was accomplished *in situ* by placing the recorded hologram back with its orientation reversed 180° . In this case, the real particle image was created from the hologram. The reconstructed particle image was then systematically scanned at regularly spaced planar slices, to make up the 3D sub-volumes of image for further processing.

The method used by Pu *et al.* for displacement extraction was actually a novel mixture of particle intensity correlation and particle tracking. In the first stage of displacement extraction, the 3D particle centroid was calculated from the stacked image slices. Once this had been implemented, the memory-intensive stacks of particle image slices were discarded. Remaining displacement analysis was carried out with the particle centroid data. In the second stage of displacement extraction, a special type of 3D particle intensity correlation, “concise cross-correlation” (CCC), was performed. This form of intensity correlation worked directly with a subset of the particle centroid position data to extract a 3C displacement vector. After this, in the third stage, the spatial measurement resolution was increased by a repeated analysis of the particle centroid data using the correlation-derived displacement to help extract the individual particle-pair displacements. Finally, in the last stage of the displacement analysis, the randomly distributed particle-pair displacement data was mapped into a higher density, regular grid of interpolated points to make further calculations more manageable. As a consequence, the technique utilised the robust characteristics of particle intensity correlation together with the higher spatial resolution inherent in particle tracking.

This system has demonstrated a number of innovative features regarding the automatic extraction of the velocity vector that are important advancements for intensity-based holographic velocimetry. However, the authors reported that the correlation processing time for 12,000 interrogation cells took 50 hours in 1997, but also indicated that it had since been decreased to roughly 7 hours.

2.5. Optical complex amplitude auto-correlation

In this section, quantitative analysis to extract 3C-3D displacement from a hologram by the technique of complex amplitude correlation (CAC) will be examined in detail since it is fundamental to the end-product of this thesis.

2.5.1 Far-field interferometry

Traditionally, holographic interferometry has been used to measure object displacement. In this way, it is found that fringes are observed on the surface of an object if it is viewed through part of the aperture of the hologram. However, if a pin-hole is used to select a small part of the reconstructed wavefront, then curved fringes appear in the aperture of the hologram that allows 3D measurement of object displacement. This technique is called far-field interferometry (Barnhart 2001).

The development of far-field holography began in 1969 (Tsujiuchi *et al.* 1969). Their work demonstrated most of the basic principles important to far-field interferometry. However, the authors did not report any quantitative measurement results in their paper. Far-field interferometry was firstly applied to holographic particle velocity measurement in 1979 by Ewan (Ewan 1979) and was further developed by Malyak *et al.* (Malyak *et al.* 1983, 1984). In many respects, the velocity measurement research of Ewan and Malyak were the same techniques found in speckle image correlation and PIV techniques. However, it is clear that Ewan and Malyak were aware of the technique's potential for 3C velocity measurement.

Far-field interferometry offered a significant difference from intensity-based measurement techniques. Whilst these latter techniques recorded the flow photographically, with analysis of the intensity information, far-field interferometry was the only method that directly recorded the scattered phase information from the particles as well. Nevertheless, all of the previous researchers of far-field interferometry had

clearly not utilized this unusual asset, which could have directly provided all three components of the displacement.

In 1986, Vlad *et al* reported their attempts at using far-field interferometry for quantitative 3C displacement measurement (Vlad *et al.* 1986). They used an off-axis holographic recording system for solid displacement measurement. A personal computer was used to automate the process, which included digital quantitative displacement analysis of the far-field interference fringes. Although the paper discussed the quadratic phase of the holographic wavefronts (that will be shown to be an indication of out-of-plane displacement), the paper only presented in-plane displacement measurements.

In 1997, Amara *et al.* published a paper concerning data extraction in far-field interferometry (Amara *et al.* 1997). A pinhole aperture was employed and placed in the reconstructed real image of the flow that was followed by a Fourier-transform lens. The far-field fringes were then projected onto a CCD camera sensor. The fringes were subsequently digitally analysed to extract three components of displacement. The reported quantitative measurements indicated a relatively poor displacement accuracy, which was shown to depend on the numerical aperture (NA) of the system. However, far-field interferometry appeared to be a promising technique for 3C displacement measurement.

2.5.2 Optical complex amplitude auto-correlation

In the last section, research on far-field interferometry was reviewed. Some of the researchers were content with 2C measurements of displacement. Others simply gave up trying to extract the out-of-plane displacement. Obviously, there has been a consistent barrier toward 3C quantitative analysis of the far-field fringes (Barnhart 2001). The problem is that traditional quantitative techniques have never been very comfortable in the analysis of circular fringes. In particular, the direct measurement of fringe curvature has always been a source of trouble. However, such analysis was precisely required for the extraction of the out-of-plane displacement.

Coupland and Halliwell recognised that fringe curvature could be measured easily by an optical Fourier transformation of the far-field fringe intensity profile. An optical complex amplitude correlation method was initially reported by them for 3C displacement extraction in 1992 (Coupland *et al.* 1992). In their method, a double-exposed hologram was used to record the particle field. The optically reconstructed real image was sampled using a small aperture, which effectively selected a small volume in the particle image field. The first-exposed optical wavefront and its shifted counterpart (second-exposed optical wavefront) emanating from the aperture were correlated in amplitude and phase by the optical Fourier transformation of the far-field fringe intensity profile (details will be given in Chapter 3). The output of complex amplitude auto-correlation was an optical field that appeared to contain three correlation peaks positioned along a line in 3D space. The central peak was a zero-order peak. Relative to the position of the central peak, two first-order peaks were situated at positions equal to the particle displacement. So it was possible to measure the full three components of velocity by locating the positions of these peaks in 3D correlation space.

There were two advantages in using optical complex amplitude correlation method. First, aberrations within the reconstructed image field no longer affected the displacement measurement accuracy (Coupland *et al.* 1997). They observed that the image of particles could be virtually lost through optical distortion but accurate particle displacement could still be extracted. The other was that for the first time the measurement of displacement in solid and fluid mechanics were no longer treated as separate items (Barnhart 2001).

Following the proposals of Coupland *et al.*, Barnhart *et al.* reported a new method, named “object-conjugate reconstruction (OCR)”, that allows an image shift to be included in a convenient manner (Barnhart *et al.* 2000). The experimental techniques of OCR combined with optical complex amplitude correlation are explained below and shown schematically in Figure 2-3 and Figure 2-4 (Barnhart 2001). The theory of complex amplitude correlation will be discussed in Chapter 3.

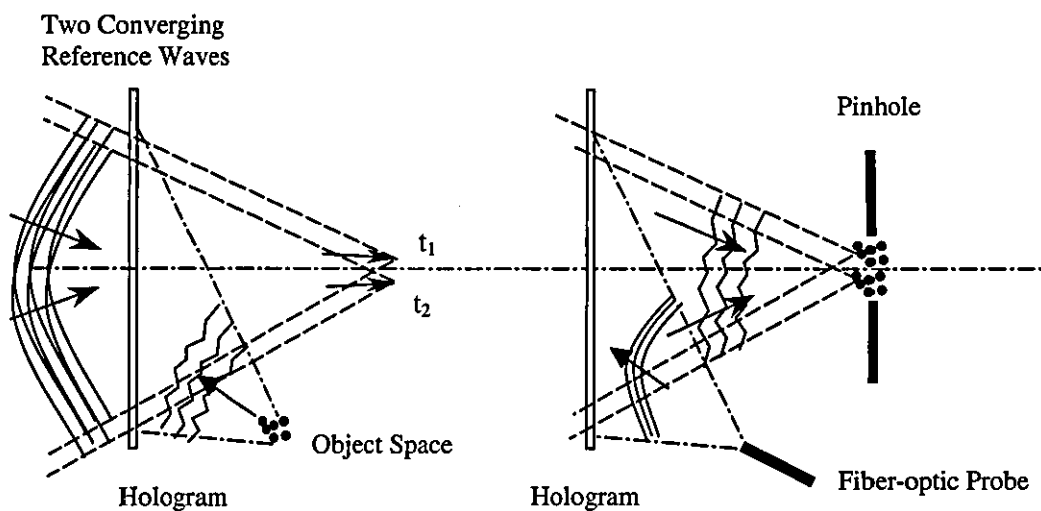


Figure 2-3 (a) Recording of hologram (b) Object-conjugate reconstruction of hologram

First of all, a double-exposure hologram is recorded by using two identical but laterally displaced converging reference waves at two different time instants, t_1 and t_2 (Figure 2-3 (a)). The object image is then reconstructed using a diverging wave from a fibre-optic probe, which is placed in the original object space (Figure 2-3 (b)). This OCR configuration generates an image of the object space at two fixed points in space. These two fixed points are defined by the two previous points of focus of the recording reference beams. Analogous to methods used in planar PIV (Adrian 1986), the resulting reconstruction introduces a constant shift between exposures that provides a known bias displacement. This image shift not only resolves directional ambiguity of the object displacement, but also is essential to successful use of complex amplitude correlation if the object displacement is purely in the z (longitudinal) direction (Barnhart 2001).

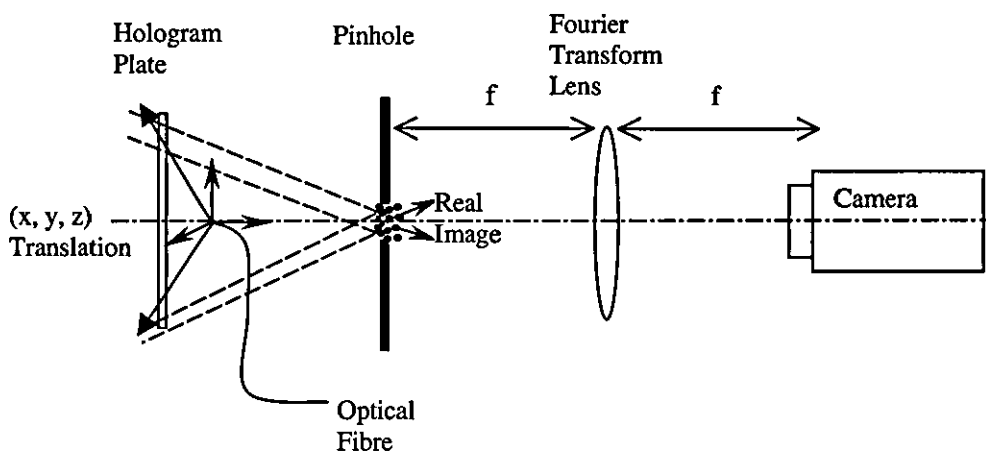


Figure 2-4 Reconstruction geometry with fibre optic illumination probe

Data extraction from an OCR hologram is shown in Figure 2-4. An optical fibre, which is mounted on a three-axis motorized translation stage and placed in the object volume, re-illuminates the recorded hologram. The two displaced, real images are produced in the space surrounding the focal points of the original recording reference beams. A stationary pinhole aperture is placed in the region surrounding the focal points of the reference waves, followed by a Fourier transform lens and the camera. After the far-field fringes in the focal plane of the lens are digitized, the optical fibre is stepped through the object space of interest, progressively sampling at selected points in space. A significant advantage of this configuration is that the pinhole-lens-camera system remains fixed, while the lightweight, movable optical fibre position determines the sample measurement coordinates (Barnhart *et al.* 2002).

After optical Fourier transformation of the sampled real image, the camera detects the 2D power spectrum of the complex field emanating from the aperture. Finally, each sampled spatial power spectrum contains the necessary information to make a single 3C displacement measurement (Coupland *et al.* 1992). In its original form, optical correlation was demonstrated by using photographic film as a spatial light modulator. Later, a liquid crystal television was used in a purpose built processor (Barnhart 2001). The results clearly demonstrated that 3C fluid velocity data can be retrieved by using complex amplitude correlation.

2.6. Digital HPIV

Although film-based HPIV is now reasonably mature it has only been adopted by a few research establishments because it is not user-friendly. The price of any gain in axial accuracy or information capacity of the holographic measurement is generally accompanied by an increase in system complexity; thus this technique becomes less attractive to general users (Meng *et al.* 2004). The newly emerged digital HPIV promises to revolutionize flow measurement and become a practical 3D velocimetry tool. By replacing the holographic film with a digital camera, digital HPIV is likely to make holographic particle imaging a routine technique in much the same way as digital PIV had brought the PIV into widespread use a decade ago.

Digital HPIV has become feasible as CCD cameras of sufficient resolution and sufficiently fast computers have become available. The holograms are recorded directly by the CCD and stored digitally. No film material involving wet-chemical or other processing is necessary. The reconstruction of the wave field, which is usually achieved optically by illumination of a conventional hologram, is performed by numerical methods. In addition to simplifying the HPIV operation, digital HPIV also expands the capability of the HPIV technique:

- (1) In the numerical reconstruction process not only the intensity, but also the phase distribution of the stored wave field can be computed from the digital hologram. This makes complex amplitude correlation for data extraction a method of choice.
- (2) Digital holograms can be pre-processed to remove noise and aberrations caused by any imperfect recording condition.
- (3) Digital HPIV is truly a 4D velocimetry technique with the cinematic recording capability of digital image sensors (Meng *et al.* 2004).

Numerical hologram reconstruction was initiated in the early 1970s (Kronrod *et al.* 1972). They sampled magnified parts of in-line and Fourier holograms recorded on a photographic plate. These digitized holograms were then reconstructed numerically. Some researchers improved the reconstruction algorithm and applied this method to particle measurement (Liu *et al.* 1987; Onural *et al.* 1987).

A digitally recorded off-axis hologram was first presented using a Kodak Megapixel CCD camera (Schnars *et al.* 1994). The original purpose of this publication was to produce a qualitative proof-of-principle test that demonstrated the technical capability of making digitally recorded off-axis holograms and then numerically constructing an image from the stored fringe pattern. Later, researchers have also reported the use of digital techniques to suppress the dc term and eliminate the twin-image in digital in-line holography (Kreis *et al.* 1997; Takaki *et al.* 1999; Cuhe *et al.* 2000).

Interesting research using a CCD camera-based digital in-line holography for flow measurements has been reported by Skarman *et al.* (Skarman *et al.* 1996; Skarman *et al.* 1999). Instead of relying on the unscattered light for its reference beam, an in-line, phase-shifted reference beam was introduced via a beam-splitter inserted between the object space and the CCD camera. After digital recording, the holographic image was numerically reconstructed to find the particle positions and velocities. The research group succeeded in experimentally demonstrating fully automated particle tracking analysis from the numerically reconstructed hologram. Although the technique was limited to small experimental volumes with relatively low numbers of particles, the effectiveness and practicability of this technique was demonstrated for automated particle velocimetry.

More recently, Meng's research group (Meng *et al.* 2004) has developed two digital HPIV systems, which are named "single-beam in-line holography with forward scattering" and "dual-beam in-line holography with 90° scattering", respectively. A 12-bit cooled CCD camera (PCO SensiCam with 1280x1024 6.7 μ m pixels) is used as the

hologram recording medium. In these digital in-line HPIV systems, the depth-of-focus problem has been effectively overcome by a novel method called particle extraction using complex amplitude (PECA). Instead of relying on the intensity image, they also make use of the complex amplitude of the reconstruction wave, which is easily accessible in numerical reconstruction. It has been found that the variance of the imaginary part of the reconstruction wave has a dipping characteristic along the depth direction, and it is minimised at the particle location. The PECA method utilizes this unique feature to extract the particle depth location. Axial accuracy of about two particle diameters can be achieved with the PECA method in spite of the extremely small numerical aperture of the digital holograms. For the velocity extraction they use a particle matching algorithm which operates on the particles' 3D coordinate data (Stellmacher *et al.* 2000).

Other researchers have also been actively looking for alternative recording materials which do not require chemical processing but still satisfy HPIV's stringent light sensitivity and spatial resolution requirements. Recently, Bacteriorhodopsin (Barnhart *et al.* 2002; Chan 2003), a type of photochromic material, has been identified as a promising replacement for silver halide films and is being used in HPIV.

The major difference between digital HPIV and film-based HPIV is the inferiority of the electronic image sensor in terms of the pixel resolution and the image format. An ideal image sensor for holographic recording in HPIV should have a comparable resolution and dimensions to those of silver halide films. However, there are still huge technological barriers to making such sensors in the foreseeable future. Besides, it would also be a formidable task to handle the images acquired by such sensors in a digital environment. With the current CCD technology, the resolution of electronic image sensors is about $100lp/mm$, which is at least one order of magnitude lower than those of holographic films. Although the spatial resolution of image sensors may never match that of silver halide films, the frame size of the image sensors is quickly approaching $35mm$ films. When such

a sensor becomes available, even moderate pixel sizes ($\sim 4\mu m$) will be sufficient to make digital HPIV a strong contender for 3D flow measurements.

2.7. Summary

Previous work on HPIV data extraction has been examined in the sections 2.3, 2.4 and 2.5. Clearly complex amplitude correlation using optical processing is attractive for 3D-3D velocity measurement. Although this technique is theoretically very robust, in practice it is limited by the performance of spatial light modulators and the speed of the mechanical devices used to search the correlation output field. With the increasing power of modern desktop computers and image processing technology, complex amplitude correlation has the potential to be implemented efficiently in a digital environment. This is the main research objective of this thesis, which is explained in Chapter 3 and 4 in detail.

The literature review presented here shows that digital HPIV is an important new direction in fluid dynamic research. In Chapter 5, a digital μ HPIV system that utilises lenses to improve the recording resolution is discussed and applied in the measurement of free jet flow in a micro-channel.

2.8. References

Adrian, R. J., 1984, "Scattering particle characteristics and their effect on pulsed laser measurements of fluid flow: speckle velocimetry vs particle image velocimetry", *Applied Optics*, vol.23, p1690.

Adrian, R. J., 1986, "Image shifting technique to resolve directional ambiguity in double-pulsed velocimetry", *Applied Optics*, vol.25, p3855-3858.

- Amara, M. K. and Bzkul, C., 1997, "Holographic particle image velocimetry: simultaneous recording of several light sheets by coherence encoding in a photorefractive crystal", *Journal of Optics*, vol. 28(4), p173-180.
- Barnhart, D. H., 2001, Whole-field holographic measurements of three-dimensional displacement in solid and fluid mechanics, PhD thesis, Loughborough University, UK.
- Barnhart, D. H., Adrian, R. J. and Papen, G. C., 1994, "Phase-conjugate holographic system for high-resolution particle-image velocimetry", *Applied Optics*, vol.133(30), p7159-7170.
- Barnhart, D. H., Halliwell, N. A. and Coupland, J. M., 2000, "Holographic particle image velocimetry: analysis using a conjugate reconstruction geometry", *Optics & Laser Technology*, vol.32, p527-533.
- Barnhart, D. H., Hampf, N., Halliwell, N. A. and Coupland, J. M., 2002, "Digital holographic velocimetry with bacteriorhodopsin (BR) for real-time recording and numerical reconstruction", 11th International Symposium on Application of Laser Techniques to Fluid Mechanics, Lisbon, Portugal.
- Barnhart, D. H., Papen, G. C. and Adrian, R. J., 1993, "Phase conjugate image reconstruction for HPIV systems", *Holographic Particle Image Velocimetry ASME*.
- Bernel, L. P. and Scherer, J., 1993, "HPIV measurements in vortical flows: lessons learned and future prospects", *Holographic Particle Image Velocimetry ASME*.
- Burch, J. M. and Tokarski, J. M. J., 1968, "Production of multiple beam fringes from photographic scatterers", *Optica Acta*, vol.115(2), p101-111.
- Chan, K. T. and Li, Y. J., 1998, "Pipe flow measurement by using a side-scattering holographic particle imaging technique", *Optics and Laser Technology*, vol.130, p7-14.

- Chan, V. S. S., 2003, "Application of holography to fluid flow measurement using Bacteriorhodopsin (BR)", International Workshop on Holographic Metrology in Fluid Mechanics, Loughborough, UK.
- Coupland, J. M. and Halliwell, N. A., 1992, "Particle image velocimetry: three-dimensional fluid velocity measurements using holographic recording and optical correlation", *Applied Optics*, vol.131(8), p1005-1007.
- Coupland, J. M. and Halliwell, N. A., 1997, "Holographic displacement measurements in fluid and solid mechanics: immunity to aberrations by optical correlation processing", *Proceedings of the Royal Society A*, 453, London.
- Cuche, E., Marguet, P. and Depeursinge, C., 2000, "Spatial filtering for zero-order and twin-image elimination in digital off-axis holography", *Applied Optics*, vol.39(23), p4070-4075.
- Dudderar, T. D. and Simpkins, P. G., 1982, "The development of scattered light metrology", *Optical Engineering*, vol.21(3), p396-399.
- Ewan, B. C. R., 1979, "Holographic particle velocity measurement in the Fraunhofer plane", *Applied Optics*, vol.118(5), p623-626.
- Feldmann, O., Mayninger, H. H. F. and Gebhard, P., 1998, "Evaluation of pulsed laser holograms of flashing sprays by digital image processing and holographic particle image velocimetry", *Nuclear Engineering and Design*, vol.1184, p239-252.
- Halliwell, N. A., 1982, *Laser Speckle and Holographic Techniques for Flow Visualization*, Memorandum No 626, Institute of Sound and Vibration Research, University of Southampton.
- Hermann, S. F. and Hinsch, K. D., 2002, "Light-in-flight holographic PIV for wind-tunnel applications", *Proceedings of the International Workshop on Holographic Metrology in Fluid Mechanics*, Loughborough, UK.

Herrmann, S. F., Geiger, M., Hinsch, K. D. and Peinke, J., 2000, "Light-in-flight holography with switched reference beams for cross-correlation in deep volume PIV", 10th International Symposium on Applications of Laser Techniques to Fluid Mechanics, Lisbon.

Hinrichs, H., Hinsch, K. D., Kickstein, J. and Bohmer, M., 1997, "Light-in flight holography for visualization and velocimetry in three-dimensional flow", *Optics Letters*, vol.122(11), p828-830.

Hinsch, K. D., Hinrichs, H., Kuhfahl, G. and P. Meinlschmidt, 1990, "Holographic recording of 3-D flow configurations for Particle Image Velocimetry (PIV)", *ICALEO*, vol.12, p121-130.

Hinsch, K. D., Hinrichs, H., Roshop, A. and Dreesen, F., 1993, "Holographic and stereoscopic advances in 3-D PIV", *Holographic Particle Image Velocimetry ASME*, vol.148, p33-36.

Hussian, F., Liu, D. D., Simmons, S. S. and Meng, H., 1993, "Holographic Particle Velocimetry: prospects and limitations", *Holographic Particle Image Velocimetry ASME*, vol.148, p1-11.

Katz, J. and Ni, H., 1993, "Problems and solutions associated with utilization of holography for three dimensional velocity measurements", *Holographic Particle Image Velocimetry ASME*, vol.148, p51-56.

Kreis, T. M. and Jtiptner, W. P. P., 1997, "Suppression of the dc term in digital holography", *Optical Engineering*, vol.136, p2357-2360.

Kronrod, M. A. and Yaroslavskii, L. P., 1972, "Reconstruction of holograms with a computer", *Sov. Phys.-Tech. Phys.*, vol.17, p333-334.

Liu, G. and Scott, P. D., 1987, "Phase retrieval and twin-image elimination for in-line Fresnel holograms", *Journal of the Optical Society of America*, vol.4(1), p159-165.

- Lozano, A., Kostas, J. and Soria, J., 1999, "Use of holography in particle image velocimetry measurements of a swirling flow", *Experiments in Fluids*, vol.127, p251-261.
- Malyak, P. H. and Thompson, B. J., 1983, "Particle velocity measurement using holographic methods", *Proceedings of SPIE*, vol.427, p172-179.
- Malyak, P. H. and Thompson, B. J., 1984, "Particle displacement and velocity measurement using holography", *Optical Engineering*, vol.123(5), p567-576.
- Meng, H., Anderson, W. L., Hussain, F. and Liu, D. D., 1993, "Intrinsic speckle noise in in-line particle holography", *Journal of the Optical Society of America A (Optics and Image Science)*, vol.10(9), p2046-2058.
- Meng, H. and Hussain, F., 1995, "In-line recording and off-axis viewing technique for holographic particle image velocimetry", *Applied Optics*, vol.134(11), p1827-1840.
- Meng, H., Pan, G., Pu, Y. and Woodward, S. H., 2004, "Holographic particle image velocimetry: from film to digital recording", *Measurement Science and Technology*, vol.15, p673-685.
- Onural, L. and Scott, P. D., 1987, "Digital decoding of in-line holograms", *Optical Engineering*, vol.126(11), p1124-1132.
- Pickering, C. J. D. and Halliwell, N. A., 1984, "Speckle photography in fluid flows: signal recovery with a two-step processing", *Applied Optics*, vol.23, p1128-1129.
- Pu, Y. and Meng, H., 2000, "An advanced off-axis holographic particle image velocimetry (HPIV) system", *Experiments in Fluids*, vol.29, p184-197.
- Schnars, U. and Jtjptner, W., 1994, "Direct recording of holograms by a CCD target and numerical reconstruction", *Applied Optics*, vol.133(2), p179-181.
- Sheng, J., Malkiel, E. and Katz, J., 2001, "One beam two view holographic particle image velocimetry system (CD-Rom)", *Proceedings of 4th International Symposium on Particle Image Velocimetry*, Gottingen.

Sheng, J. and Meng, H., 1998, "A genetic algorithm particle pairing technique for 3D velocity field extraction in holographic particle image velocimetry", *Experiments in Fluids*, vol.12, p461-473.

Skarman, B., Becker, J. and Wozniak, K., 1996, "Simultaneous 3D-PIV and temperature measurements using a new CCD-based holographic interferometer", *Flow Measurement and Instrumentation*, vol.7, p1-6.

Skarman, B., Wozniak, K. and Becker, J., 1999, "Digital in-line holography for the analysis of Benard convection", *Flow Measurement and Instrumentation*, vol.110, p91-97.

Stellmacher, M. and Obermayer, K., 2000, "A new particle tracking algorithm based on deterministic annealing and alternative distance measures", *Experiment in Fluids*, vol.28, p506-518.

Stitou, A. and Riethmuller, M. L., 2001, "Extension of PIV to super resolution using PTV", *Measurement Science and Technology*, vol.12, p1398-1403.

Takaki, Y., Kawai, H. and Ohzu, H., 1999, "Hybrid holographic microscopy free of conjugate and zero-order images", *Applied Optics*, vol.38, p4990-4996.

Trolinger, J. D., Belz, R. A. and Farmer, W. M., 1969, "Holographic techniques for the study of dynamic particle fields", *Applied Optics*, vol.8(5), p957-960.

Trolinger, J. D., Rottenkolber, M. and Elandaloussi, F., 1997, "Development and application of particle image velocimetry techniques for microgravity applications", *Measurement Science and Technology*, vol.8, p1573-1583.

Tsujiuchi, J., Takeya, N. and K. Matsuda, 1969, "Mesure de la deformation d'un objet par interferometrie holographique", *Optica Acta*, vol.16(6), p709-722.

Vlad, V. I., Popa, D. and Solomon, S., 1986, "Hybrid holographic-digital processing system for three-dimensional displacement measurement", SPIE Proceedings, vol.1700, p344-351.

Zhang, J., Tao, H. and Katz, J., 1997, "Turbulent flow measurement in a square duct with hybrid holographic PIV", Experiments in Fluids, vol.123, p373-381.

Chapter 3 : Theoretical Background of Complex Amplitude Correlation

3.1. Introduction

The purpose of this chapter is to introduce the basic principles and theory that are used in this thesis to describe holographic three-component (3C) displacement measurement. Section 3.2 re-examines three-dimensional (3D) complex amplitude correlation (CAC) measurement analysis mathematically. Using a formulation of scalar diffraction in 3D vector space, it is shown, for the first time, that 3D-CAC provides a field that is the exact correlation of the propagating fields that are the reconstruction of the first and second exposure images. Section 3.3 explains the implementation of 3D-CAC digitally and shows some results simulated in MatLab. Discussion of more specific development, application and results will be left to the remaining chapters. However, the efforts detailed in the remainder of this thesis are all based on the basic principles introduced here.

3.2. 3D complex amplitude correlation

As reviewed in chapter 2, optical complex amplitude correlation analysis was introduced by Coupland and Halliwell, and uses the complex amplitude of the reconstruction wave that was uniquely available in HPIV (Coupland *et al.* 1992). In the following analysis the monochromatic, scalar diffraction theory of Fourier Optics (Goodman 1996) is used to derive an expression for the complex amplitude of a wavefront at the sampled volume region centred on the middle of the aperture (shown in Figure 2-4). For the first time, this is presented as a full 3D analysis using wave-vector notation. As will be seen, if the

complex field distribution of a monochromatic disturbance is Fourier-analyzed throughout the space, the various spatial Fourier components can be identified as plane waves travelling in different directions away from that region. Since the numerical aperture of the hologram is large, the optical field in three dimensions is considered using a wave-vector notation.

Let the complex field at a position vector $\mathbf{r}=(r_x, r_y, r_z)$ be represented by $U(\mathbf{r})$. Accordingly, $U(\mathbf{r})$ can be decomposed into its spectrum of plane-wave components $S(\mathbf{k})$ defined by the 3D Fourier transformation,

$$S(\mathbf{k}) = \int_{-\infty}^{+\infty} U(\mathbf{r}) \exp(-2\pi j \mathbf{k} \cdot \mathbf{r}) d\mathbf{r} \quad (3-1)$$

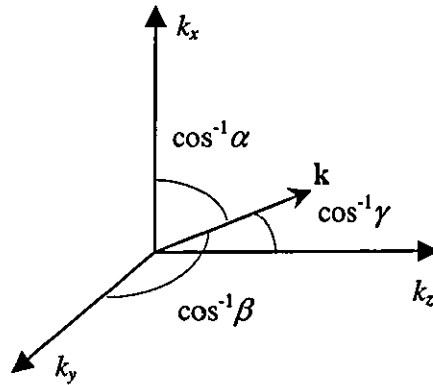
where wave vector $\mathbf{k}=(k_x, k_y, k_z)$ and $d\mathbf{r}$ conventionally denotes the scalar quantity $dr_x dr_y dr_z$. Clearly the field at any point in space can be found by inverse Fourier transformation of its spectrum, and is defined as,

$$U(\mathbf{r}) = \int_{-\infty}^{+\infty} S(\mathbf{k}) \exp(2\pi j \mathbf{k} \cdot \mathbf{r}) d\mathbf{k} \quad (3-2)$$

With reference to Equation (3-1), it is noted that the equation for a unit-amplitude plane wave $B(\mathbf{r})$ propagating with direction cosines (α, β, γ) (as illustrated in Figure 3-1), relative to an origin at the centre of the aperture, is given by

$$B(\mathbf{r}) = \exp\left[\frac{2\pi j}{\lambda} (\alpha r_x + \beta r_y + \gamma r_z)\right] \quad (3-3)$$

Note that the direction cosines are interrelated through $\gamma = \sqrt{1 - \alpha^2 - \beta^2}$ and λ is the wavelength. Thus $S(\mathbf{k})$ can be regarded as a decomposition of the optical field $U(\mathbf{r})$ into plane waves each propagating with direction cosines (α, β, λ) given by

Figure 3-1 The wave vector \mathbf{k}

$$\alpha = \lambda k_x, \beta = \lambda k_y, \gamma = \lambda k_z \quad (3-4)$$

and

$$|\mathbf{k}|^2 = 1/\lambda^2 \quad (3-5)$$

In this way any monochromatic optical field propagating in a linear isotropic homogeneous medium (LIH) can be decomposed into a plane wave spectrum in wave-vector space that is defined on the surface of a sphere of radius $1/\lambda$, shown in Figure 3-2. In the analogous study of periodic structures in solid state physics this sphere is usually referred to as the Ewald sphere (Ashcroft et al., 1976).

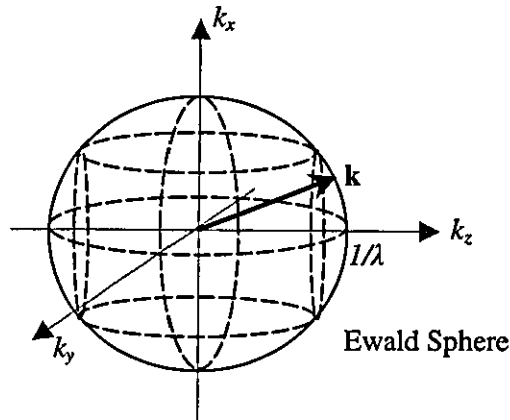


Figure 3-2 Ewald Sphere

The complex amplitude of each plane wave component is given by $S(\mathbf{k})d\mathbf{k}$ evaluated at $k_x = \alpha/\lambda$, $k_y = \beta/\lambda$ and $k_z = \gamma/\lambda$. Finally note that the power spectral density, $P(\mathbf{k})$, is defined as

$$P(\mathbf{k}) = |S(\mathbf{k})|^2 \quad (3-6)$$

Using this approach, the optical field transmitted by the sampling aperture $U(\mathbf{r})$ can be written as the sum of the reconstructed fields, so that

$$U(\mathbf{r}) = U_1(\mathbf{r}) + U_2(\mathbf{r}) \quad (3-7)$$

where $U_1(\mathbf{r})$ and $U_2(\mathbf{r})$ represent the complex wavefields which correspond to the images of the seeding particles formed in the aperture at the times of the first and second exposures respectively. For mathematical simplicity the windowing effect of the aperture itself is neglected. If it is assumed that the particle images move in unison a distance \mathbf{s} between exposures, the second exposure field $U_2(\mathbf{r})$ is identical to $U_1(\mathbf{r})$ but shifted by \mathbf{s} , such that,

$$U_2(\mathbf{r}) = \exp(j\varphi)U_1(\mathbf{r}-\mathbf{s}) \quad (3-8)$$

and

$$U(\mathbf{r}) = U_1(\mathbf{r}) + \exp(j\varphi)U_1(\mathbf{r}-\mathbf{s}) \quad (3-9)$$

where φ , the phase difference between the field illuminating the particle at the times of the first and second exposures respectively, is a function of the displacement vector \mathbf{s} . It is noted that any additional image-shift (for ambiguity removal) can be included in the object displacement. In this way, the spectrum defined by Equation (3-1) is given by

$$S(\mathbf{k}) = \int_{-\infty}^{+\infty} [U_1(\mathbf{r}) + \exp(j\varphi)U_1(\mathbf{r}-\mathbf{s})] \exp(-2\pi j\mathbf{k}\cdot\mathbf{r}) d\mathbf{r} \quad (3-10)$$

Substituting this equation in Equation (3-6) and using the Fourier shift theorem, the power spectral density $P(\mathbf{k})$ of the optical field $U(\mathbf{r})$ transmitted by the sampling aperture can be written

$$\begin{aligned} P(\mathbf{k}) &= \left| \int_{-\infty}^{+\infty} U(\mathbf{r}) \exp(-2\pi j\mathbf{k}\cdot\mathbf{r}) d\mathbf{r} \right|^2 \\ &= 2P_1(\mathbf{k})[1 + \cos(2\pi\mathbf{k}\cdot\mathbf{s} - \varphi)] \end{aligned} \quad (3-11)$$

where $P_1(\mathbf{k})$ is the power spectral density corresponding to the first exposure image. This equation can be interpreted in general as a set of curved fringes that modulate the power spectral density of the optical field produced by the distribution of scattering particles.

Using vector notation and the autocorrelation theorem, the autocorrelation field, $R(\mathbf{r})$, is given by the inverse Fourier transformation of the power spectral density distribution such that,

$$\begin{aligned}
 R(\mathbf{r}) &= \int_{-\infty}^{+\infty} P(\mathbf{k}) \exp(2\pi j \mathbf{k} \cdot \mathbf{r}) d\mathbf{k} \\
 &= R_1(\mathbf{r}) \otimes [2\delta(\mathbf{r}) + \exp(j\varphi) \delta(\mathbf{r} - \mathbf{s}) + \exp(-j\varphi) \delta(\mathbf{r} + \mathbf{s})]
 \end{aligned} \tag{3-12}$$

where $R_1(\mathbf{r})$ is the autocorrelation of the optical field describing the first (and second) exposure images, \otimes denotes convolution and δ is the Dirac delta function. $R_1(\mathbf{r})$ consists of a peak at the origin with a magnitude proportional to the sum of the scattered intensity from each particle and noise resulting from uncorrelated particle images. With reference to Equation 3-12, the intensity distribution in the output space of the autocorrelation consists of three dominant peaks as shown in Figure 3-3. The first term is the self-correlation of the double exposure record. Relative to the position of the first term peak, the second and third term peaks are situated at positions equal to plus and minus the particle displacement. In this way, the particle image displacement can be found by searching the correlation field for the highest intensity peak. Original work in this area used optical methods to produce an optical field proportional to the 3D correlation of the transmitted field and searched the correlation field for the brightest point (Coupland et al., 1992). Clearly, if the complex amplitude $U(\mathbf{r})$ or the power spectrum $P(\mathbf{k})$ is known numerically, the 3D correlation can be calculated digitally. The following Section will explain the implementation of this 3D-CAC process analysis digitally in a step-by-step manner.

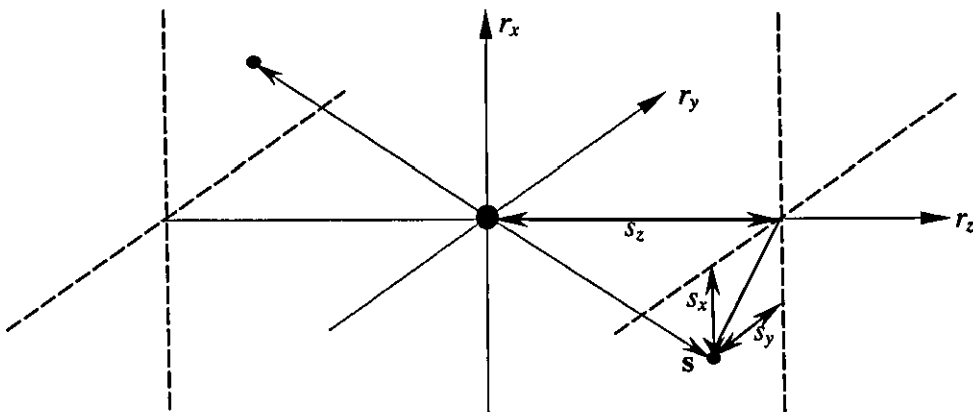


Figure 3-3 3D complex amplitude auto-correlation output

3.3. Digital 3D complex amplitude correlation

The 3D-CAC analysis outlined above describes complex HPIV analysis in a concise mathematical manner; it does, however, give a rather pessimistic impression of the computation required. Since, in k -space, monochromatic fields are represented purely by the 2D surface of the Ewald sphere, the superposition integral of Equation (3-2) reduces to a 2D surface integral. In this way, a field with no counter-propagating plane wave components (i.e., forward propagating) is represented by a half sphere in k -space and can be defined unambiguously by the projection of its wave vector components in a (CCD camera) plane. For example, a field that is propagating at an angle to the z axis is entirely described by its k_x and k_y components. This is what is measured by digitizing the power spectrum that is viewed in the far focal plane of a convex lens. In order to implement 3D-CAC, this measurement needs to be related to the power spectrum specified on the surface of the Ewald sphere.

As the wave vector components in k -space are interrelated through Equation(3-5), the far-field fringe pattern distribution, described by its k_x and k_y wave vector components in a plane, can in effect be projected back onto the surface of the half Ewald sphere to give the power spectrum $P(\mathbf{k})$ as shown in Figure 3-4. This is the key step in digital complex amplitude correlation analysis. This part of the 3D power spectrum distribution is then used to compute the 3D autocorrelation by the 3D inverse fast Fourier transformation to give the correlation illustrated in Figure 3-3.

The following digital procedure involves an iterative search through the complex-correlation space to determine the accurate 3D position of the correlation peak. When the correlation peak covers more than one pixel, its location can be determined at sub-pixel level by interpolation. Two interpolation methods that are frequently used are the peak centroid analysis and the Gaussian curve fitting. The centroid estimator is based on the fact that the centroid of a symmetric object is equal to the position of the object. The

Gaussian peak fit is based on the notion that the displacement-correlation peak has an approximately Gaussian shape. Despite the differences in behaviour, the two estimators are quite similar (Westerweel 1997).

Overall digital 3D-CAC is composed of the four main steps as shown in Figure 3-5. A computer program has been written in MatLab in order to implement the procedure presented above. More details about the computational efficiency and accuracy of the digital 3D-CAC will be discussed in Chapter 4. The program has also been used to compute the 3C displacement in μ HPIV described in Chapter 5.

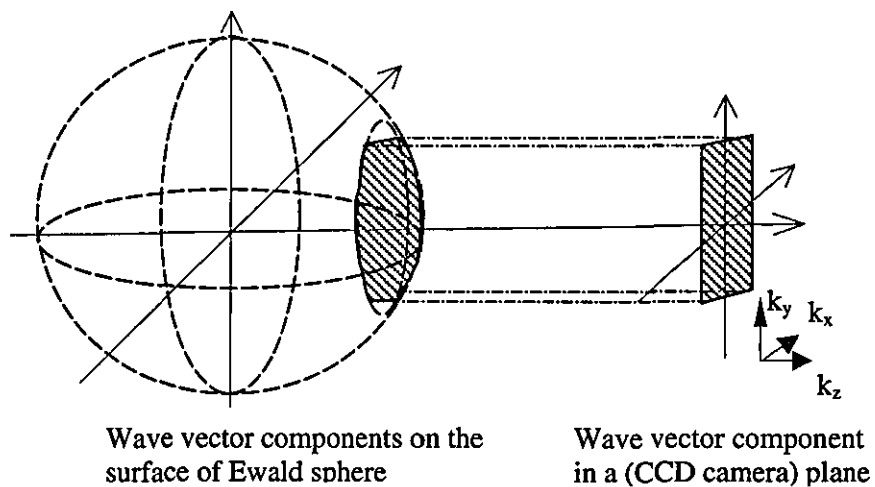


Figure 3-4 k-space mapping

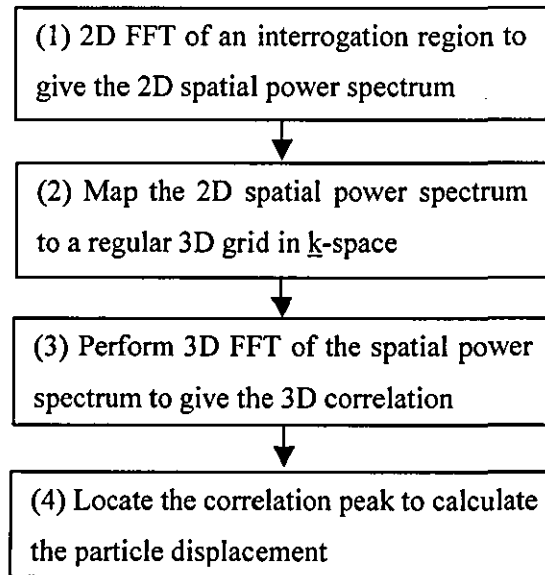


Figure 3-5 Flow chart of digital 3D-CAC

3.4. Summary

The method of 3D complex amplitude correlation presented in this chapter provides a mathematical basis that is exploited in the remaining chapters. The method manipulates both the phase and the amplitude of the recorded signal and because of this it is inherently immune to imaging aberration (Coupland *et al.* 1996). The digital implementation of the method has been discussed. However, 3D fast Fourier transformation (as well as 3D peak searching) is computationally intensive. For a typical fringe pattern digitized to a 256x256 pixels resolution it requires approximately 400M floating-point operations using 3D FFT methods and it may take many days to extract the data from a holographic record using current desktop computers. Therefore, the basic approaches presented here must be modified in practice for successful application. A new method of analysis has been considered and is introduced in Chapter 4.

The main contribution of this chapter is the definition of the 3D complex amplitude correlation using a formulation of scalar diffraction in 3D vector space.

3.5. References

Coupland, J. M. and Halliwell, N. A., 1992, "Particle image velocimetry: three-dimensional fluid velocity measurements using holographic recording and optical correlation", *Applied Optics*, vol.131(8), p1005-1007.

Coupland, J. M. and Halliwell, N. A., 1996, "Holographic particle image velocimetry: immunity from aberration by optical information processing", *Proceeding of IMechE.*, City University, London, UK.

Goodman, J. W., 1996, *Introduction to Fourier Optics*. New York, McGraw-Hill.

Westerweel, J., 1997, "Fundamentals of digital particle image velocimetry", *Measurement Science and Technology*, vol.8, p1379-1392.

Chapter 4 : Digital Shearing Method

4.1 Introduction

In this chapter a new digital method is introduced to extract the 3C-3D particle displacement data from a hologram. The method is based on far-field interferometry and complex amplitude correlation (CAC) (Coupland *et al.* 1992). By analogy with similar techniques in classical interferometry, this technique is named the *digital shearing method*. Section 4.2 explains the basic principle and presents the formulation derived from CAC. Like optical correlation analysis, it is inherently immune to image aberration. However, digital shearing is not a direct digital implementation of optical correlation and a considerable saving in computation time results. Section 4.3 demonstrates the power of the method by MatLab simulation and discusses its performance with reference to optical analysis. Comparison of the accuracy and computational efficiency of digital shearing and digital 3D-CAC method is presented in Section 4.4. The simulated results show that the digital shearing method has comparable accuracy to digital 3D correlation but is significantly faster and more memory efficient. Experiments have been performed to demonstrate the implementation of the theory, which are described in section 4.5. Finally Section 4.6 gives a summary of the digital shearing method.

4.2 Theory of digital shearing method

Optical and digital methods have been introduced to implement CAC in previous chapters. Although CAC is theoretically the most robust method to locate spatial repetition in a signal, when applied optically, it is limited by the performance of spatial light modulators

and the speed of the mechanical devices used to search the output field (Barnhart 2001). 3D-CAC can be calculated digitally, however, this computation is intensive. For this reason, the *digital shearing method* has been developed.

It was shown in Chapter 3 that in practice a hologram records only a portion of the scattered field represented by a region on the Ewald sphere. Accordingly only a portion of the power spectrum can be measured. By considering only the x - y projection of this portion of the power spectral density, $P(k_x, k_y)$, the computational complexity could be reduced considerably. According to Equations (3-5) and (3-11) in Chapter 3, $P(k_x, k_y)$ can be written in 2D Cartesian components as

$$P'(k_x, k_y) = 2P_l(k_x, k_y) \left\{ 1 + \cos \left[2\pi k_x s_x + 2\pi k_y s_y + 2\pi s_z (\lambda^{-2} - k_x^2 - k_y^2)^{1/2} - \varphi \right] \right\} \quad (4-1)$$

With image shifting, the total particle image displacement $\mathbf{s} = (s_x, s_y, s_z)$ is the sum of the particle displacement $\mathbf{s}_p = (s_{px}, s_{py}, s_{pz})$ and the image shift $\mathbf{s}_1 = (s_{ix}, s_{iy}, s_{iz})$. Without loss of generality the image shift is defined to be in the x direction only, defined by a unit vector \hat{i} , such that $\mathbf{s}_1 = s_{ix} \hat{i}$. In addition it is assumed that the power spectral density corresponding to the first exposure, $P_l(k_x, k_y)$, is slowly varying such that, to within a multiplicative constant, the total power spectral density, $P'(k_x, k_y)$, can be written as

$$P'(k_x, k_y) = 2 + \exp[-j(2\pi k_x s_{ix} - \varphi)] \exp\{-2\pi j[k_x s_{px} + k_y s_{py} + s_{pz} (\lambda^{-2} - k_x^2 - k_y^2)^{1/2}]\} \\ + \exp[j(2\pi k_x s_{ix} - \varphi)] \exp\{2\pi j[k_x s_{px} + k_y s_{py} + s_{pz} (\lambda^{-2} - k_x^2 - k_y^2)^{1/2}]\} \quad (4-2)$$

Since the image shift is larger than the particle displacement, it is straightforward to isolate the centre term in this expression by spatial filtering in the x -direction. This term is called $W(k_x, k_y)$ and it is noted that it corresponds to the spectrum of a unit amplitude

point source emanating from a point defined by the particle image displacement vector s_p , such that

$$W(k_x, k_y) = \exp\{-2\pi j[k_x s_{px} + k_y s_{py} + s_{pz}(\lambda^{-2} - k_x^2 - k_y^2)^{1/2}]\} \quad (4-3)$$

If two single-exposure holograms are taken, this term can be obtained by calculating the cross-spectrum. Considering the form of the interference fringes, if the displacement is purely in the x and y directions then the phase increases linearly with the components k_x and k_y , and if a phase map is presented parallel (Youngs type) fringe are observed. If however, the displacement is in the z -direction, then circular (Haidinger type) fringes are observed in the phase map. In essence, therefore, the problem is to measure the wavefront curvature and this is done in a manner that is analogous to a wavefront shearing interferometer. Accordingly, shearing symmetrically both the wavefront and its conjugate but in the inverse k_x -direction and then multiplying the two sheared terms $W(k_x - \Delta k_x, k_y)$ and $W^*(k_x + \Delta k_x, k_y)$ defines $P_w(k_x, k_y)$, thus,

$$\begin{aligned} P_w(k_x, k_y) &= W(k_x - \Delta k_x, k_y) W^*(k_x + \Delta k_x, k_y) \\ &= \exp \left\{ \begin{aligned} &-2\pi j[-2\Delta k_x s_{px} + s_{pz}(\lambda^{-2} - (k_x - \Delta k_x)^2 - k_y^2)^{1/2}] \\ &-s_{pz}(\lambda^{-2} - (k_x + \Delta k_x)^2 - k_y^2)^{1/2} \end{aligned} \right\} \end{aligned} \quad (4-4)$$

where * here denotes the complex conjugate. Expanding the terms of $(k_x - \Delta k_x)^2$ and $(k_x + \Delta k_x)^2$, the phase of this function, θ , can be written

$$\begin{aligned} \theta &= -2\pi \left\{ -2\Delta k_x s_{px} + s_{pz} [(\lambda^{-2} - \Delta k_x^2 - k_y^2) - (k_x^2 - 2\Delta k_x k_x)]^{1/2} \right. \\ &\quad \left. - s_{pz} [(\lambda^{-2} - \Delta k_x^2 - k_y^2) - (k_x^2 + 2\Delta k_x k_x)]^{1/2} \right\} \\ &= -2\pi \left\{ -2\Delta k_x s_{px} + s_{pz} (\lambda^{-2} - \Delta k_x^2 - k_y^2)^{1/2} \left[1 - \frac{k_x^2 - 2\Delta k_x k_x}{\lambda^{-2} - \Delta k_x^2 - k_y^2} \right]^{1/2} \right. \\ &\quad \left. - s_{pz} (\lambda^{-2} - \Delta k_x^2 - k_y^2)^{1/2} \left[1 - \frac{k_x^2 + 2\Delta k_x k_x}{\lambda^{-2} - \Delta k_x^2 - k_y^2} \right]^{1/2} \right\} \end{aligned} \quad (4-5)$$

Expanding $[1 - \frac{k_x^2 - 2\Delta k_x k_x}{\lambda^{-2} - \Delta k_x^2 - k_y^2}]^{1/2}$ and $[1 - \frac{k_x^2 + 2\Delta k_x k_x}{\lambda^{-2} - \Delta k_x^2 - k_y^2}]^{1/2}$ as a Taylor series and collecting the terms in powers of k_x ,

$$\begin{aligned} \theta &= -2\pi\{-2\Delta k_x s_{px} \\ &+ s_{pz}(\lambda^{-2} - \Delta k_x^2 - k_y^2)^{1/2}[1 - \frac{k_x^2 - 2\Delta k_x k_x}{2(\lambda^{-2} - \Delta k_x^2 - k_y^2)} + \frac{(k_x^2 - 2\Delta k_x k_x)^2}{8(\lambda^{-2} - \Delta k_x^2 - k_y^2)^2} + \text{high order terms}] \\ &- s_{pz}(\lambda^{-2} - \Delta k_x^2 - k_y^2)^{1/2}[1 - \frac{k_x^2 + 2\Delta k_x k_x}{2(\lambda^{-2} - \Delta k_x^2 - k_y^2)} + \frac{(k_x^2 + 2\Delta k_x k_x)^2}{8(\lambda^{-2} - \Delta k_x^2 - k_y^2)^2} + \text{high order terms}]\} \\ &= -2\pi\{-2\Delta k_x s_{px} + s_{pz}[\frac{2\Delta k_x k_x}{(\lambda^{-2} - \Delta k_x^2 - k_y^2)^{1/2}} - \frac{\Delta k_x k_x^3}{(\lambda^{-2} - \Delta k_x^2 - k_y^2)^{3/2}} + \text{high order terms}]\} \end{aligned} \quad (4-6)$$

For the reconstruction geometry shown in Figure 2-4 of Chapter 2, it is noted that the far-field intensity distribution recorded by a camera is directly related to power in each plane-wave component as shown in Figure 4-1. To map a plane wave represented by a wave vector (k_x, k_y) onto a point (x, y) in its focal plane, it is straightforward to show that

$$k_x = x\lambda^{-1}(x^2 + y^2 + f^2)^{-1/2} \quad (4-7)$$

$$k_y = y\lambda^{-1}(x^2 + y^2 + f^2)^{-1/2} \quad (4-8)$$

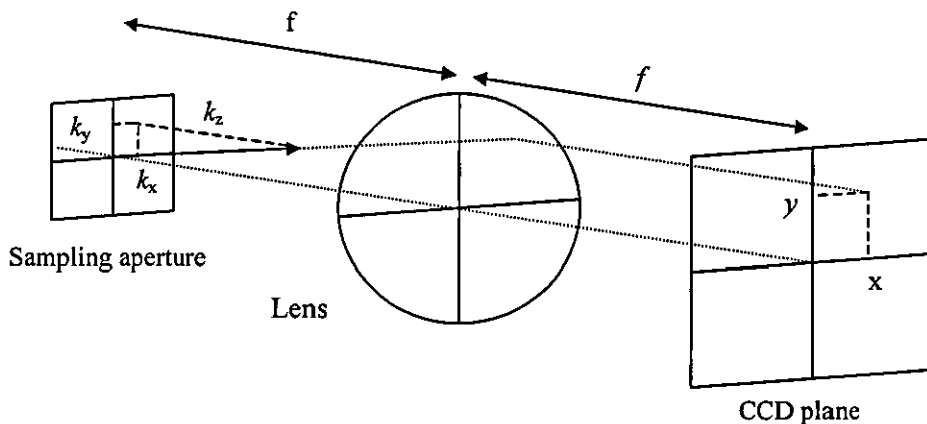


Figure 4-1 Wave-vector geometry

As the numerical aperture (NA) is typically less than 0.5, the wavefront $W(k_x, k_y)$ is only measured over a region bounded by $|k_x| < k_{xmax}$ and $|k_y| < k_{ymax}$, where $k_{xmax} = 0.408/\lambda$ and $k_{ymax} = 0.408/\lambda$ (putting $x = y = 1$ and $f = 2$, for example). The function $P_w(k_x, k_y)$ is therefore defined over the overlap region such that $|k_x| < k_{xmax} - \Delta k_x$ and $|k_y| < k_{ymax}$. In order that $P_w(k_x, k_y)$ be defined over half the area of the wavefront $W(k_x, k_y)$ (i.e. 50%) overlap we require $|\Delta k_x| = k_{xmax} / 2$. Consequently for the case defined by NA=0.5, we have $|k_x| < 0.204/\lambda$, $|k_y| < 0.408/\lambda$ and $|\Delta k_x| < 0.204/\lambda$. Using these values it is found that, even at the extreme aperture, the third order term in k_x accounts is less than 2.5% of the first order term and hence can be neglected. To a good approximation Equation (4-6) can be therefore written

$$P_w(k_x, k_y) = \exp(-2\pi j\theta_s) \exp\left\{-2\pi j\left[\frac{2\Delta k_x k_x s_{pz}}{(\lambda^{-2} - \Delta k_x^2 - k_y^2)^{1/2}}\right]\right\} \quad (4-9)$$

where θ_s is a phase constant. Finally, a change of variables is made such that:

$$K_x = \frac{2\Delta k_x k_x}{(\lambda^{-2} - \Delta k_x^2 - k_y^2)^{1/2}}, \quad K_y = k_y \quad (4-10)$$

And

$$\begin{aligned} P_w^z(K_x, K_y) &= P_w\left[\frac{(\lambda^{-2} - \Delta k_x^2 - k_y^2)^{1/2} K_x}{2\Delta k_x}, K_y\right] \\ &= \exp[-2\pi j(s_{pz} K_x + \theta_s)] \end{aligned} \quad (4-11)$$

With these co-ordinate changes, it can be seen that the final distribution is a linear phase ramp. The rate of change of phase is proportional to the particle image displacement in the z-direction, s_{pz} , and can be found by Fourier transformation such that,

$$\begin{aligned}
 R_w^z(r_x, r_y) &= \iint P_w^z(K_x, K_y) \exp[2\pi j(K_x r_x + K_y r_y)] dK_x dK_y \\
 &= \exp(j\theta_s) \delta(r_x - s_{pz}, r_y)
 \end{aligned} \tag{4-12}$$

In this way the z -displacement s_{pz} is identified by the location of the peak in this distribution, and can be used to find the particle image displacement in the x and y -directions, s_{px} and s_{py} . Accordingly, multiplying the field $W(k_x, k_y)$ of Equation (4-3) by the complex exponential $\exp[2\pi j s_{pz} (\lambda^{-2} - k_x^2 - k_y^2)^{1/2}]$ and Fourier transforming to give,

$$\begin{aligned}
 R_w^{xy}(r_x, r_y) &= \iint W(k_x, k_y) \exp[2\pi j s_{pz} (\lambda^{-2} - k_x^2 - k_y^2)^{1/2}] \exp[2\pi j(k_x r_x + k_y r_y)] dk_x dk_y \\
 &= \delta(r_x - s_{px}, r_y - s_{py})
 \end{aligned} \tag{4-13}$$

Again the displacements in the x and y -directions are found from the position of the peak. The proposed digital shearing method described above can be summarized as the following steps shown in Figure 4-2 and are illustrated through MatLab simulation in next section.

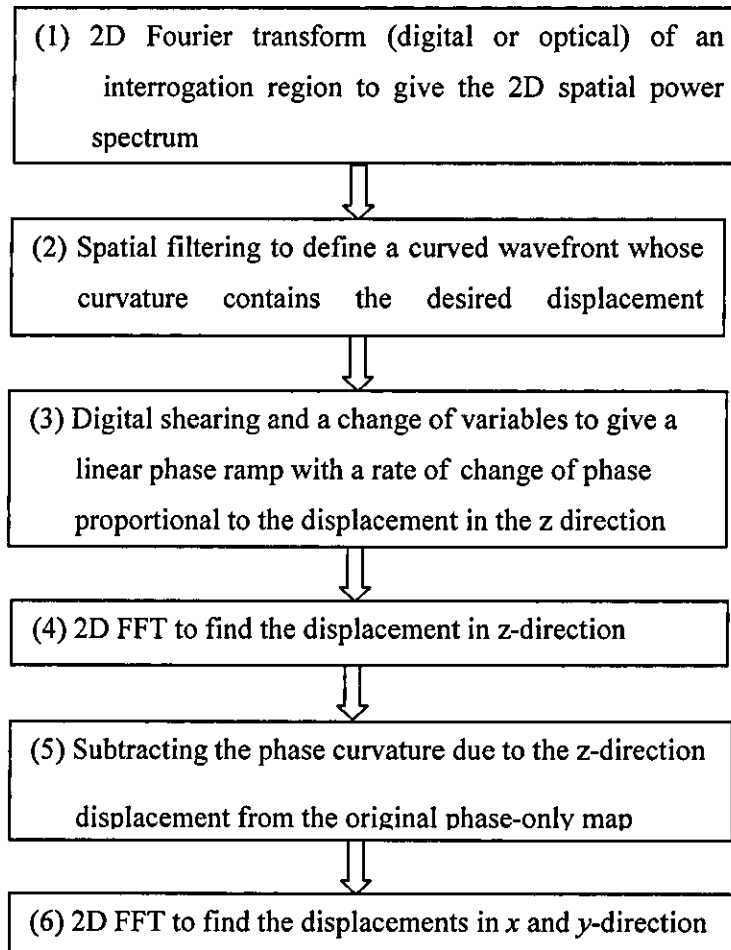


Figure 4-2 Flow chart of digital shearing method

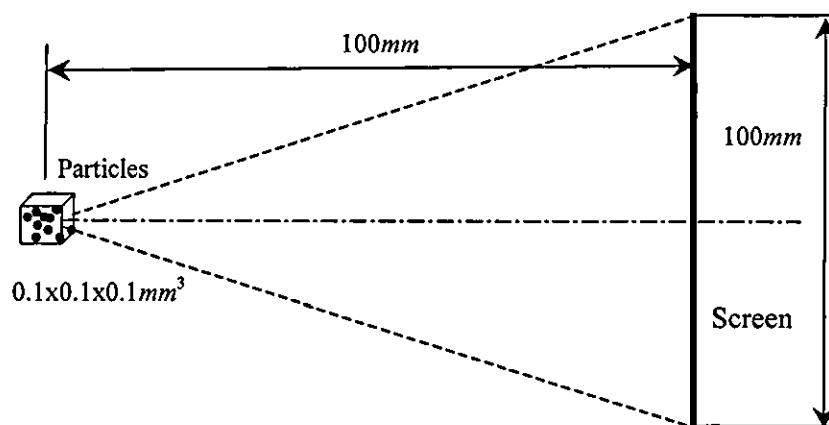


Figure 4-3 Geometry of fringe pattern generation

4.3 Simulated experiment

In order to demonstrate the implications of the theory presented above, several controlled experiments are simulated in MatLab. To begin, the fringe pattern is generated by the superposition of the light scattered by a small group of particles at the times of first and second exposures. The co-ordinates of the first exposure particle images are randomly generated within a cubic volume of $0.1 \times 0.1 \times 0.1 \text{ mm}^3$. Second exposure position co-ordinates are computed by adding the particle image displacement, which are $10 \mu\text{m}$ in the x and y directions and $15 \mu\text{m}$ in the z direction. As shown in Figure 4-3, a distant screen is located at a distance of 100 mm from the particles, which satisfies the Fraunhofer condition (the observation distance $z \gg 2l^2/\lambda \approx 30 \text{ mm}$, where $l=0.1 \text{ mm}$ and $\lambda=0.632 \times 10^{-3} \text{ mm}$) (Goodman 1996). The far-field intensity distribution is therefore observed on the screen, which is calculated directly by adding the spherical waves originating from the particle position co-ordinates. For the case defined by $\text{NA} \approx 0.5$, the size of the screen is $100 \text{ mm} \times 100 \text{ mm}$. In this way, approximately circular fringes are observed on the screen as shown in Figure 4-4.

For the geometry of fringe pattern generation shown in Figure 4-3, it is noted that the far-field intensity distribution recorded by the screen is directly related to power in each plane-wave component. To map a plane wave represented by a wave vector (k_x, k_y) onto a point (x, y) on the screen with the distance of z , it is straightforward to show that $k_x = x\lambda^{-1}(x^2 + y^2 + z^2)^{-1/2}$ and $k_y = y\lambda^{-1}(x^2 + y^2 + z^2)^{-1/2}$. The fringe pattern is accordingly converted into k_x and k_y components, shown in Figure 4-5. It can be seen that the dominant pattern consists of circular fringes.

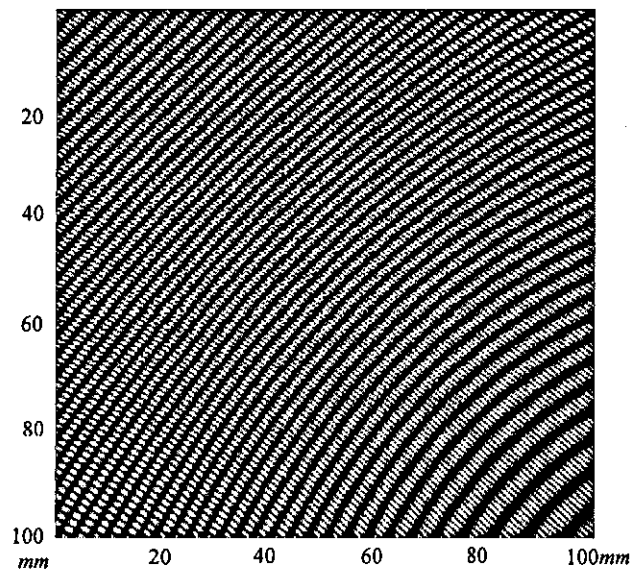


Figure 4-4 The far field fringe pattern

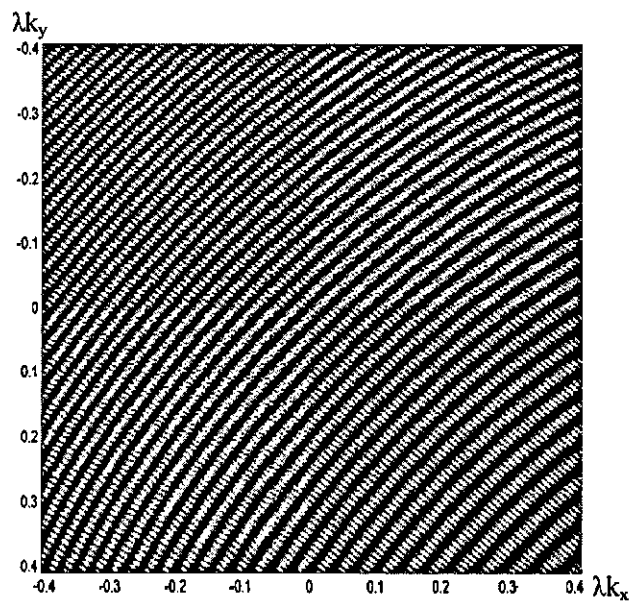


Figure 4-5 The far-field fringe pattern as a function of wave vector components

This fringe distribution is then spatially filtered by calculating the Fast Fourier Transform (FFT), removing the negative half-plane and zero order (DC term) and taking the inverse FFT. The result of this operation defines a curved wavefront whose curvature contains the desired displacement information. Figure 4-6 shows a phase-only map of this curved wavefront (modulo 2π).

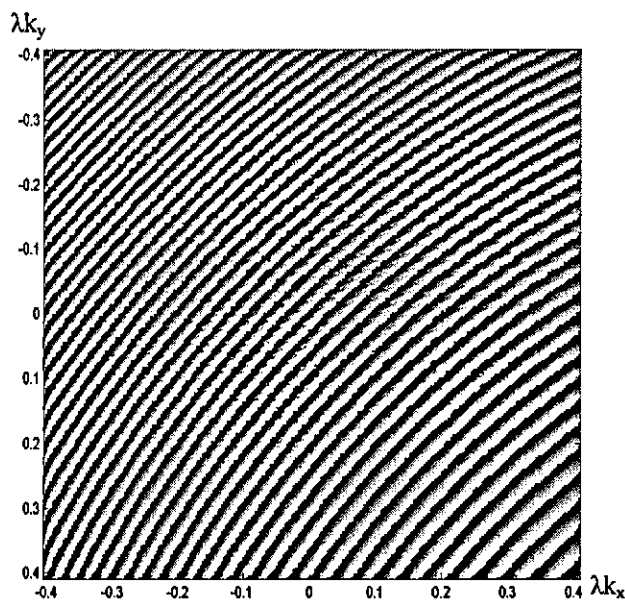
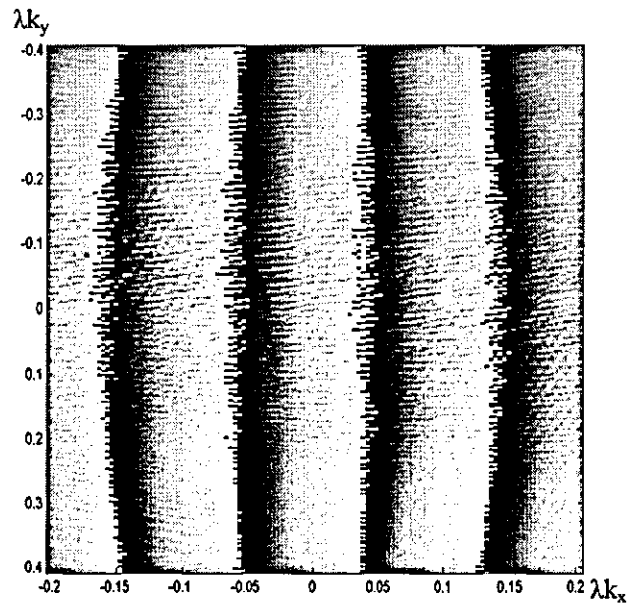
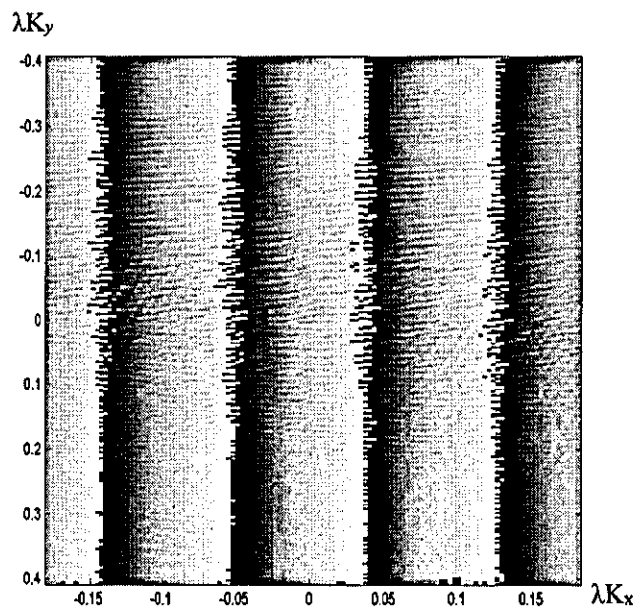


Figure 4-6 Phase-only map of the curved wavefront (modulo 2π)

In order to measure the wavefront curvature, the phase of the negative half plane of the phase distribution shown in Figure 4-6 (i.e. the left-hand side) is taken and subtracted from that of the positive half plane (the right hand side). This is equivalent to wavefront shearing and Figure 4-7 shows the image calculated by this method. Nearly parallel fringes are clearly visible. A change of variables, defined by Equation (4-10), renders the fringes parallel as shown in Figure 4-8. It is thought that, the noise in the fringes of Fig. 4-5, 4-6, 4-7 and 4-8 are caused by the interpolation processing of k_x and k_y components.

Figure 4-7 Sheared phase distribution (modulo 2π)Figure 4-8 Sheared phase distribution with a change of variable (modulo 2π)

This distribution can be thought of as a tilted plane wave or a linear phase ramp with a rate of change of phase proportional to the displacement in the z direction. As such the z displacement can be found by FFT. Figure 4-9 shows the result of this operation and it can be seen that a well-defined peak is clearly visible and its position (in the x direction) is determined by the z displacement.

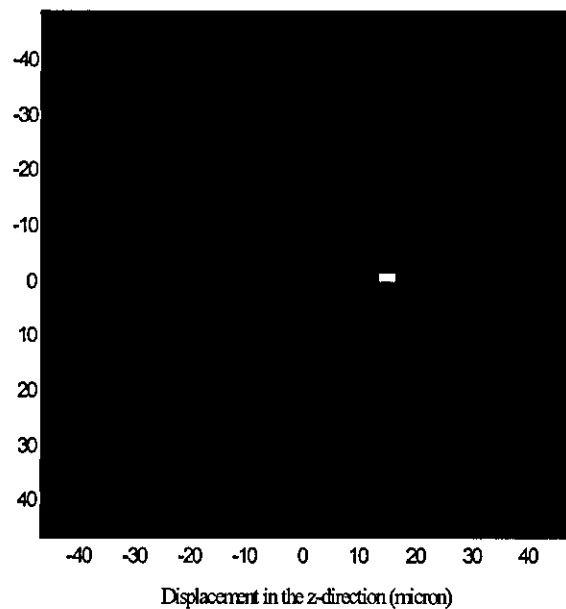


Figure 4-9 Squared modulus of FFT of complex exponential
of the phase shown in Figure 4-8

The last operation is to calculate the x and y image displacements. Figure 4-10 shows the original phase-only map of Figure 4-6 with the phase curvature due to the s_z displacement subtracted. In a similar manner to before, we now have approximately parallel fringes with some curvature, which is probably caused by the error of the computed z displacement. The FFT of this distribution, shown in Figure 4-11, gives a clear signal peak with position related with the displacement in the x and y direction.

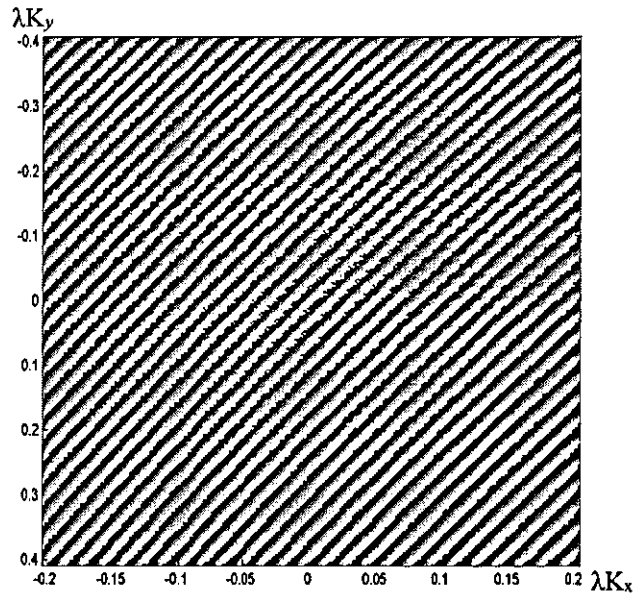


Figure 4-10 Original phase-only map (Figure 4-6) with curvature (due to s_z displacement) subtracted

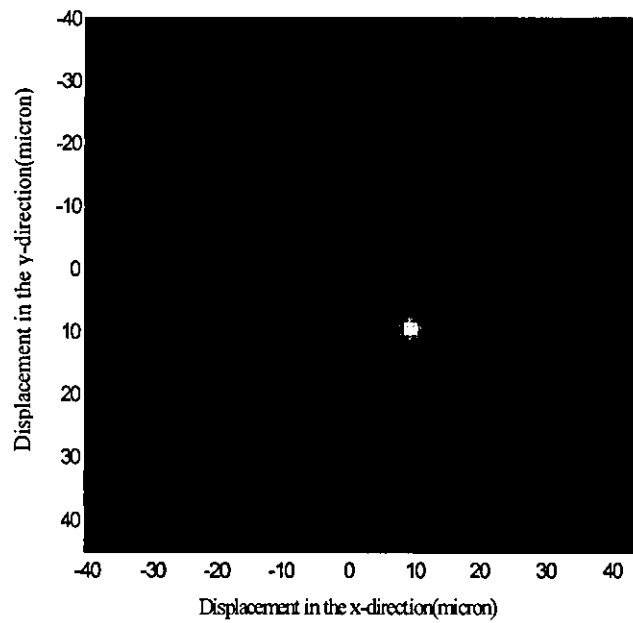


Figure 4-11 Squared modulus of FFT of complex exponential of the phase shown in Figure 4-10

At this point it is worth commenting on the speed of the method. The final result has been computed using a total of four 2D FFT operations and these represent the dominant computational overhead. Using an input of 256x256pixels resolution, this requires approximately 4M floating-point operations and it is estimated that the other essential computations (coordinate transforms) require approximately 1M floating-point operations. The digital shearing method therefore affords a considerable time saving over the full three-dimensional correlation approach (approximately 400M floating-point operations).

It might be expected that this saving would be at the expense of accuracy or robustness. To assess this hypothesis the accuracy of the digital shearing method has been tested for a range of simulated particle image displacements and a varying number of particle image pairs within the region. Figure 4-12, Figure 4-13 and Figure 4-14 present the comparison between the computed and pre-assigned displacement in the x , y and z directions respectively. It can be seen that the results agree well and the method appears to be tolerant to the particle image location and the number of particle images.

The independence of the measurements of x , y and z displacement has been also tested. Table 4-1 shows the pre-assigned and (mean) measured x , y and z displacements for samples of 10 particle images. Here the z displacement is much larger than the x - y displacement. These results show that the x and y displacement measurements are not influenced to any great extent by the large z displacement. However, there is some evidence of a small systematic error in the measurement of y (the positive non-zero value) and z (the negative value) displacement. It is thought that, the error results from the quantization process.

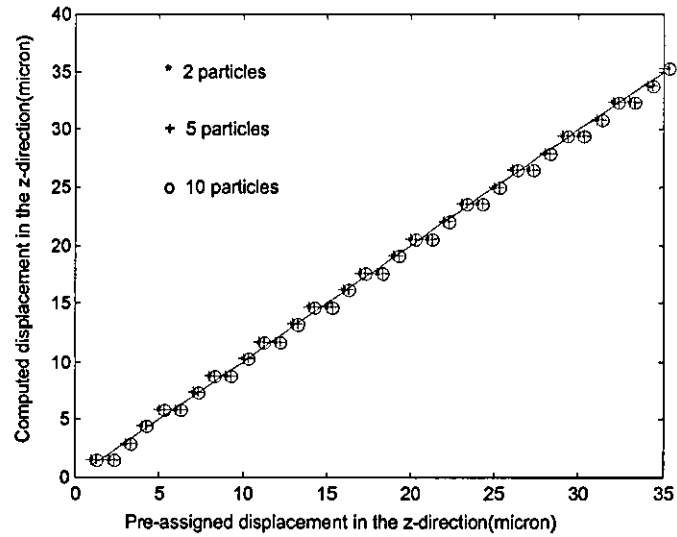


Figure 4-12 A comparison between the computed and pre-assigned displacement in z direction (Pre-assigned displacements in x and y directions are $10\mu\text{m}$, respectively)

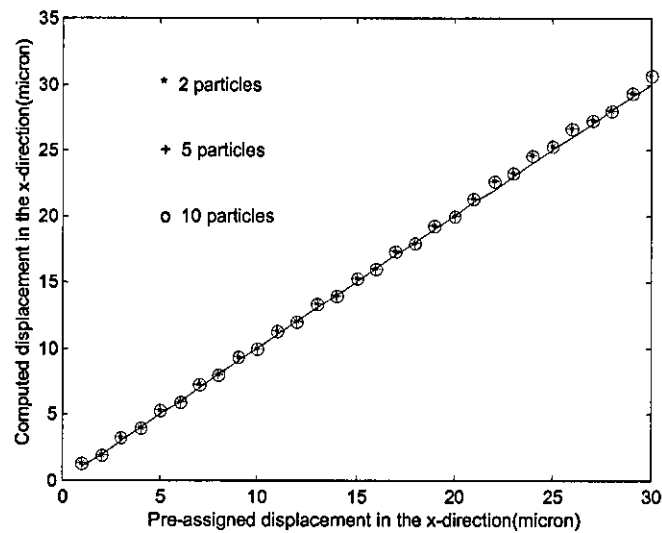


Figure 4-13 A displacement comparison in x-direction (Pre-assigned displacements in y and z directions are $10\mu\text{m}$ and $15\mu\text{m}$, respectively)

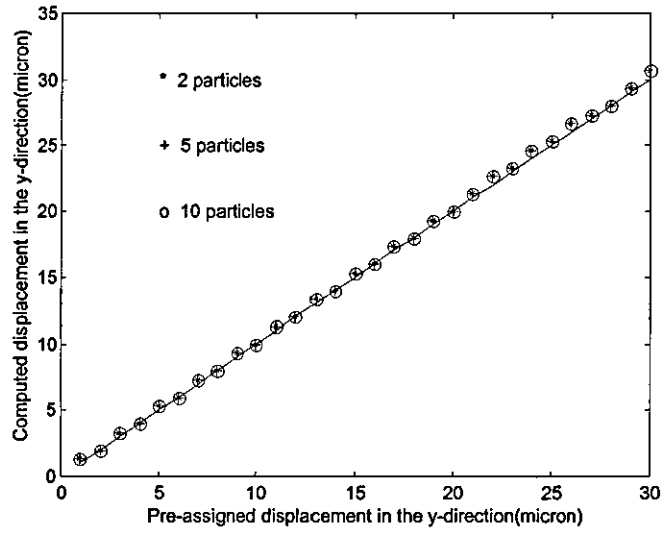


Figure 4-14 A displacement comparison in y -direction
(Pre-assigned displacements in x and z directions are $10\mu m$ and $15\mu m$, respectively)

Table 4-1 Independence of x , y and z displacement measurements

Assigned Displacement (μm)			"Measured" Displacement (μm)		
x	y	z	\bar{x}	\bar{y}	\bar{z}
5	0	50	5.0	0.2	49.2
10	0	50	9.9	0.2	48.5
15	0	50	14.8	0.2	49.0

4.4 Comparison of the digital shearing and CAC method

To ascertain the accuracy and computational efficiency of the digital shearing and 3D-CAC processing schemes, numerically generated HPIV images are used with prescribed displacements. The first exposure image is generated by randomly populating it with particles assumed to behave as randomly phased point sources. The second exposure image is computed by adding the pre-assigned particle image displacement (with image shift $10\mu\text{m}$). The particle density is set at 10 particles per $0.1\times 0.1\times 0.1\text{mm}^3$ volume.

4.4.1 Computational performance

Compared to direct computation, the fast Fourier transformation (FFT) method is very efficient, reducing the number of computations for N points from N^2 to the order of $N\log_2 N$. In this way $N\times N\times N$ 3D correlation for HPIV displacement extraction takes $O(3N^3\log_2 N)$ operations. In contrast, the digital shearing method described above has computed the final result using a total of four 2D FFT operations and one coordinate transformation. Each 2D FFT takes $O(2N^2\log_2 N)$ operations which represent the dominant computation overhead. Each coordinate transformation takes $O(N^2)$ operations. The digital shearing method thus requires $O(8N^2\log_2 N + N^2)$ operations or a saving of a factor of about $8/3N$ compared to 3D correlation operations for an array of $N\times N$ elements. The digital shearing method therefore affords a considerable time saving over the digital 3D correlation approach. As the number of pixels increases this effect becomes more pronounced.

The computational speeds of these two methods are presented in Table 4-2 when simulated by MatLab6 with a 2.0GHz Intel P4 PC running Windows XP. The speed of the digital shearing method is readily apparent. For 128×128 pixels images, it is about 40 times faster than digital 3D correlation approach (and 20 times faster for 64×64 pixels images).

Table 4-2 Computational performance of digital shearing and 3D correlation methods

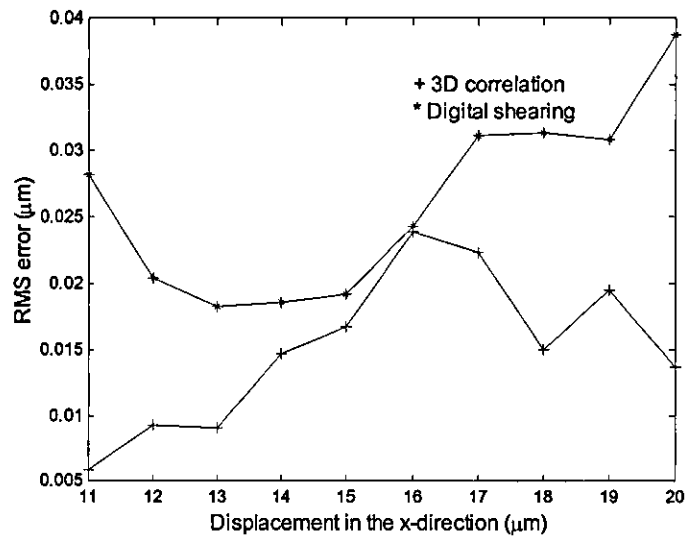
Scheme	Time (ms)
128x128pixels image	
Digital shearing	124
3D correlation	4780
64x64pixels image	
Digital shearing	50
3D correlation	1060

4.4.2 Accuracy

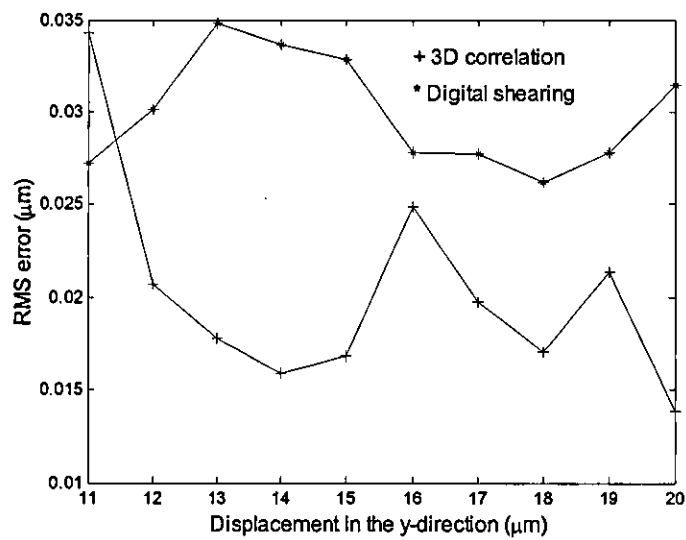
The relative accuracy of digital shearing and CAC methods was examined by analysing regions with different displacement Δx , Δy and Δz . Every combination of integer displacement in the range 11-20 μm (with image shift 10 μm) was considered. Thus 1000 random images with integer displacements were generated. Correlation peaks were found to sub-pixel accuracy using three-point Gaussian curve fits.

Considering the RMS errors (Figure 4-15), the two methods show some irregularity. The reason for this is that, with FFT correlation, the peak can assume an asymmetric shape due to randomly located particles with randomly generated intensities. Thus, sub-pixel Gaussian curve fitting of the peaks, as was done here, will yield random errors in the computed peak location. The RMS errors of these two methods show qualitative similarity in the x and y -direction, which is less than 0.04 μm , however, the 3D correlation method shows slightly better performance. In the digital shearing method, extracting the z displacement is necessary before the procedure of removing the curvature of the far field fringe pattern. The RMS errors in the x and y directions then are affected by the accuracy of the computed peak location in the z direction and so the RMS errors in the x and y directions are slightly higher. However, the digital shearing method shows better

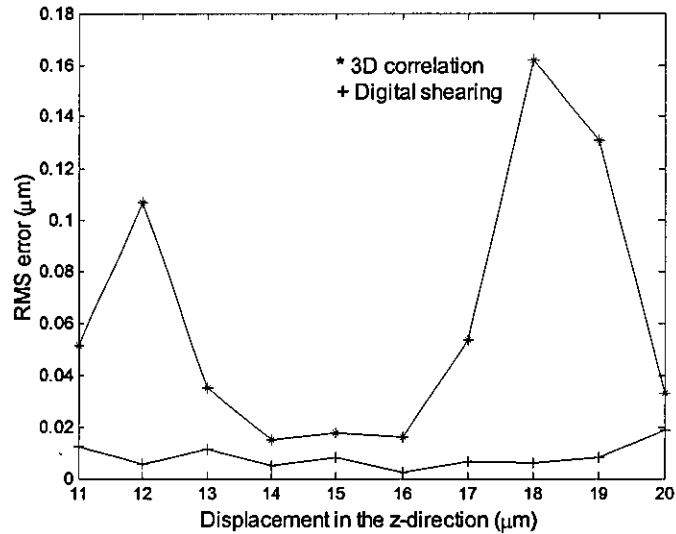
performance in the z-direction. It is thought that these are due to windowing effects and more constant data would be obtained if Hanning window was applied in k-space. Overall, the digital shearing method provides comparable accuracy to 3D correlation technique.



(a) x-direction



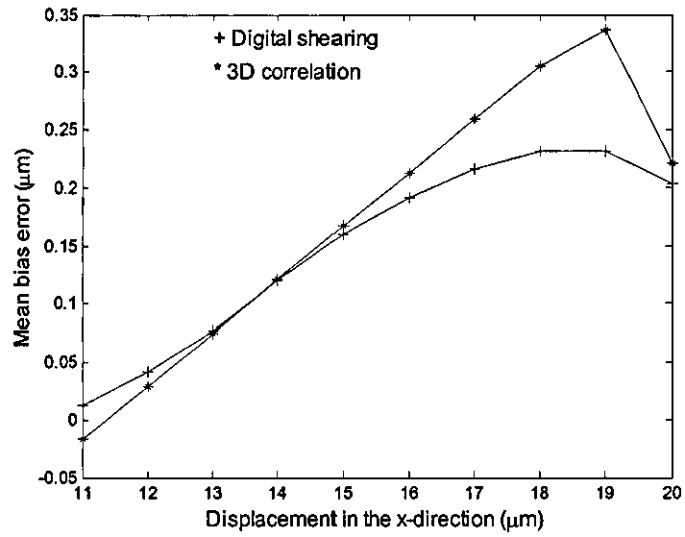
(b) y- direction



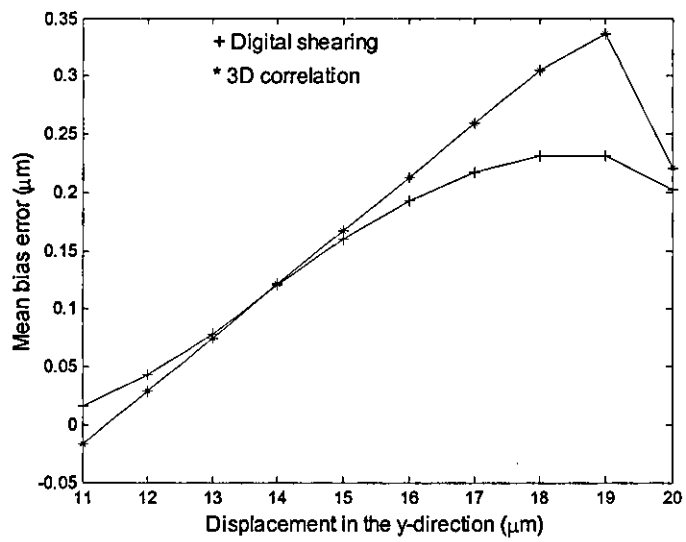
(c) z- direction

Figure 4-15 Variation of RMS error for digital shearing and 3D correlation methods

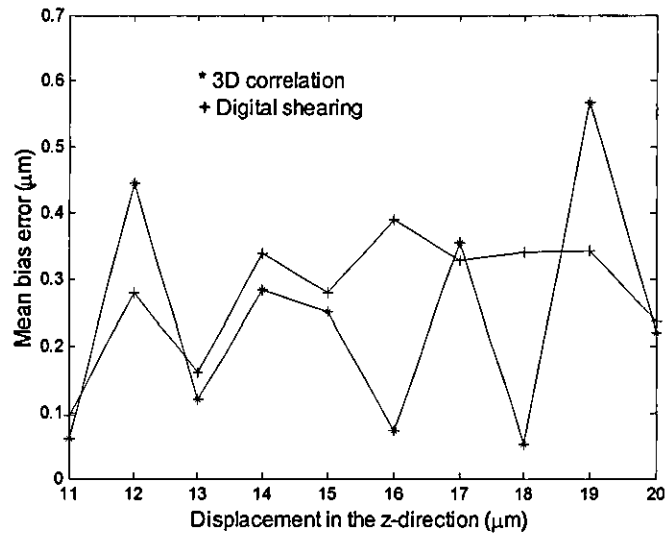
Turning to the mean bias errors, shown in Figure 4-16, the two methods show a proportional increase as the displacement increases in x and y -direction but there is no clear trend as in the RMS error in the z -direction. For the 3D correlation method, the power spectral density is mapped onto the \mathbf{k} -space surface of the Ewald sphere and it is suspected that the sampling interpolation procedure results in the bias errors. In the digital shearing method it is noted that Equation (4-9) is an approximation. At a NA of 0.5 there is about 8% error in this term and it is observed that this results in an increased width of the correlation peak. In this case, the three-point Gaussian curve fit does not provide a good approximation of the actual peak shape. However, for the digital shearing method, the mean bias errors are comparable in magnitude to the 3D correlation method. Further improvements may be expected by optimizing the sub-pixel interpolation routine with respect to the shape of the discrete correlation peak.



(a) x-direction



(b) y-direction



(c) z-direction

Figure 4-16 Variation of mean bias error for digital shearing and 3D correlation methods

The outcome of the accuracy tests is summarized in Table 4-3. Examining the two methods, the relative errors incurred are smaller than 3%. Considering the computational efficiency discussed above, the digital shearing method can provide acceptable displacement measurements and is nearly 2 orders of magnitude faster than the CAC technique. Note that the results in Figure 4-15 and Table 4-3 cannot be compared directly to the data in Table 4-1 because they are simulated by a slightly different procedure. The results in Table 4-1 are simulated without the image shift and a three-point Gaussian fit is used to determine peak position in the later work.

Table 4-3 Mean errors magnitude over the complete 11-20 μm range

Scheme	RMS error (μm)	Mean bias error (μm)
3D correlation		
x-direction	0.01	0.15
y-direction	0.02	0.15
z--direction	0.06	0.39
Digital shearing		
x-direction	0.03	0.15
y-direction	0.03	0.15
z--direction	0.01	0.28

4.5 Experimental results

In section 4.3 the digital shearing method has been demonstrated using simulated data for a range of displacements. This section will illustrate the method applied to HPIV data recorded on 35mm photographic film. The film was Kodak Technical Pan 2415 having a maximum resolution of 200lp/mm and can be used as a direct replacement for holographic emulsion providing the interference image is magnified by about 6 times.

The digital shearing method can be digitally implemented by cross-correlation of reconstructed particle images from two single-exposure holograms. The recording geometry of OCR method (shown in Figure 2-4), which allows an image shift to be included, is not necessary for the digital shearing method. In this case, a forward scatter geometry was chosen for reasons of efficiency and simplicity as shown in Figure 4-17.

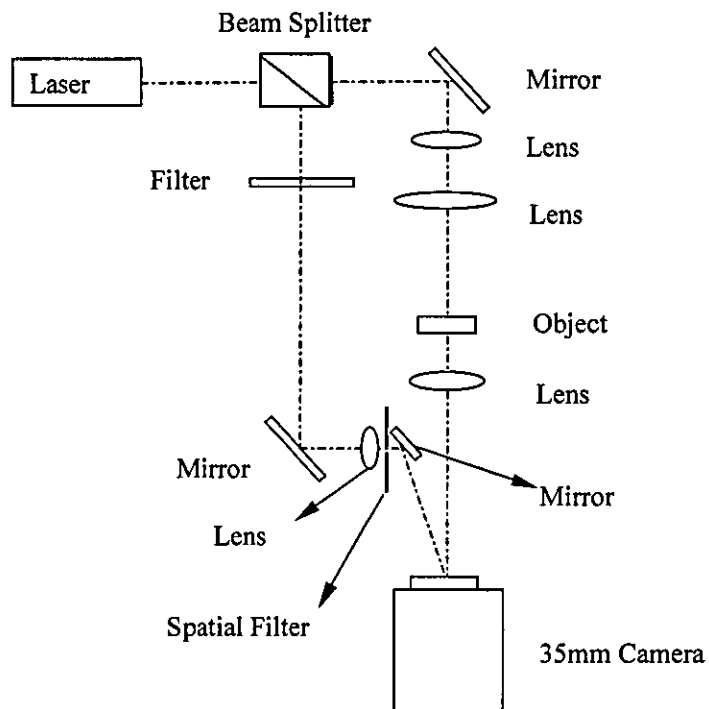


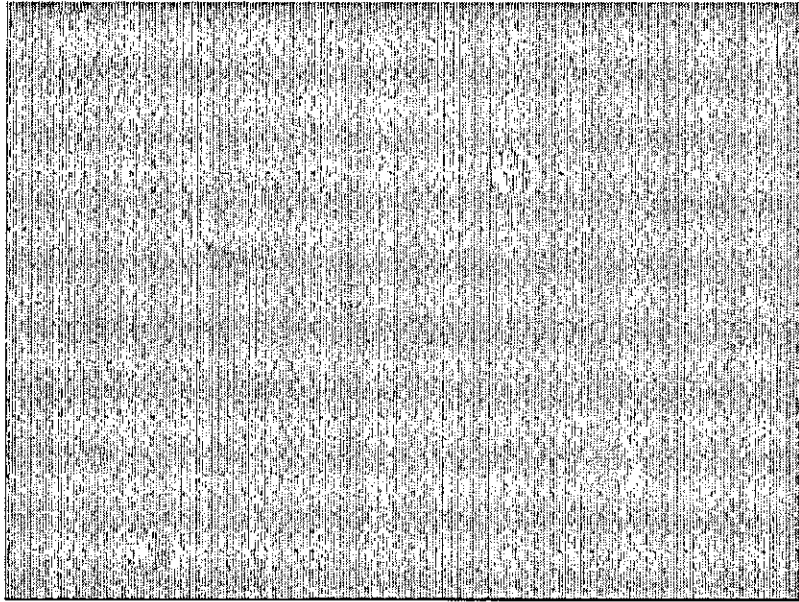
Figure 4-17 Recording Geometry

In essence, an image plane hologram is formed at the film with a magnification of 6 times using a reversed 50mm, F/2 Pentax lens. For the purposes of this experiment the object was a plate of glass that was sparsely sprayed with a mist of fine particles of approximately 10-50 μm in diameter and is illuminated by a collimated, axial object beam. An off-axis reference beam diverges from a (virtual) point that is in the far focal plane of the imaging lens and mixes with the light scattered from the object. In this way the phase curvature introduced by the imaging process is exactly matched by the curvature of the reference beam such that straight interference fringes are observed in the film plane in the absence of any object (this aspect is shown theoretically in Chapter 5 concerning μHPiV).

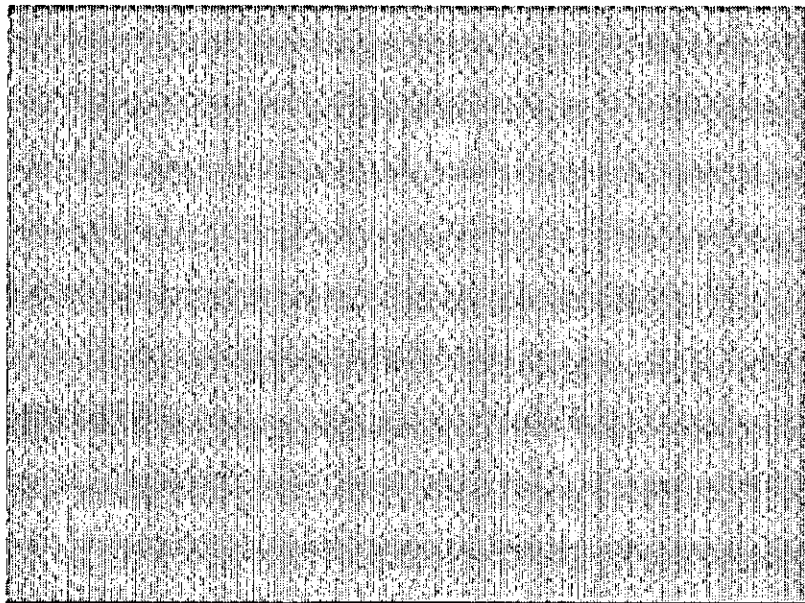
The laser used was a Q-switched, diode pumped, doubled Nd: YAG laser with about 100 μJ per pulse. Holograms were taken with a pre-defined displacement of the slide between exposures. The 35mm negatives were processed in Kodak D19 developer and initially scanned into digital format using the professional flat bed scanner. However, it was found that the true resolution of the professional scanner was about 100lp/mm and was insufficient to scan the 35mm film with the required resolution of 320lp/mm. The reconstructions presented below were accomplished by digitizing a small area of the negative using a Nikon microscope (10x). As the hologram was recorded using the forward scattering geometry with an imaging lens, the numerical aperture of the digitized field is not restricted by this process.

Digitized holographic images taken from the 35mm film that corresponds to about 0.15x0.1mm² in the object space are shown in Figure 4-18 a) and b). High frequency, vertical fringes can be seen in the first and second exposure images corresponding to a pitch of about 0.35 $\mu\text{m}/\text{cycle}$ in the object space. Once digitized, the complex amplitude in the plane of the film at the time of the exposure can be demodulated numerically in the normal way (multiplying by a linear phase ramp and low pass filtering). The complex amplitude in the plane of the object is found by scaling this according to the

magnification. The magnitude of the corresponding, demodulated images are shown in Figure 4-19.



a) First exposure hologram



b) Second exposure hologram

Figure 4-18 First and second exposure hologram

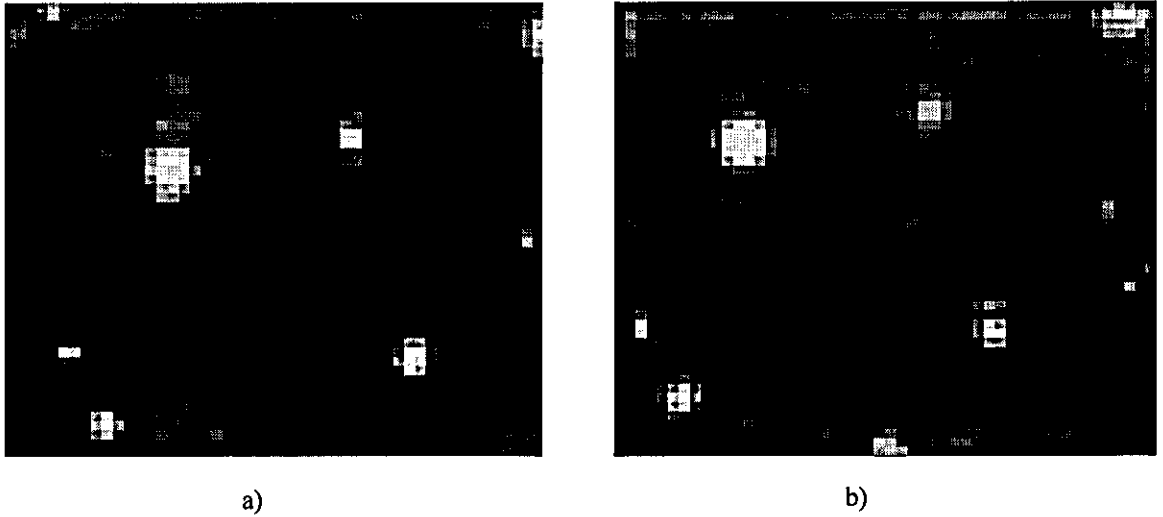


Figure 4-19 Reconstructed particle images from

Figure 4-18 a) and b)

The phase of the cross-spectrum was calculated and is displayed as a grey-scale phase map in Figure 4-20. Although there is significant noise (probably due to the digitization process), curved fringes can be seen clearly that appear to be centred toward the bottom right hand corner of the image.

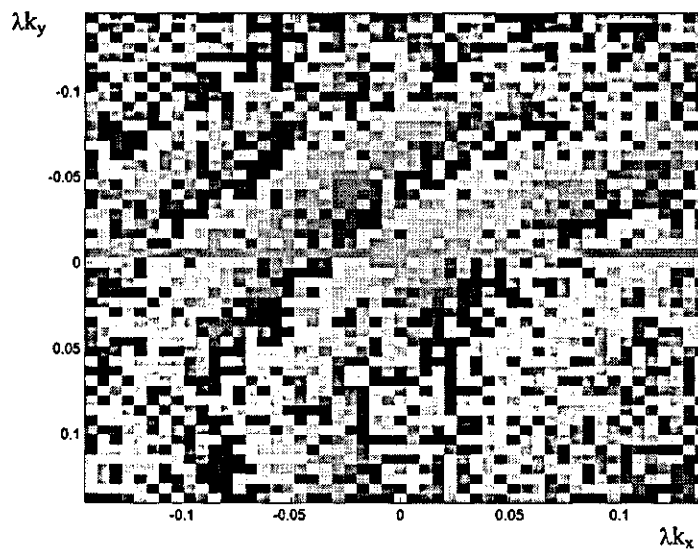


Figure 4-20 Phase map of cross-spectrum (module 2π)

The sheared and co-ordinate transformed phase map is shown in Figure 4-21. About one and a half cycles of horizontal fringes can be seen (note shear is vertical in this case).

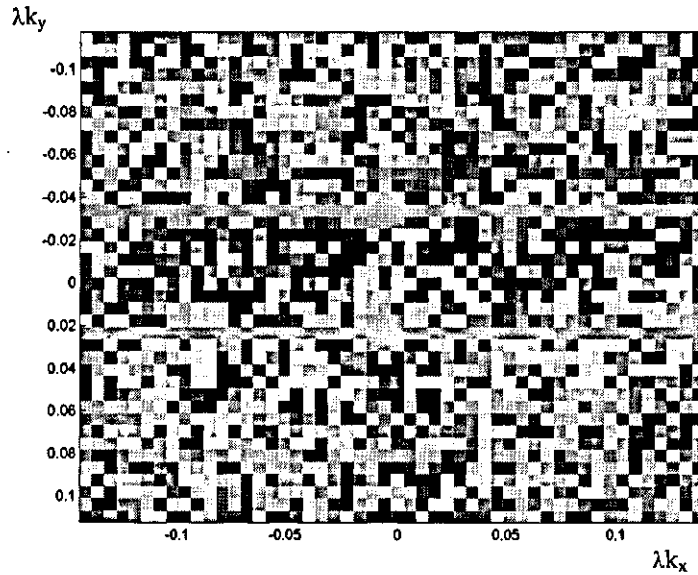


Figure 4-21 Phase map of co-ordinate transformed sheared cross-spectrum (modulo 2π)

The displacement in the z -direction is found by Fourier transformation of this distribution. In order to increase the signal resolution, the zero padding is used to perform interpolation. A clear signal peak can be seen in Figure 4-22.

Finally the curvature of the fringes displayed in the phase map of Figure 4-21 is removed using the measured z -displacement as shown in Figure 4-23.

In this case the x and y displacements are found by Fourier transformation. This is shown in Figure 4-24 and once again the signal peak can be clearly identified as required.

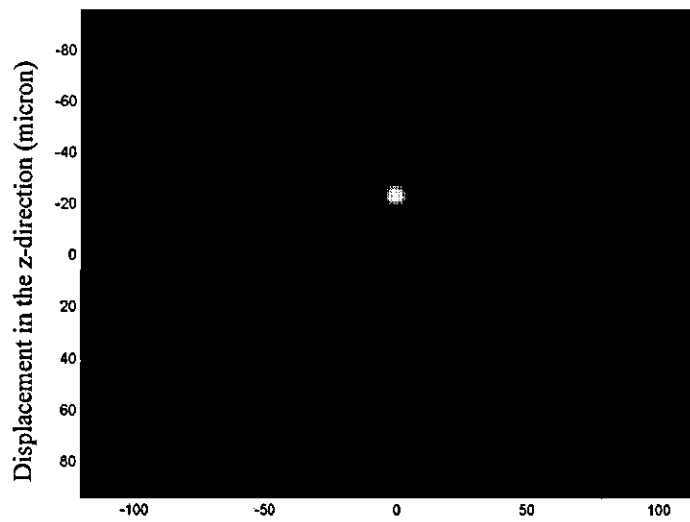


Figure 4-22 Squared Modulus of FFT of complex exponential of the phase illustrated in Figure 4-21 (after zero padding)

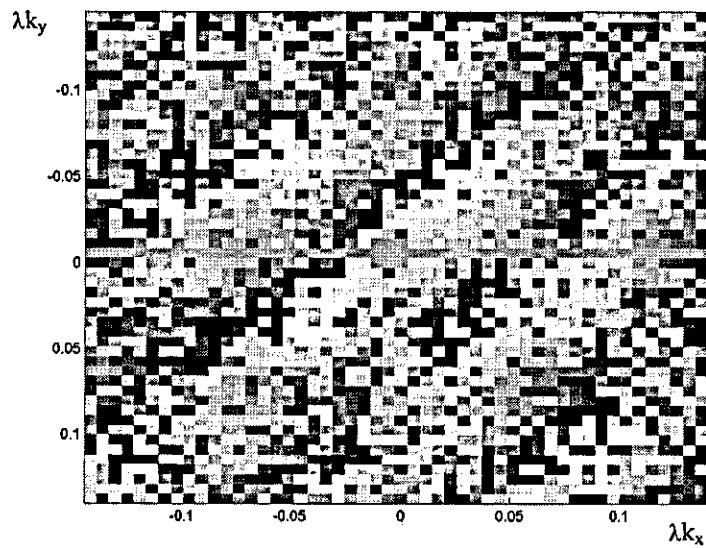


Figure 4-23 Original phase map of cross-spectrum (Figure 4-20) with curvature subtracted (modulo 2π)

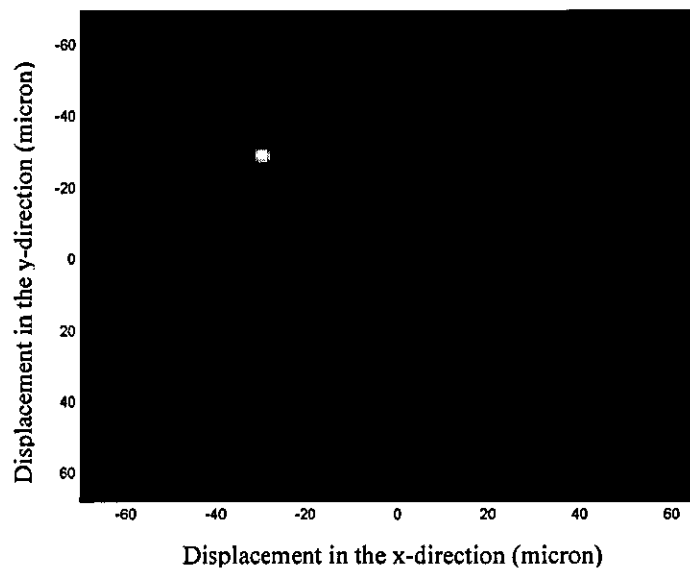


Figure 4-24 Squared modulus of FFT of complex exponential of the phase illustrated in

Figure 4-23 (after zero padding)

4.6 Summary

In this chapter, a new method to extract particle image 3D displacement from a double exposure or two single-exposure HPIV hologram(s) has been proposed and demonstrated. In contrast to the digital 3D-CAC, it has been shown that all three components of particle image displacement can be retrieved using 2D FFT operations and approximate coordinate transformations. Since HPIV recordings necessarily utilise large numerical apertures (NA) the method has been analysed using a wave-vector approach to specify the coordinate transformations. Using a MatLab simulation the method has been illustrated in a step by step manner showing the effect of each operation. The simulation has also been used to assess the accuracy of the method and its tolerance to variations in the number of particle images.

The performance of the digital shearing and three-dimensional correlation methods has also been examined in terms of the computational efficiency and measurement accuracy.

The simulated results show that the digital shearing method can provide much higher speed and comparable accuracy to the 3D correlation technique. From the initial simulations it has been found that the digital shearing method is around 40 times faster than 3D-CAC for 128x128 pixels image. From the analysis, the digital shearing method only requires about $3/8N$ of the operations required by 3D correlation for an array of $N \times N$ elements. Thus the digital shearing method affords a considerable time saving over the full 3D correlation approach. As the number of pixels increases, this becomes more pronounced.

Errors in the digital shearing technique are due to the following influences: the accuracy of the computed peak location in the z direction, the proposed approximation in Equation (4-9) and the smaller image shifts.

The digital shearing method has been illustrated in the analysis of recordings made on 35mm photographic film. As only single experimental data is obtained, it is impossible to analyse the experimental errors and accuracy of the technique at this stage and more experimental data should be obtained in the future work.

4.7 References

- Barnhart, D. H., 2001, Whole-field holographic measurements of three-dimensional displacement in solid and fluid mechanics, PhD thesis, Loughborough University, UK.
- Coupland, J. M. and Halliwell, N. A., 1992, "Particle image velocimetry: three-dimensional fluid velocity measurements using holographic recording and optical correlation", *Applied Optics*, vol.131(8), p1005-1007.
- Goodman, J. W., 1996, *Introduction to Fourier Optics*. New York, McGraw-Hill.

Chapter 5 : Micro Holographic Particle Image Velocimetry

5.1 Introduction

In this chapter, Micro Holographic Particle Image Velocimetry (μ HPIV) is introduced for 3C-3D measurement of flow structures within microfluidic devices. Firstly, the Micro Particle Image Velocimetry (μ PIV) method for 2C-2D velocity measurement is reviewed in Section 5.2. The difference between μ PIV and macro PIV is explained. Section 5.3 presents the basic principles of μ HPIV. Digital recording using a holographic microscope and numerical reconstruction is exploited throughout. Although the digital shearing method has been shown to work efficiently and accurately with simulated data and would be expected to work well for μ HPIV, a bug in the program prevented its use. Due to time constraint, the bug was unresolved and the analysis was performed using complex amplitude cross-correlation for data extraction. In Section 5.4 an example of digital μ HPIV application is presented, which is the velocity measurement of a micro-scale jet flow. In Section 5.4.1, the experimental layout to take digital holograms of micro-scale fluid flow is introduced. In Section 5.4.2, the measurement results are examined and discussed. Section 5.4.3 discusses vector cluster analysis, which is of concern in the implementation and application of μ HPIV. The conclusion of this chapter is given in section 5.5.

5.2 Review of μ PIV

Rapid progress in micro- and nano-technologies has fuelled a growing interest to develop microfluidic devices that can manipulate and transport relatively small volumes of fluid. For further development of microfluidic devices, e.g., Micro-Electro-Mechanical systems (MEMS) (Rai-Choudhury 2000) or lab-on-a-chip devices (<http://www.lab-on-a-chip.com/home/index.aspx>), quantitative measurements of micro scale flow have been required to understand the physics of the transport process with spatial resolutions of the order of a few microns. The PIV technique has been well established for macroscopic flows (Adrian 1991), however, it is limited to maximum spatial resolutions of 0.2–1.0mm (Urushihara *et al.* 1993) using typical hardware. In order to achieve micro scale velocity measurements, novel developments in PIV image recording hardware, flow-tracing particles, system design, and analysis software are required (Wereley *et al.* 2003).

μ PIV refers to application of PIV to measure velocity fields of fluid motion with length scales of order 100 μ m, and with spatial resolutions of order 1-10 μ m (Wereley *et al.* 2003). This technique was introduced by Santiago *et al.* in 1998 as a means to investigate flow structures of two components in the object plane of a microscope (Santiago *et al.* 1998) and was further improved by Meinhart *et al.* (Meinhart *et al.* 1999). Essentially, it is the same as digital PIV, but the particle images are taken from the object plane of a microscope. So the recorded particle image plane is defined by the depth of the field rather than by a light sheet. Only two component planar velocities are measured. Figure 5-1 is a schematic of a typical μ PIV system, originally described by Meinhart *et al.* (Meinhart *et al.* 1999). The illumination light is delivered to the microscope through beam-forming optics, which can consist of a variety of optical elements that will sufficiently modify the light so that it will fill the objective lens, and illuminate the microfluidic device. The microfluidic test section must have at least one optically transparent wall, so that it can be viewed through the microscope lens. Typically, the

working fluid is directed through the microfluidic device by pressure or induced electrokinetically. The working fluid is often seeded with fluorescent particles. A Barrier filter is positioned between the mirror and the relay lens. The barrier filter is usually a low pass filter that filters out the illumination light that is reflected by the surface of the test section or scattered by the particles. A sensitive large-format interline-transfer CCD camera is commonly used to record the particle image fields.

In his initial experiments, Santiago measured the surface-tension driven Hele-Shaw flow around a roughly cylindrical obstruction with a $30\mu\text{m}$ axis. A bulk velocity of $50\mu\text{m/s}$ was measured with a spatial resolution of $6.9\mu\text{m}\times 6.9\mu\text{m}\times 1.5\mu\text{m}$, based on the size of the interrogation window and the depth-of-field of the microscope. Each interrogation spot was overlapped by 50%, producing approximately 900 vectors over a $120\mu\text{m}\times 120\mu\text{m}$ field.

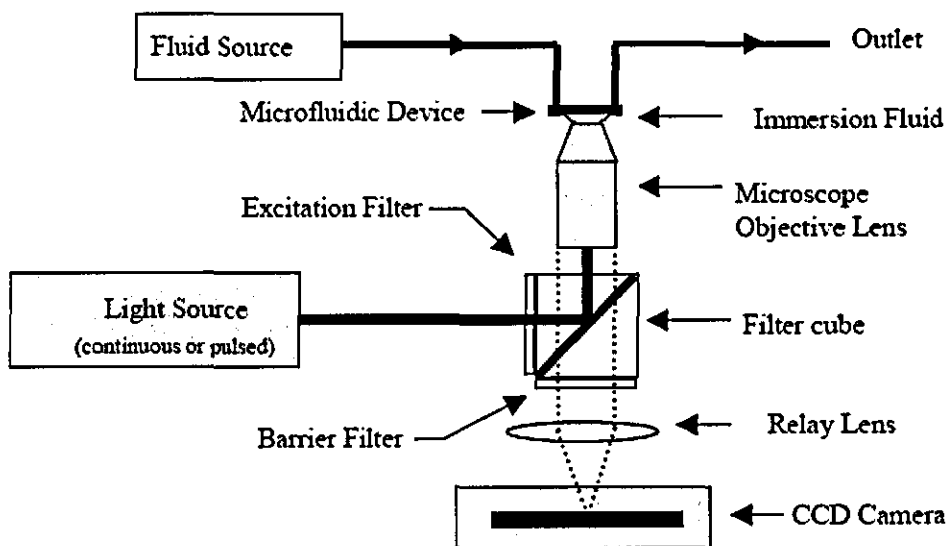


Figure 5-1 Schematic of a μPIV system (after Meinhart et al)

Two fundamental characteristics differentiate μ PIV and conventional macro-PIV. One is that the particles become so small that the effects of Brownian motion must be addressed. In Santiago's work, the effect of Brownian motion was eliminated by an eight-image time-averaged method. Another research group has developed a spatially averaged, time-resolved particle tracking velocimetry (SAT-PTV) method in order to eliminate the effect of Brownian motion in an unsteady flow (Yamamoto *et al.* 2003). These methods could be applied to eliminate the effect of Brownian motion in the μ HPIV technique.

The other fundamental problem that differentiates μ PIV from conventional macro-PIV is the illumination source, which is typically not a light sheet but an illuminated volume of the flow. This is because diffraction effects mean that it is impossible to produce a light sheet that is the order of a wavelength thick. Later work (Meinhart *et al.* 1999), considered the need of high numerical aperture (NA), sparse seeding and ensemble averaged results, to ensure that the plane of interest is sufficiently well defined. Velocity measurements of laminar flow with a higher spatial resolution close to the wall ($13.6\mu\text{m} \times 0.9\mu\text{m} \times 1.8\mu\text{m}$) and a lower resolution away from the wall ($13.6\mu\text{m} \times 4.4\mu\text{m} \times 1.8\mu\text{m}$) were obtained in a $30\mu\text{m} \times 300\mu\text{m} \times 25\text{mm}$ rectangular microchannel.

The first μ PIV measurement in circular tubes was obtained by Koutsiaris *et al.* (Koutsiaris *et al.* 1999). They used a 20W Halogen lamp to illuminate the a glycerol suspension of $10\mu\text{m}$ diameter glass spheres flowing through $\sim 200\mu\text{m}$ diameter glass capillaries. The $10\mu\text{m}$ diameter particle size allowed for relatively short exposure times with continuous illumination. The spatial resolution of these measurements was approximately $26\mu\text{m}$.

The μ PIV technique has been applied to a variety of flow regimes. A few of these examples range from fundamental studies of fluid motion (Tretheway *et al.* 2002), to

practical applications such as commercial inkjet print heads (Meinhart *et al.* 2000), and BioMEMS devices like electrokinetic-based devices (Santiago 2001).

Currently, μ PIV is able to deliver thin 2D planes of velocity measurement that can be scanned in the third dimension to construct two-component, three-dimensional velocity measurement within a volume. It is clear that, if a reference beam is brought into the CCD sensor plane, a hologram of the seeding particles is then recorded by the CCD camera in a similar way to the photographic HPIV shown in Figure 4-16. It should therefore be possible to make 3C-3D measurement of small scale flows. This is what the author refers to as μ HPIV and is discussed in detail in the following sections.

5.3 Digital μ HPIV

As described in Chapter 2, in parallel efforts, researchers have investigated HPIV as a means to make three-component velocity measurements from a three-dimensional volume of interest. Unlike scanning PIV, HPIV relies on holography to record and retrieve 3D images of the tracer particles, from which 3C-3D displacements of the particles are extracted. In particular, 3D-CAC analysis of the wavefront data stored by a hologram has been shown to be inherently tolerant to aberrations induced by poor quality windows for example (Coupland *et al.* 1996). A variant of HPIV is presented to measure 3C-3D fluid velocity within micro-fluidic devices, which is called Micro Holographic Particle Image Velocimetry (μ HPIV).

In recent years digital HPIV has become an attractive technique due to its simple implementation. Digital HPIV includes three basic steps, the same as the conventional HPIV, but implemented in purely digital environment. Firstly, a CCD camera records holograms of flow tracer particles. The holograms are then numerically reconstructed to estimate the original object wave. Finally, from the reconstructed wave field, particle 3D

velocities can be extracted. Compared to conventional holographic techniques, digital recording and numerical reconstruction of holograms offer new possibilities in optical metrology. Since the hologram is coded numerically as a digitized image, it is not necessary to process a photographic plate to reconstruct a real image. Moreover, the numerical reconstruction of the complex amplitude allows straightforward access to phase (Grilli *et al.* 2001).

The large pixel size of electronic image sensors is often seen as the major barrier for digital HPIV. However, the effective pixel size can be arbitrarily chosen by employing imaging lenses in the holographic recording system if the flow field is small. High numerical aperture recording can be made on current CCDs with no loss of information. In this section the implementation of μ HPIV is demonstrated with a standard CCD imaging device in a purely digital environment.

5.3.1 Digital recording

To make simultaneous holographic recording of micro scale flow, a transmission microscope utilizing coherent detection is used. Figure 5-2 illustrates the principle of digital μ HPIV. The object beam passes through the flow of interest and carries the information of the seeded particles. The seeded particles are imaged to the CCD plane by the objective lens (which introduces a phase curvature). To increase SNR a high-pass optical filter is used to stop the DC component in the object beam. For holographic recording, a reference beam is brought into the CCD plane. If a reference beam is well conditioned to diverge from a point that is in the (virtual) far focal plane of the imaging objective lens, the phase curvature introduced by the imaging process is exactly matched by the curvature of the reference beam. This is proved in the following section.

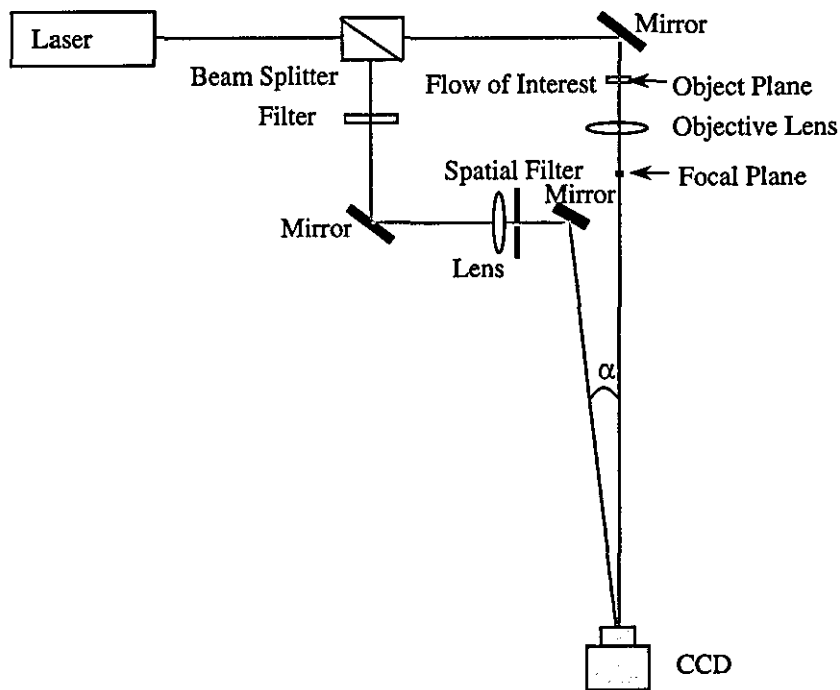


Figure 5-2 Digital micro HPIV

According to paraxial imaging theory, the image complex amplitude U_i at coordinates (x_i, y_i) at a distance z_i behind the lens is given in terms of the object complex amplitude $U_o(x_o, y_o)$, such that,

$$U_i(x_i, y_i) = \left[\frac{1}{M} U_o\left(-\frac{x_i}{M}, -\frac{y_i}{M}\right) \otimes h(x_i, y_i) \right] \exp\left[j \frac{\pi}{\lambda z_i} \left(1 + \frac{1}{M} \right) (x_i^2 + y_i^2) \right] \quad (5-1)$$

where M represents the magnification of the system, \otimes denotes convolution and $h(x_i, y_i)$ is the point-spread function. In practice, the impulse response, $h(x_i, y_i)$, defines diffraction limit and hence the minimum size of the recorded particle images. To simplify the analysis, however, the diffraction limit is assumed to be sufficient to resolve the optical field and the image complex amplitude $U_i(x_i, y_i)$ of Equation (5.1) is a magnified

version of the object amplitude distribution multiplied by a quadratic phase distribution such that,

$$U_i(x_i, y_i) = U_o\left(-\frac{x_i}{M}, -\frac{y_i}{M}\right) \exp\left[j\frac{\pi}{\lambda z_i}\left(1 + \frac{1}{M}\right)(x_i^2 + y_i^2)\right] \quad (5-2)$$

In this work the off-axis reference beam, $U_r(x_i, y_i)$ diverges from a (virtual) point that is in the far focal plane of the imaging object lens. This is essentially the image of a tilted plane wave in the object plane and as such, the complex amplitude of the reference beam $U_r(x_i, y_i)$ can be written as

$$U_r(x_i, y_i) = \exp(j2\pi x_i \sin \alpha / \lambda) \exp\left[j\frac{\pi}{\lambda z_i}\left(1 + \frac{1}{M}\right)(x_i^2 + y_i^2)\right] \quad (5-3)$$

where α is the angle between the reference beam and the object beam (Figure 5-2).

Finally, the intensity distribution at the CCD plane $I(x_i, y_i)$ is given by

$$I(x_i, y_i) = 1 + |U_o|^2 + U_o\left(-\frac{x_i}{M}, -\frac{y_i}{M}\right) \exp(-j2\pi f_{x_i} x_i) + U_o^*\left(-\frac{x_i}{M}, -\frac{y_i}{M}\right) \exp(j2\pi f_{x_i} x_i) \quad (5-4)$$

where $f_{x_i} = \frac{\sin \alpha}{\lambda}$ is the spatial frequency of the carrier fringes and λ is the wavelength.

It can be seen that the phase curvature introduced by the imaging process is exactly matched by the curvature of the reference beam, as shown in Figure 5-3, such that straight carrier fringes are observed in the CCD array plane in the absence of any object. In this way, the carrier modulated intensity distribution $I(x_i, y_i)$ can be thought of as a holographic recording of the optical field in *the object plane of the objective* (shown in Figure 5-4). It is noted, however, that the carrier frequency can be much higher than that which could be physically created by introducing a reference wave on the object side of the objective lens.

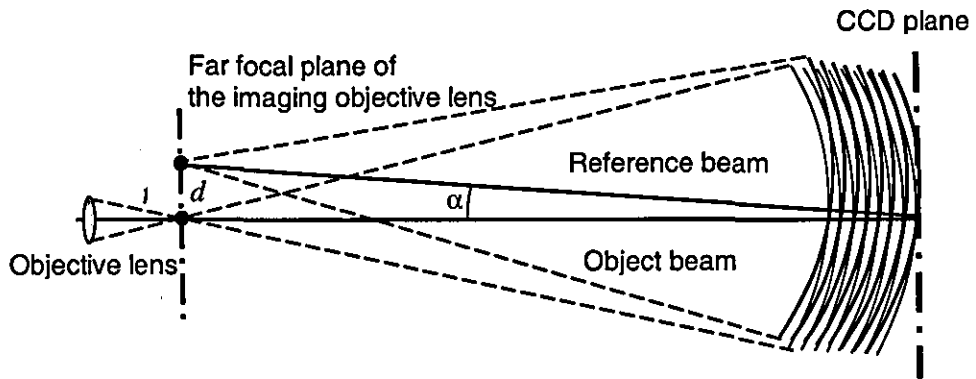


Figure 5-3 Phase curvature match

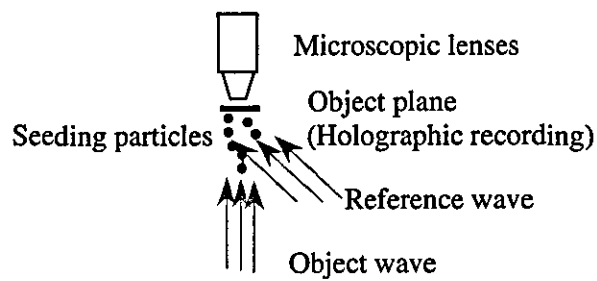


Figure 5-4 A holographic recording of the optical field in the object plane of the objective.

A practical problem in recording an off-axis hologram using a CCD camera is the restriction of the angle between the reference and object wave due to the spatial frequency limitation. The light-sensitive material used to record holograms must resolve the interference pattern resulting from superposition of the object and reference wave. Holographic emulsions have resolutions up to $5000lp/mm$. With these materials, holograms with angles between the reference and the object wave of up to 180° can be recorded. However, the typical pixel size of a CCD is only of about $\Delta x \approx 5\mu m$. The corresponding maximum resolvable spatial frequency calculated by

$$f_{\max} = 1/2\Delta x \quad (5-5)$$

is therefore of about $100lp/mm$. As the spatial frequency of the carrier fringes $f_{x_i} = \frac{\sin \alpha}{\lambda}$, the maximum angle between the reference and the object wave is restricted to a few degrees (3°).

The limited angle between the reference and object wave means that only low NA lensless off-axis holograms can be made. However, this problem can be solved in μ HPIV. As shown in Figure 5-3, the distance between the reference and the object beam in the focal plane of the objective lenses, d , can be calculated by the geometry to give

$$d \approx \frac{(M-1)\phi \tan \alpha}{2NA} \quad (5-6)$$

where ϕ is the diameter of the objective lenses, M is the magnification of the imaging system. For the author's μ HPIV experiment (described in Section 5.4), where M is the order of 14 and NA is about 0.25, the distance d is about 2ϕ . This distance is wide enough to assemble the optical elements to take large numerical aperture, off-axis, digital holograms.

5.3.2 Numerical reconstruction

In conventional digital holography the Fresnel-Kirchoff integral is used to calculate the intensity and the phase distribution of the reconstructed real image, however, the direct numerical processing of the Fresnel-Kirchoff integral is time consuming. In the case of the digital μ HPIV recording described above, the whole optical field can be reconstructed by the Fast Fourier Transform (FFT) based convolution approach more efficiently.

As the intensity distribution $I(x_i, y_i)$ recorded by the CCD camera is thought of as a magnified holographic recording of the optical field in the object plane of the objective, the signal can be demodulated to find the complex amplitude in the object plane of the imaging system. Using a 2D Fourier transform to demodulate the recorded carrier intensity distribution $I(x_i, y_i)$ of Equation (5-4), we have

$$\begin{aligned} \text{FT}[I(x_i, y_i)] = & \delta(f_x, f_y) + \text{FT}[|U_o|^2] + \text{FT}[U_o(-\frac{x_i}{M}, -\frac{y_i}{M})]\delta(f_x - f_{x_i}, f_y) \\ & + \text{FT}[U_o^*(-\frac{x_i}{M}, -\frac{y_i}{M})]\delta(f_x + f_{x_i}, f_y) \end{aligned} \quad (5-7)$$

where δ is a delta function and FT represents Fourier transformation. Isolating the third term of Equation (5-7), using inverse Fourier transformation and then scaling by the system magnification, the optical field complex amplitude in the object plane of the microscope $U_o(x_o, y_o; 0)$ can then be obtained.

Since it is usual for the object plane of the imaging system to be somewhere within the flow field, the optical field in different planes can be reconstructed from this plane using the free-space propagation equation. The object spatial frequency spectra in the object plane $S(k_x, k_y; 0)$ is given by the Fourier transformation of optical field complex amplitude, such that

$$S(k_x, k_y; 0) = \iint U_o(x_o, y_o; 0) \exp[-2\pi j(k_x x_o + k_y y_o)] dk_x dk_y \quad (5-8)$$

The spatial frequency spectra at a parallel plane z can be calculated by following the frequency plane formulation of free-space propagation,

$$S(k_x, k_y; z) = S(k_x, k_y; 0) H(k_x, k_y; z) \quad (5-9)$$

where $H(k_x, k_y; z) = \exp(j2\pi z \sqrt{1/\lambda^2 - k_x^2 - k_y^2})$ is the transfer function of the wave propagation. The optical field complex amplitude at a parallel plane z can be obtained by taking an inverse Fourier transform of Equation (5-9),

$$U_o(x_o, y_o; z) = \iint S(k_x, k_y; z) \exp[2\pi j(k_x x_o + k_y y_o)] dk_x dk_y \quad (5-10)$$

From the analysis above, the whole process to calculate the optical field complex amplitude can be carried out more efficiently using the fast Fourier transform algorithm.

5.3.3 Data extraction

In digital μ HPIV two single-exposure holograms separated by a short time are recorded by CCD camera. By numerical reconstruction the complex amplitudes of the two recorded particle fields are then available for further processing. Each reconstructed particle field is divided into a grid of small sections or interrogation areas. The complex amplitude of the optical field transmitted by the corresponding interrogation areas can be decomposed into its spectrum of plane-wave components respectively defined by the two-dimensional Fourier transformation, from which the cross-spectral density can be calculated. The cross-spectral density is then used to extract the 3D displacement by digital shearing method or 3D complex amplitude correlation method. The detailed processing steps are the same as described in previous chapters.

This process is repeated at each interrogation area within the optical field, resulting in a 3D map of velocity vectors to describe the flow. The proposed processing method described above can be summarized as the following steps shown in Figure 5-5 and are illustrated in next section.

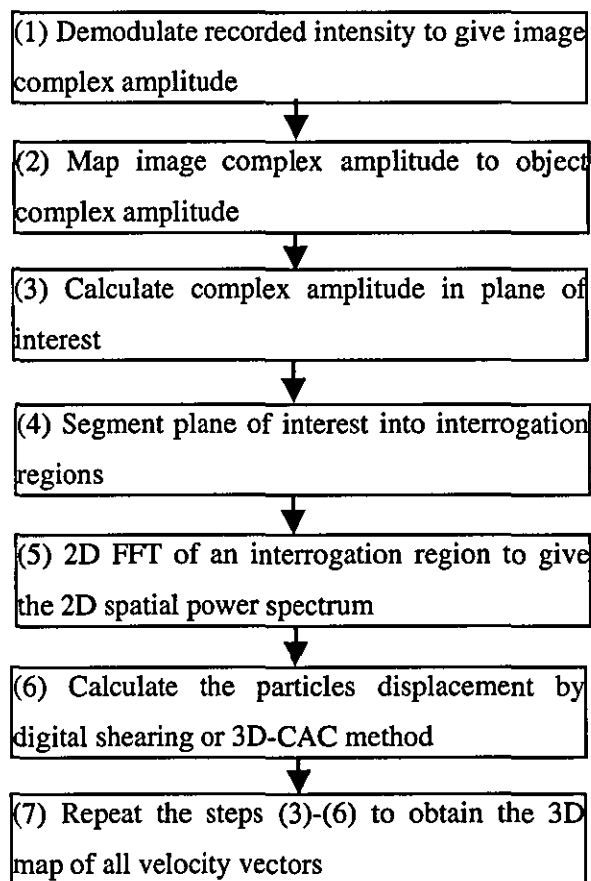


Figure 5-5 Flow chart of the digital μ HPIV

5.4 3C-3D measurement of the micro-scale jet flow

The principle of digital μ HPIV has been described in previous section. In this section, the digital μ HPV method will be applied to velocity measurement in micro-scale fluid mechanics. A micro-scale jet flow was designed for the μ HPIV experiment. Numerical reconstruction and data extraction is implemented, following the procedure described in section 5.3. Practical problems, such as vector clustering, are then discussed.

5.4.1 Experimental layout

The experimental configuration shown in Figure 5-6 is based on Figure 5-2, which is used to make simultaneous holographic recording of the jet flow inside a micro-channel. A Q-switched, diode pumped, frequency doubled Nd: YAG laser is used as the optical source. The collimated laser beam (wavelength $\lambda=532nm$) is divided by the beam splitter into two beams: one of these, the object beam, is a spherical wave produced by an objective lens of focal length $55mm$ and $f\#=2$; the other one is a reference beam which diverges from a (virtual) point that is in the far focal plane of the imaging lens. The magnification of the imaging system is 14. The hologram pattern is digitized by a CCD camera and straight interference fringes are observed in the CCD array plane in the absence of any object. The system NA is restricted by the objective lens $f\#$ to about 0.25, the field of view (corresponding to the size of the field in the object plane) was approximately $600\mu m \times 500\mu m$. As the maximum fringe frequency of the interference pattern which can be resolved by the CCD camera array is the inverse of twice the pixel size ($6.8\mu m$), this gives a maximum reference beam angle, α , of about 2.5° .

The pulsed laser and the CCD camera are synchronous controlled by the software on a PC. The software was written in MatLab. The PixeLink PL-A630 CCD array of 1280x1024pixels operating at 3fps is used to record a sequence of holograms.

The micro-channel comprises of a quartz glass capillary 50mm long with a cross section 5mm by 2mm (shown in Figure 5-7). The liquid (deionised water) is seeded with hollow glass micro-spheres approximately 5 μ m in diameter. The liquid is delivered into the capillary by a hypodermic needle with a diameter of 0.25mm and the flow rate is approximately 0.5mm³/s.

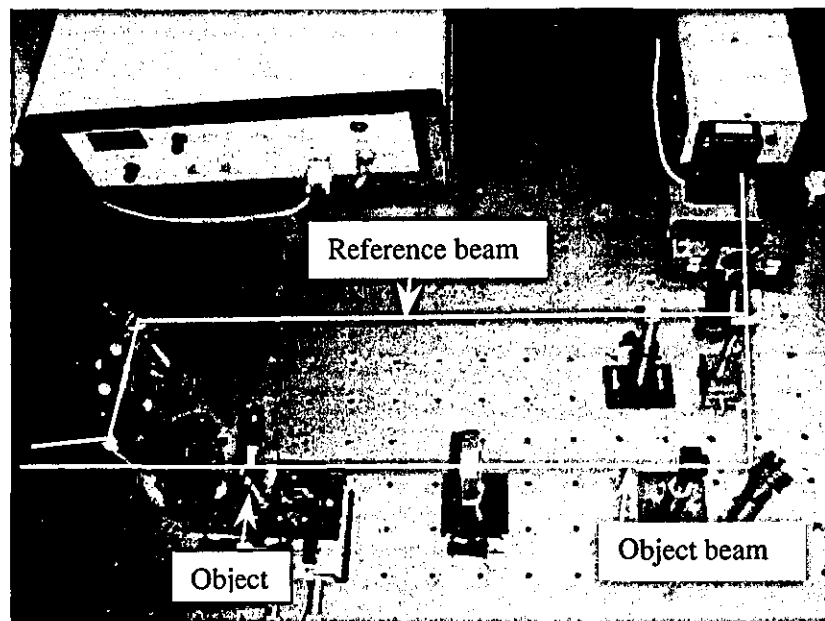
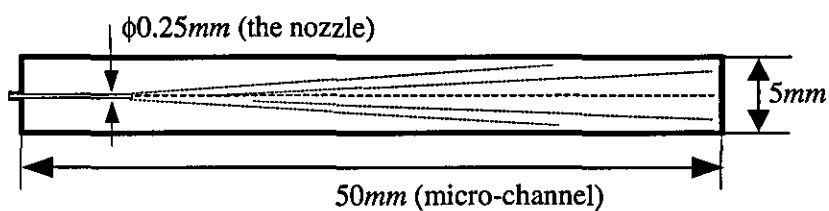
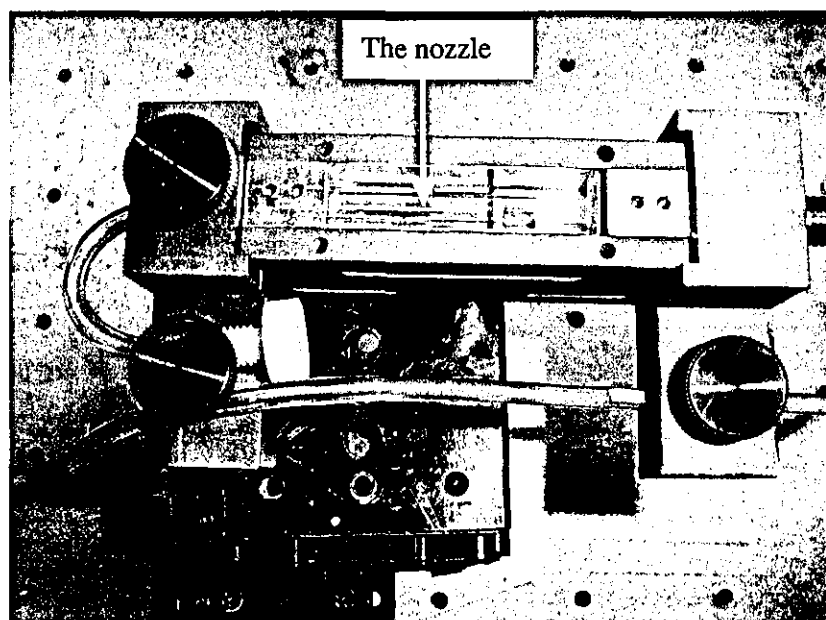


Figure 5-6 Off-axis forward scattering μ HPIV imaging system



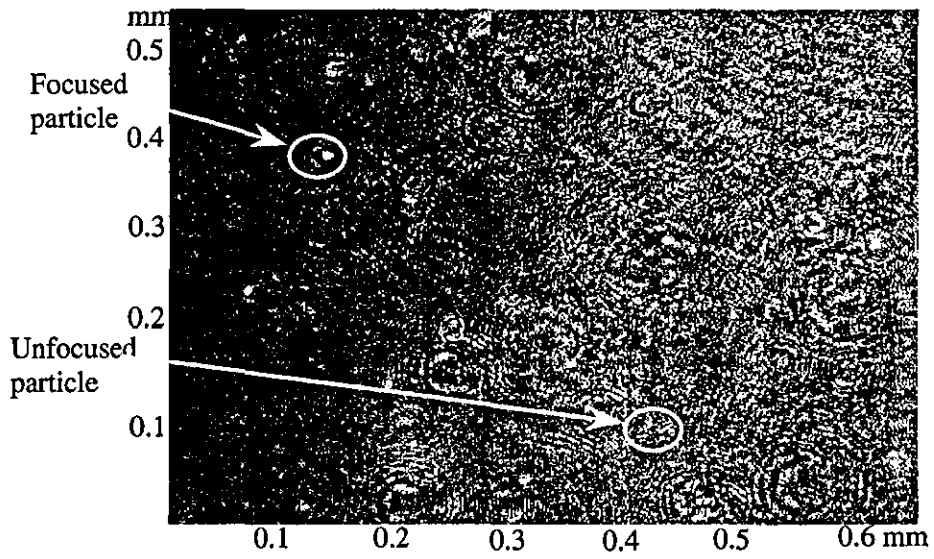
(a) Dimensional sketch



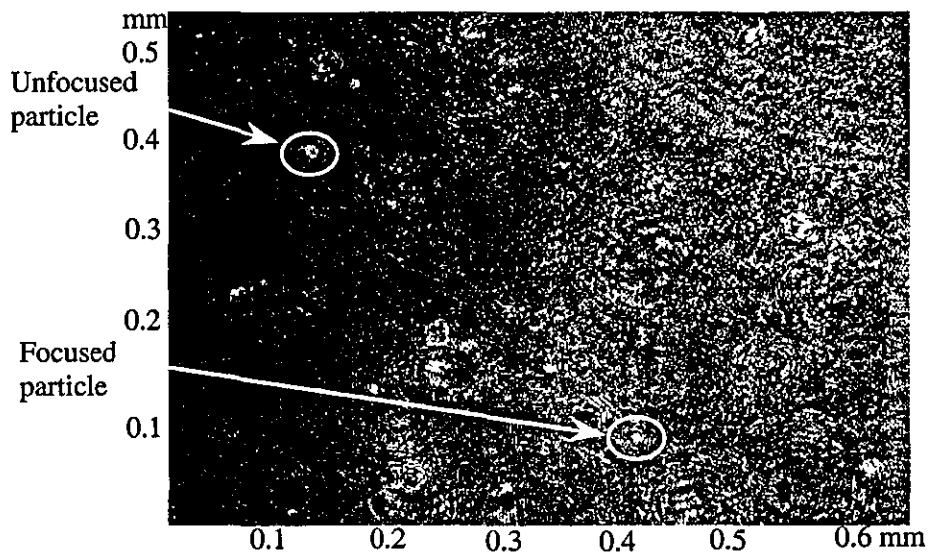
(b) Experimental configuration

Figure 5-7 Micro channel

Figure 5-8 (a) and (b) show the first and second exposure holograms of free jet fluid flow respectively, which is recorded by the set-up described above. It can be clearly seen that the particle marked with circle on the top-left side is in-focus in the first exposure hologram and out-of-focus in the second hologram.



(a)



(b)

Figure 5-8 (a) First and (b) second exposure hologram

5.4.2 Experimental results

After the digital holograms are recorded and transferred into the computer, the real challenge is to extract the particle displacement. The analysis of each sequential pair of particulate holograms was as follows. First the optical field was reconstructed in 20 planes separated by $30\mu\text{m}$ by demodulating the recorded intensity to find the complex amplitude, and using the frequency plane formulation of free-space propagation as discussed in section 5.3.2. Figure 5-9 presents the numerical reconstructed particle images at the object plane from Figure 5-8. Figure 5-10 and Figure 5-11 present the reconstructed particle images at distance $z=-0.12\text{mm}$ and $z=-0.21\text{mm}$ from the object plane respectively. It can be seen that the sub-picture marked with white box is focused at $z=-0.12\text{mm}$ (Figure 5-10).

Subsequently, the particle velocity is calculated using complex amplitude cross-correlation technique on each 64×64 pixels interrogation area of this field. When projecting into the fluid, the correlation windows are about $30\mu\text{m}\times 30\mu\text{m}$. The interrogation spots are overlapped by 50%, yielding a velocity-vector spacing of $15\mu\text{m}\times 15\mu\text{m}$. Figure 5-12 shows the 3D cross-correlation intensity of marked sub-pictures in the Figure 5-9, Figure 5-10 and Figure 5-11, respectively. In all, 25,600 cross-correlations were calculated in this way from each pair of holographic images.

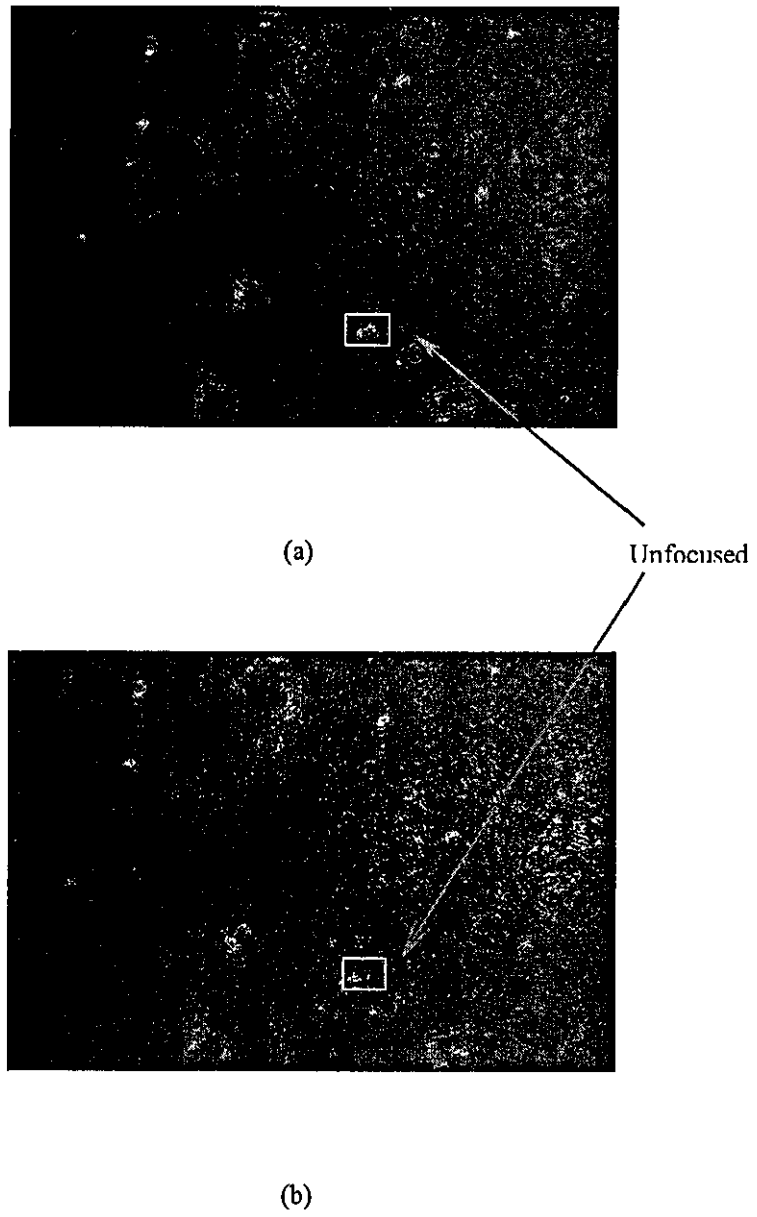


Figure 5-9 Reconstructed particle image from Figure 5-8

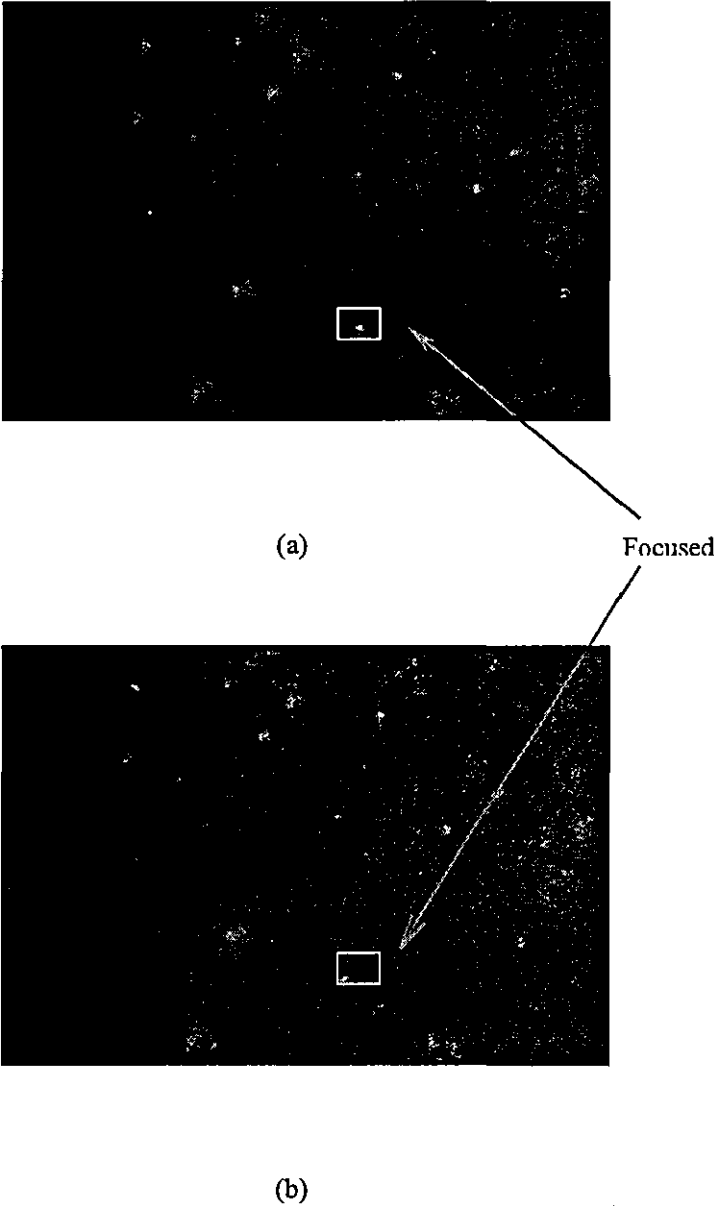


Figure 5-10 Reconstructed particle image at $z=-0.12mm$

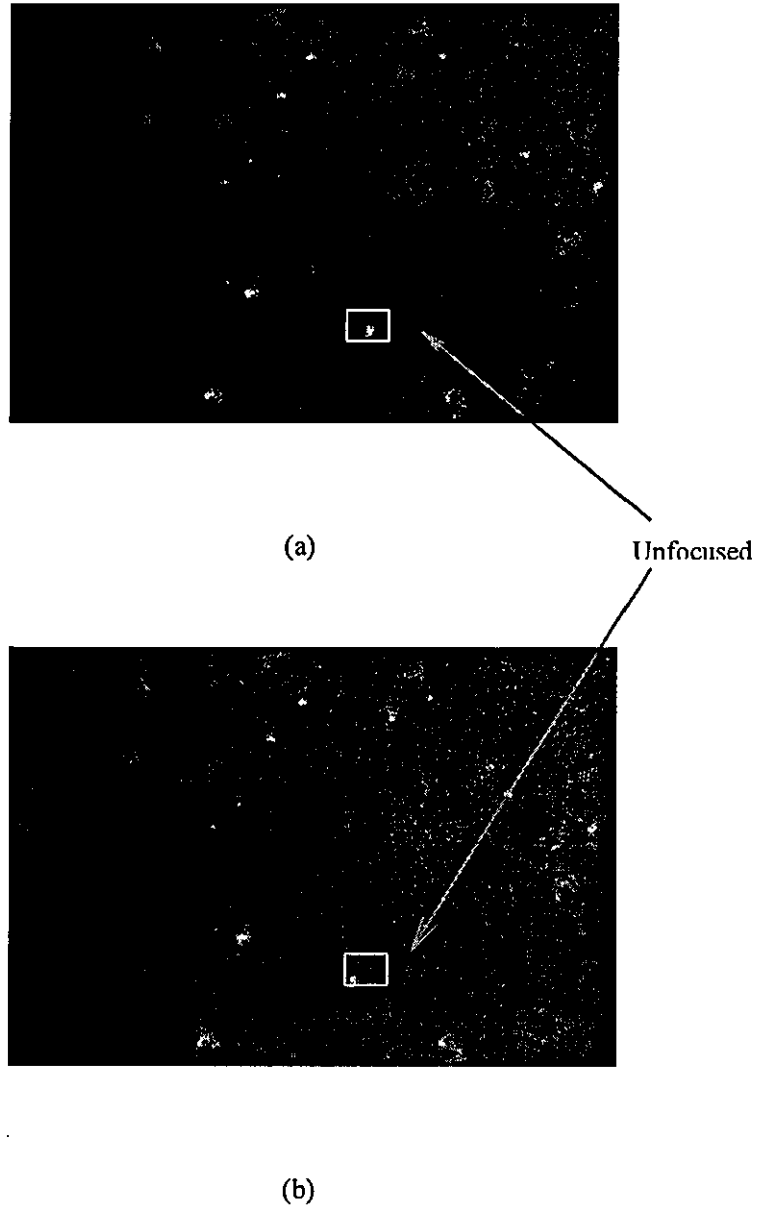
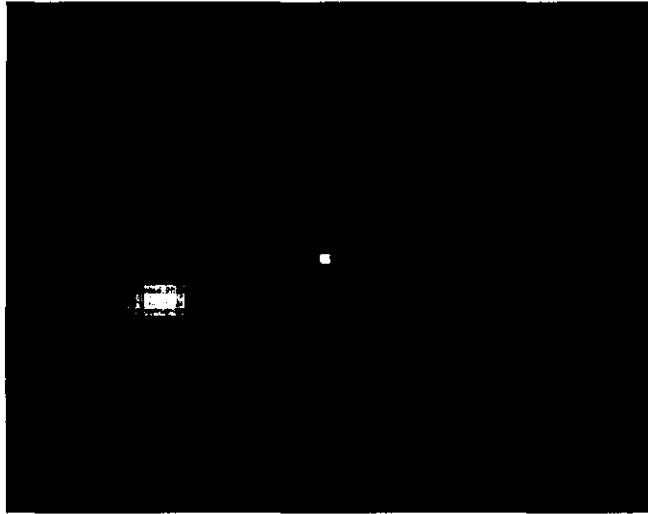
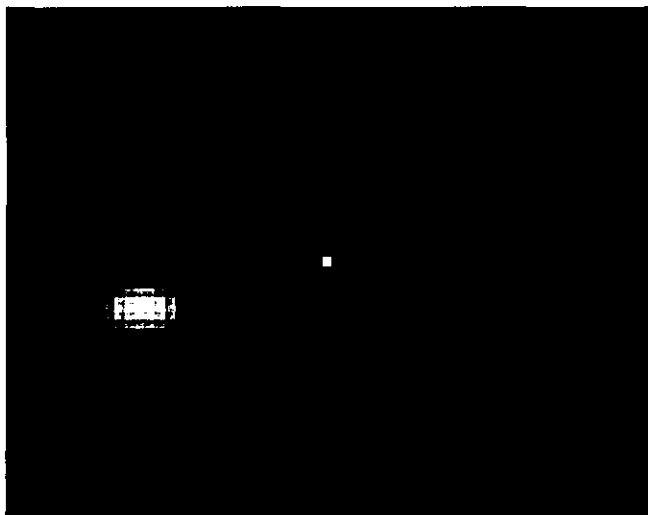


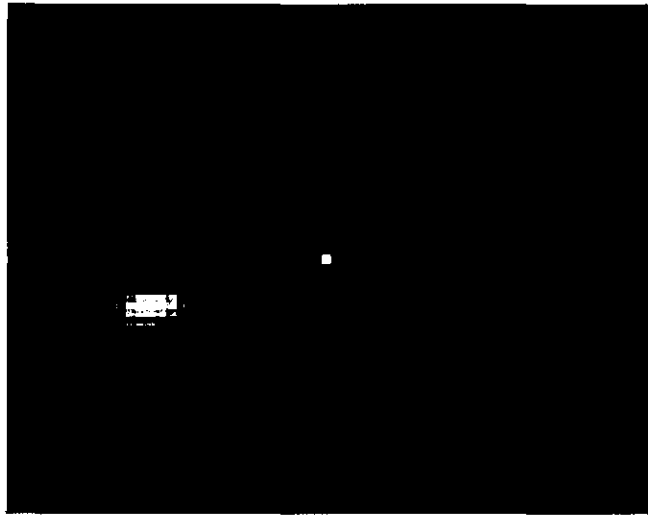
Figure 5-11 Reconstructed particle image at $z=-0.21mm$



(a)



(b)



(c)

Figure 5-12 3D cross-correlation intensity of marked sub-pictures in the (a) Figure 5-9, (b) Figure 5-10 and (c) Figure 5-11 (the centre pixel is a zero velocity reference)

5.4.3 Vector cluster analysis

In all the μ HPIV experiments to date, the flow was relatively sparsely seeded with $5\mu m$ hollow glass micro-spheres and this has highlighted some fundamental issues concerning the analysis procedure. For the case of sparse seeding, it is noted that a correlation signal is observed above the background (stationary noise caused by scattering from windows etc.) over a cluster of interrogation regions. This is most noticeable in the depth direction. Figure 5-13 displays the magnitude of the cross-correlation peak as a function of depth-ordinate, z , for a set of interrogation regions and it can be seen that the signal could be attributed to a particle located approximately $0.12mm$ from the object plane of the microscope. Figure 5-14 shows the corresponding 3C particle displacement vectors that have been extracted from the correlation peak position. It can be deduced that the displacement of this particle is approximately $\Delta x = -28.38\mu m$, $\Delta y = -9.02\mu m$ and $\Delta z = 4.12\mu m$

and these measurements are reasonably consistent over the space defined by the width of the peak in Figure 5-13.

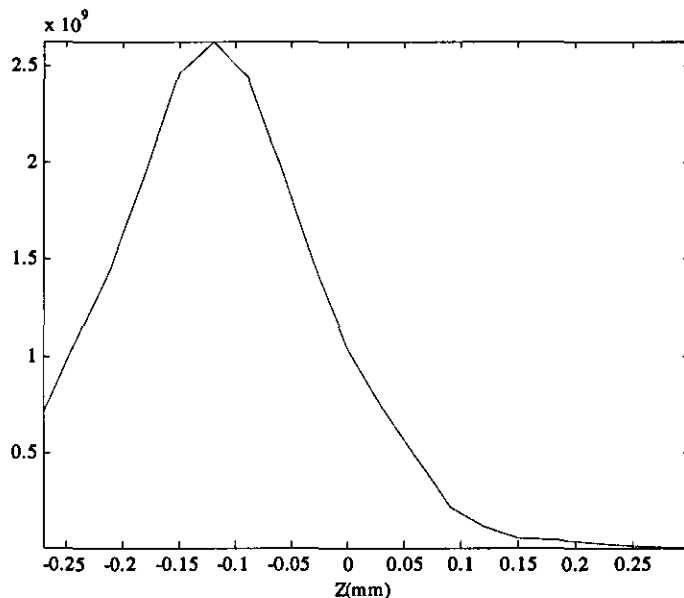


Figure 5-13 The correlation peaks of marked sub-pictures throughout the z-direction

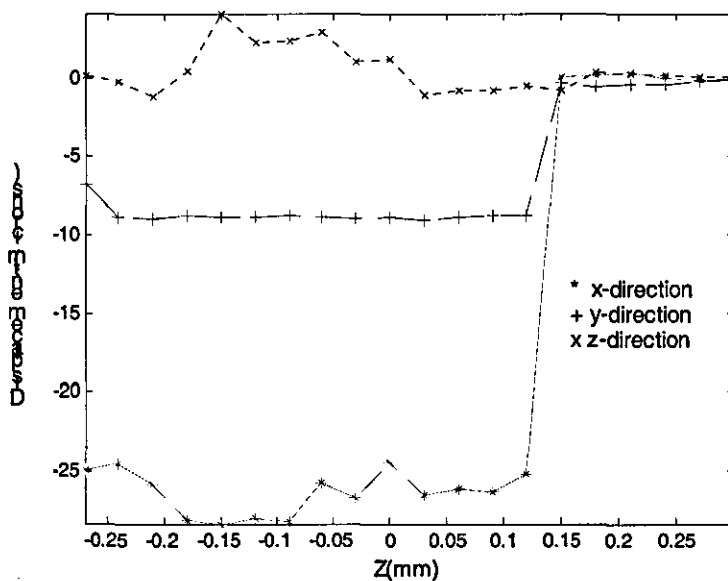
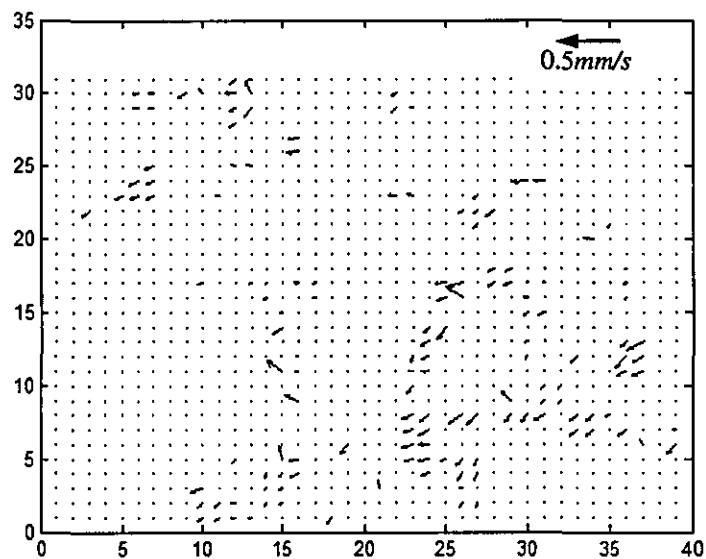
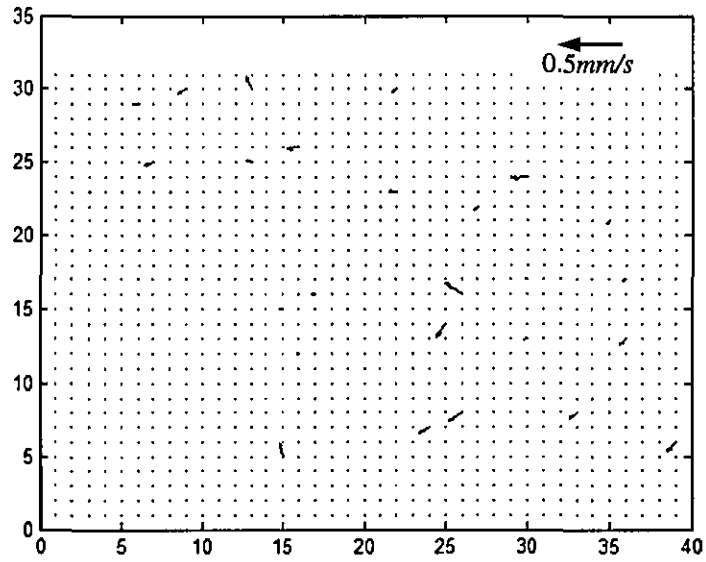


Figure 5-14 The calculated three-component displacement vectors from the correlation peaks position throughout the depth-direction of the flow volume

It is clear from the results that a method is needed to assign the measured displacement to a velocity at a particular point in the flow. As the seeding concentration is increased, there could be a number of peaks in each correlation. These peaks correspond to the movement of particles that are both in and out-of-focus. However, the largest correlation peak is expected to correspond to the brightest particle image. A suitable method is needed to locate this in 3D space. The method used here is to cluster the measured data into regions identified by high correlation strength (as shown in Figure 5-13). The measured velocity is then ascribed to the geometric centre of this cluster and all other data from the cluster is discarded. Figure 5-15 (a) and (b) shows the in-plane two components velocity map in the image plane before and after the measurement data is identified, respectively. Using this approach 137 vectors have been extracted from the 25,600 correlation measurements and are shown in the quiver plot of Figure 5-16. These vectors that have been simultaneously measured throughout the $0.5 \times 0.6 \times 0.6 \text{ mm}^3$ volume clearly show behaviour of the jet flow.



(a)



(b)

Figure 5-15 In-plane two components velocity map in the image plane (a) before and (b) after the measurement data is identified

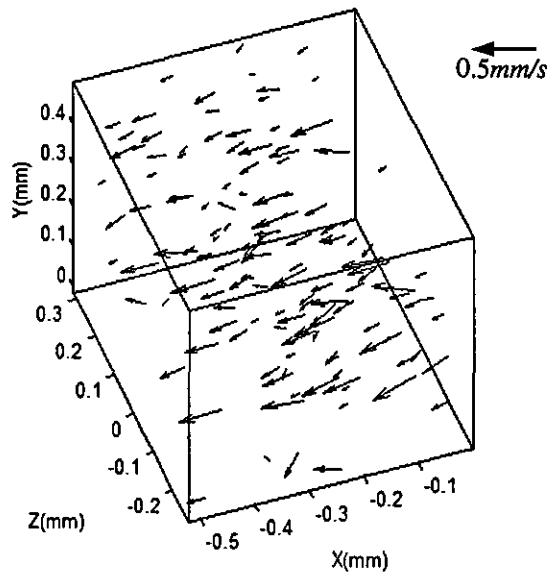


Figure 5-16 Three-dimensional velocity map of free jet fluid flow (137 vectors in the size of $0.5 \times 0.6 \times 0.6 \text{ mm}^3$ volume)

5.5 Summary

In this chapter digital μ HPIV has been investigated as a means to make 3C-3D measurements in micro-fluidics. In particular, digital holographic recording and numerical reconstruction has been discussed in detail. As the off-axis reference beam diverges from a point in the far focal plane of the imaging lens, the phase curvature introduced by this imaging lens is cancelled and the carrier modulated intensity distribution can be thought of as a holographic recording of the optical field in the object plane of the objective. The complex amplitude of the optical field in any plane is reconstructed by a FFT based convolution approach, which is more efficient than the direct numerical processing.

Digital μ HPIV has been applied to make 3C-3D measurements of the micro-scale jet flow. An object of about $0.5\text{mm} \times 0.6\text{mm}$ has been magnified 14 times and imaged into the CCD camera. The flow field has been numerically reconstructed into 20 planes with the interval of $30\mu\text{m}$. Complex amplitude correlation has been applied to each $30\mu\text{m} \times 30\mu\text{m}$ interrogation area (with 50% overlap) to calculate the seeding particle displacement. The results clearly demonstrate the potential of μ HPIV with complex amplitude correlation analysis for 3C-3D velocity measurements in micro-fluidics.

One interesting feature of the analysis procedure applied here is the method by which vectors are assigned to a point in space. For the case of sparse seeding, it was found that a cluster of interrogation regions provided the same measurement of particle displacement. In the analysis procedure this cluster was identified and the measured displacement was applied to the interrogation region at the centre of the cluster. In this way 137 vectors have been obtained from the 25,600 correlations.

The number of vectors measured by the technique would clearly be improved through seeding the flow more densely, however, the SNR will decrease proportionally due to the

contribution of out-of-focus particles. In practice there needs to be a balance between SNR and the density of seeding particles that includes contributions from light scattered by dirty windows and other artefacts in the optical path. An experimental programme to determine the information capacity of μ HPIV is discussed in the following chapter.

5.6 References

Adrian, R. J., 1991, "Particle-imaging technique for experiment fluid dynamics", *Ann. Rev. Fluid. Mech.*, vol.23, p261-304.

Coupland, J. M. and Halliwell, N. A., 1996, "Holographic particle image velocimetry: immunity from aberration by optical information processing", *Proceeding of IMechE.*, City University, London, UK, p359-376.

Grilli, S. and Ferraro, P., 2001, "Whole optical wavefields reconstruction by digital holography", *Optical Express*, vol.9(6), p294-302.

Koutsiaris, A. G., Mathioslakis, D. S. and Tsangaris, S., 1999, "Microscope PIV for velocity-field measurement of particle suspensions flowing inside glass capillaries", *Measurement Science and Technology*, vol.10, p1037-1046.

Meinhart, C. D., Wereley, S. T. and Santiago, J. G., 1999, "PIV measurement of a microchannel flow", *Experiment in Fluids*, vol.27, p414-419.

Meinhart, C. D. and Zhang, H. S., 2000, "The flow structure inside a microfabricated inkjet printhead", *Journal of MEMS*, vol.9(1), p67-75.

Rai-Choudhury, P., Ed. 2000, *MEMS and MOEMS: Technology and Applications*, SPIE Press Monography.

Santiago, J. G., 2001, "Electroosmotic flows in microchannels with finite inertial and pressure forces", *Anal. Chem.*, vol.73, p2353-2365.

Santiago, J. G., Wereley, S. T., Meinhart, C. D., Beebe, D. J. and Adrian, R. J., 1998, "A micro particle image velocimetry system", *Experiment in Fluids*, vol.25(4), p316-319.

Tretheway, D. and Meinhart, C. D., 2002, "Fluid slip near hydrophobic microchannel walls", *Physics of Fluids*, vol.14(3), pL9-L12.

Urushihara, T., Meinhart, C. D. and Adrian, R. J. (1993). Investigation of the logarithmic layer in pipe flow using particle image velocimetry in near-wall turbulent flows. Elsevier. al., R. M. C. S. e. Amsterdam: 433-466.

Wereley, S. T. and Meinhart, C. D. (2003). *Micron-Resolution Particle Image Velocimetry. Diagnostic Techniques for Microfluidics*. Breuer, K., Springer Verlag.

Yamamoto, T., Inaba, S., Y.Sato, Hishida, K. and Maeda, M., 2003, "Measurement in microchannel by laser induced molecular tagging and micro-PIV", *Sixth International Conference on Micro-TAS*, p1-13.

Chapter 6 Conclusions and Further Work

6.1 Conclusions and main contributions

This thesis has discussed work with two main objectives. One is to develop a high speed digital analysis approach to extracting 3C-3D data from holograms. This is a continuation of the work on the complex amplitude correlation analysis that was originally proposed by Coupland and Halliwell (Coupland *et al.* 1992). The other is to investigate digital μ HPIV, a method capable of measuring micro-scale fluid flow.

The main contributions that have been achieved in this thesis are summarized as follows:

(1) Definition of 3D-CAC using a formulation of scalar diffraction in 3D vector space.

A review, with specific focus on the various HPIV data extraction techniques, was presented. In particular, optical CAC was examined. The method manipulates both the phase and the amplitude of the recorded signal and because of this it is inherently immune to imaging aberration (Coupland *et al.* 1996). Although complex amplitude correlation is theoretically the most robust method to locate spatial repetition in a signal (when applied optically), it is limited by the performance of spatial light modulators and the speed of the mechanical devices used to search the output field (Barnhart 2001). In order to implement CAC digitally, the theory of CAC has been re-examined through a formulation of scalar diffraction in 3D vector space. The 2D spatial frequency spectrum is mapped onto the 3D surface of the Ewald sphere and CAC can then be implemented digitally using a single 3D FFT. However, 3D FFTs (as well as 3D peak searching) are computationally intensive.

A new technique, named the *digital shearing method*, has been developed to extract 3C particle displacement data digitally.

(2) Proposition, implementation and application of the digital shearing method.

Following the analysis of digital 3D-CAC, the digital shearing method has been introduced and defined. The formulation of the digital shearing method and its fast implementation has been discussed. In contrast to digital 3D-CAC, it has been shown that all three components of particle image displacement can be retrieved using 2D FFT operations and approximate coordinate transformations. Using a MatLab simulation the method has been illustrated in a step-by-step manner showing the effect of each operation. The performance of the digital shearing and 3D-CAC methods in terms of the computational efficiency and measurement accuracy has been evaluated. The simulated results have shown that the digital shearing method can provide much higher speed and comparable accuracy than the 3D correlation technique. From the analysis, the digital shearing method only requires about $3/8N$ of the operations required by the 3D-CAC method for an array of $N \times N$ elements. Thus the digital shearing method affords a considerable time saving over the full 3D correlation approach. As the number of pixels increases this effect becomes more pronounced. The method has also been tested by experiments, in which holograms were recorded on 35mm photographic films.

(3) Proposition, implementation and application of digital μ HPIV for 3C-3D measurement of micro-scale flow structures.

Digital μ HPIV has been investigated as a means to make 3C-3D measurements in micro-scale flow. The principle of digital μ HPIV has been analysed. In particular digital holographic recording and numerical reconstruction is discussed in detail. As the off-axis reference beam is diverged from a point that is in the far focal plane of the imaging lens, the carrier modulated intensity distribution can be thought of as a holographic recording

of the optical field in the object plane of the objective. The whole optical field complex amplitude has been reconstructed by the fast Fourier transformation based on the convolution approach, which is more efficient than the direct numerical processing. Practical issues of digital μ HPIV including vector cluster analysis and spatial frequency limitations have been discussed. Spatial frequency in μ HPIV recording is limited by the effective CCD pixel size and this can be arbitrarily chosen through the choice of magnification. For the case of sparse seeding, it was found that a cluster of interrogation regions provided the same measurement of particle displacement. In the analysis procedure this cluster was identified and the measured displacement was applied to the interrogation region at the centre of the cluster. Digital μ HPIV and CAC have been demonstrated in a real micro fluid flow. An object of $0.5\text{mm} \times 0.6\text{mm}$ was magnified 14 times and imaged into the CCD camera. The flow field has been numerically reconstructed in 20 planes separated by $30\mu\text{m}$. CAC has been applied to each $30\mu\text{m} \times 30\mu\text{m}$ interrogation area (with 50% overlap) to calculate the seeding particle displacement. Cluster analysis has been used to assign the right vectors in the right position. In this way 137 vectors have been obtained from the 25,800 correlations. The results clearly have demonstrated the potential of μ HPIV with complex amplitude correlation analysis for 3C-3D velocity measurements in micro-fluidics.

The work described in this thesis has been summarised and published in five papers.

These thesis-related papers are:

H. Yang, N. A. Halliwell and J. M. Coupland (2004), "Digital μ PIV: 3C-3D measurement of free jet fluid flow in the micro-channel", 12th International Symposium on Applications of Laser Technique to Fluid Mechanics, Lisbon, Portugal, Paper No. 5.5

H. Yang, N. A. Halliwell and J. M. Coupland (2004), "Application of digital shearing method to extract 3C velocity data in holographic PIV", *Measurement of Science and Technology*, Vol.15, p694-699

H. Yang, N. A. Halliwell and J. M. Coupland (2003), "Digital shearing method to extract three-dimensional velocity data in holographic PIV", *Applied Optics*, Vol.42, p6458-6464

H. Yang, N. A. Halliwell and J. M. Coupland (2003), "A comparison of digital shearing and 3D correlation analysis methods", *Proceedings of the International Society for Optical Engineering*, Vol.5191, San Diego, USA, p52-58

H. Yang, N. A. Halliwell and J. M. Coupland (2003), "Extraction of 3C velocity data in holographic PIV", *Proceedings of the International Workshop on Holographic Metrology in Fluid Mechanics*, Loughborough, UK, p167-176

6.2 Suggestions for further work

In order to further improve the performance of μ HPIV and the digital shearing method, further investigation is suggested through the following.

(1) Algorithm efficiency improvement

As discussed in Chapter 4, the digital shearing method uses a total of four 2D FFT operations and other essential computations to calculate the final result. Using an input resolution of 256x256 pixels, FFT operations require approximately 4Mflops and it is estimated that the other essential computations require approximately 1M floating-point operations. Coordinate transforms represent the dominant computational overhead in the other essential computations. The MatLab-based method developed in this thesis is

efficient in the centre of k_x and k_y coordinate but there are some NaN (Not a Number) produced near the edge of k_x and k_y components. The origins of these singularities are unknown but should be eliminated by coding another interpolation routine.

(2) Background noise removal

The background noise may be successfully removed by subtracting background images from μ HPIV recordings. An image of the background could be obtained by averaging of μ HPIV recordings. Because the particles are randomly distributed and quickly move through the camera view area, their image will disappear in the averaged recording. However, the image of the background (including boundary and particles adhered to the well, etc.) maintains the same brightness distribution in the recording, because it does not move or change.

(3) Dense seeding to improve spatial resolution

137 vectors have been obtained with vector cluster analysis in the case of the sparse seeding in this thesis. The vector number could be improved through seeding more densely. However, SNR will decrease as the density of seeding particles is increased. Clearly there needs to be a balance between SNR and the density of seeding particles. An experiment to determine the information capacity of μ HPIV needs to be performed in the future work.

(5) Effects of Brownian motion

Brownian motion is the random thermal motion of a particle suspended in a fluid (Probstein 1994). The motion results from collisions between fluid molecules and suspended particles. When the seed particle size becomes small, the effect of Brownian motion on the accuracy of μ HPIV has to be considered. The relative error due to

Brownian motion can be estimated by $\varepsilon = \frac{1}{u} \sqrt{\frac{2D}{\Delta t}}$, where D is the Brownian diffusion coefficient, u is the flow velocity and Δt is the time interval between pulses (Santiago *et al.* 1998). This Brownian error establishes a lower limit on the measurement interval Δt since, for short time, the measurement is dominated by the uncorrelated Brownian motion. Also, errors due to Brownian motion place a lower limit on the size of the particle that can be used to achieve the desired velocity measurement accuracy. The product of the size of particle and the measurement interval is dependent on the flow velocity of the experiment.

Since the errors due to Brownian motion are unbiased, they can be substantially reduced by averaging over several particle images in a single interrogation spot and over several realizations. The error decreases as $1/\sqrt{N}$, where N is the total number of particles in the average (Bendat *et al.* 1986). Another method would be to track the motion of individual particles as they move through the fluid effectively increasing the measurement time. Further work is required to investigate error reduction by averaging and tracking methods.

6.3 References

Barnhart, D. H., 2001, Whole-field holographic measurements of three-dimensional displacement in solid and fluid mechanics, PhD thesis, Loughborough University, UK.

Bendat, J. S. and Piersol, J. G., 1986, Random data: analysis and measurement procedures. New York, Wiley.

Coupland, J. M. and Halliwell, N. A., 1992, "Particle image velocimetry: three-dimensional fluid velocity measurements using holographic recording and optical correlation", Applied Optics, vol.131(8), p1005-1007.

Coupland, J. M. and Halliwell, N. A., 1996, "Holographic particle image velocimetry: immunity from aberration by optical information processing", Proceeding of IMechE., City University, London, UK.

Probstein, R. F., 1994, Physicochemical Hydrodynamics: an introduction. New York, John Wiley & Sons.

Santiago, J. G., Wereley, S. T., Meinhart, C. D., Beebe, D. J. and Adrian, R. J., 1998, "A micro particle image velocimetry system", Experiment in Fluids, vol.25(4), p316-319.

